UNIVERSITY OF COPENHAGEN
FACULTY OF SCIENCE

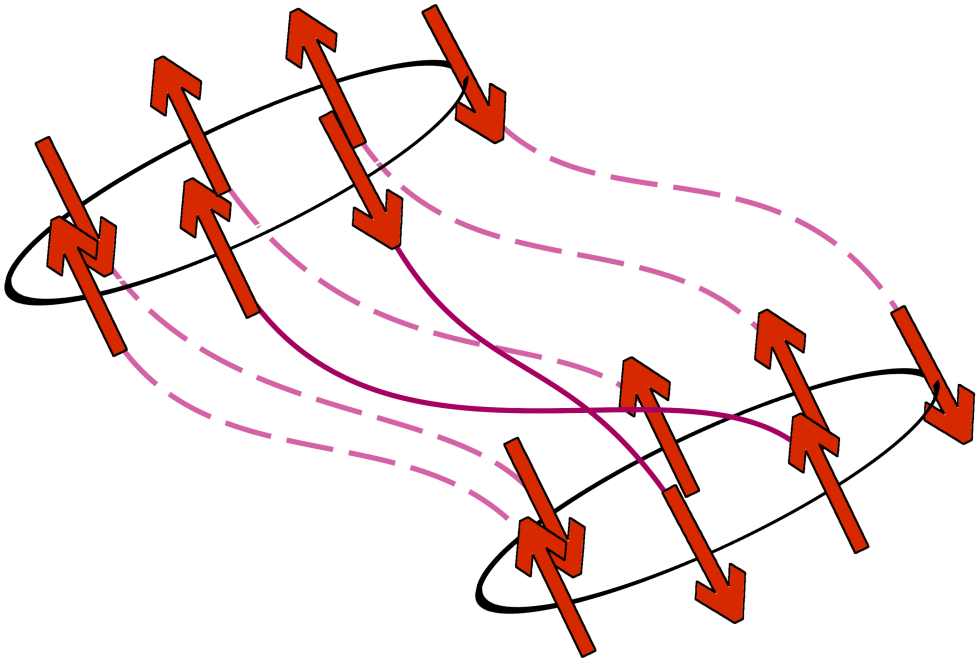

Master Thesis

Spectral Integrability In γ_i-Twisted $\mathcal{N} = 4$ Super Yang-Mills Theory

Random Matrix Theory For Non-Unitary Spin Chains

Anna Liv Paludan Bjerregaard

Supervisor: Anne Spiering
Co-supervisor: Matthias Wilhelm

Submitted: May 19, 2023

Abstract

Recently, the use of Random Matrix Theory methods in the context of gravitational systems has gained much attention. This similarly motivates their application in the study of the dual conformal field theories to learn more about universal properties of observables in these theories. An important example is maximally supersymmetric Yang-Mills theory, where the anomalous dimension spectra have been shown to manifest the model's planar integrability, while at the non-planar level the spectra can be described by Random Matrix Theory, revealing the quantum chaotic nature of the model. The goal of this project is to further these analyses, in particular in a specific limit of planar $\mathcal{N} = 4$ Super Yang-Mills theory with large imaginary twisting parameters. A specific case of this is the so-called Fishnet theory, which is integrable to all orders of the coupling constant g_{YM}, but becomes chaotic at certain truncations of the perturbative expansion in g_{YM}. In this project the anomalous dimension spectrum of Fishnet theory is studied and found to deviate from the Poissonian statistics usually seen for integrable systems. Similar but less pronounced deviations are found in the spectrum of a related $SU(3)$ sector. In the case of Fishnet theory these deviations are analyzed using the Coordinate Bethe Ansatz.

Contents

Contents **3**

1 Introduction: Chaos, a Quantum Phenomenon **5**

2 RMT and Chaotic Quantum Systems **9**
2.1 RMT and Spectral Integrability 9
2.1.1 Hermitian Ensembles 10
2.1.2 Non-Hermitian Ensembles 11
2.2 Measures of Spectral Integrability 11
2.2.1 Level Spacings and Unfolding 12
2.2.1.1 Real Spectra 12
2.2.1.2 Complex Spectra 14
2.2.2 Level Spacing Ratios 16

3 Spin Chains and $\mathcal{N} = 4$ SYM **20**
3.1 $\mathcal{N} = 4$ SYM 20
3.1.1 Supersymmetry and Conformality 21
3.1.2 Field Contents 23
3.1.3 Spin Chains and the Dilatation Operator 24
3.2 γ_i-Twisted $\mathcal{N} = 4$ SYM 28
3.2.1 Fishnet Theory 29
3.2.2 The Non-Eclectic $SU(3)$ Sector 31
3.3 The XXZ Spin Chain 32
3.3.1 Deformations and Integrability Breaking 34
3.3.1.1 NNN Coupling 35
3.3.1.2 Random Magnetic Field 36
3.4 Desymmetrisation 36

4 Spectral Integrability for $\mathcal{N} = 4$ SYM **39**
4.1 Fishnet Theory 40
4.1.1 Spectra 40
4.1.2 Level Spacings 45
4.1.3 Level Spacing Ratios 49
4.2 Non-Eclectic SU(3) Sector 51
4.2.1 Spectra 52

4.2.2 Level Spacings 54
4.2.3 Level Spacing Ratios 56
4.3 Discussion 58
4.3.1 Fishnet Degeneracies From Bethe Root Combinatorics 59

5 Conclusions **62**

A Numerical Details **65**
A.1 Constructing Spin Chain Hamiltonians 66
A.2 Generating RMT Matrices 68
A.3 Unfolding the XXZ Spin Chain 69
A.4 Solving Fishnet Bethe Equations 70

Bibliography **72**

Chapter 1

Introduction: Chaos, a Quantum Phenomenon

Anyone who uses words "quantum" and "chaos" in the same sentence should be hung by his thumbs on a tree in the park behind the Niels Bohr Institute.
- Joseph Ford [1]

Chaotic systems have always been of great interest in classical mechanics, both for physicists and others merely fascinated by the visuals of double pendulums. Especially in the areas of fluid dynamics, climate physics, and many-body physics in general, it is of the utmost importance to understand the features of chaotic systems. For those of us studying quantum mechanics we might ask ourselves how such a concept translates to microscopic scales, where classical mechanics is no longer of use. Chaos is commonly understood visually as a divergence of phase-space paths that are initially close together when evolving in time, a concept which may seem outside the scope of quantum mechanics as the Heisenberg uncertainty principle does not allow for the concept of such paths to begin with. However, we know that classical mechanics is a limit of quantum mechanics, meaning that chaotic behavior must manifest itself somehow. The question of quantum chaos has been studied extensively since the conception of quantum mechanics this past century and has been met with varying degrees of enthusiasm, as illustrated in the Joseph Ford quote above. Luckily, Ford's assumption of maleness allows me, a woman, a loophole which I shall be exploiting during the entirety of this thesis.

Let us start with definitions. Classically chaotic systems are most precisely defined in Hamiltonian formalism using generalized coordinates q_i and their conjugate momenta p_i. A Hamiltonian, $H(q_1, \ldots, q_N, p_1, \ldots, p_N)$ with N independent degrees of freedom is said to be chaotic if the amount of independent conserved quantities I_i, such that $\{I_i, H\} = \{I_i, I_j\} = 0$[1], is smaller than N [2]. If not, the system is said to be *integrable*. Chaotic behavior can be in-

[1] $\{\cdot, \cdot\}$ are the Poisson brackets of classical mechanics.

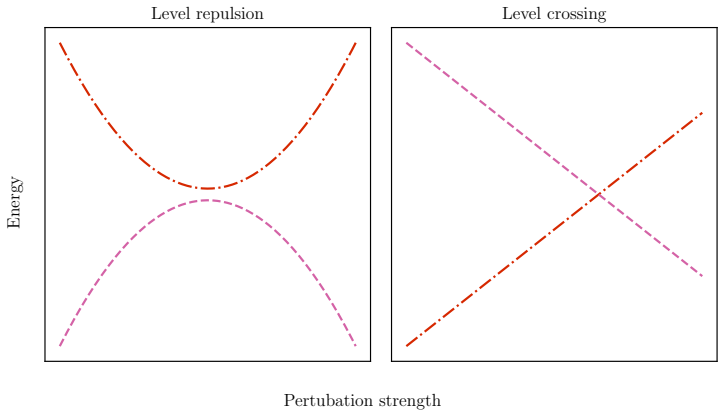

Figure 1.1: Level repulsion and crossing for perturbed energy levels.

tuitively understood as a high sensitivity to initial conditions. Phase-space points initially close together may become exponentially separated under time evolution of the system, whereas for integrable systems this distance may only increase like a polynomial in time [3]. Essentially, one needs arbitrarily precise knowledge of initial conditions to preserve determinism of chaotic systems on large time scales (hence why weather reports are never more than a few days ahead).

The ultimate goal of most classical mechanics is to solve for the dynamics of objects – i.e. their position and momentum as a function of time, as these are what we can observe through experiments. In quantum mechanics however, we typically look for eigenvalues of operators, so perhaps a natural place to look for chaotic behavior would be in the spacings between eigenvalues – mirroring the distance between phase-space paths in the classical picture. Consider a two-level quantum system with a perturbation that changes the energies such that they initially approach each other. As the strength of the perturbation increases the energies can either cross or repel each other, as shown in fig. 1.1. In [4, 5] these spectral properties are interpreted as signatures of chaos (level repulsion) and integrability (level crossing) respectively. This is the origins of the Bohigas-Gianonni-Schmidt (BGS) conjecture, which more precisely states a relation between the level spacings of chaotic quantum systems and those of certain ensembles of random matrices. The BGS conjecture has been studied in great detail for many Hermitian quantum systems, see [1, 6, 7, 8] for examples relevant to this thesis.

The spectral properties of a quantum system may reveal or provide evidence for the integrability of the model (or lack thereof), but in this thesis we will take an integrable quantum system to be one which eigenvalues can be expressed exactly as an expression of the physical parameters of the system. For example, the hydrogen atom is an integrable system since the energy levels can be found as functions of the parameters of the system $E_n = -{}^{m_e e^4}/_{8h^2\epsilon_0^2 n^2}$ [9, chapter 4]. Similarly the energy eigenvalues of the Heisenberg XXZ spin chain, discussed in detail in section 3.3, can be found as exact expressions of the length of the

chain and the amount of propagating magnons. This is what marks difference between "integrable" and "solvable" as any quantum system can, in principle, be solved by finding the Hamiltonian as a matrix and diagonalising it. However sometimes in the literature "solveable" is used to mean "integrable", and we will use the term like that throughout this thesis. In summation this thesis will test the BGS conjecture by looking at some systems we know to be integrable (or chaotic) and examining whether the spectral properties match this claim.

A context within modern theoretical physics in which integrability is of great interest is AdS/CFT correspondence – a duality which relates string theories on Anti-de Sitter (AdS) spacetimes to conformal field theories (CFT's) on the boundary of said AdS spacetime. In other words AdS/CFT correspondence allows a d-dimensional CFT to be described by a $(d+1)$-dimensional string theory or vice-versa and as such specific examples are often denoted as $\mathrm{AdS}_{d+1}/\mathrm{CFT}_d$. Crucially, the duality is strong/weak in terms of the coupling of the related theories, meaning that if the string theory is weakly coupled the CFT is strongly coupled and vice-versa. This means that we can solve one side using perturbation theory, a well established method both in CFT and in string theory. However the strong side of the duality requires special attention as it requires evaluation at all orders in the non-vanishing coupling. If one of the sides can be shown to be integrable, we can solve both sides of the duality and possibly provide insight into the general case of AdS/CFT [10, 11]. Studying AdS/CFT correspondence would allow for developements in theories of quantum gravity, as well as provide a method of calculating observables in some strongly coupled condensed matter systems.

Black holes are some of the most fascinating objects in modern theories of gravity and we have known them to be thermal objects since Hawking's work in the 1970's, see [12] for a review. [13] found that black hole geometries in the AdS side can be generated by a "scrambling" of eigenstates on the CFT side leading to a chaotic quantum system. [14] and [15] discuss a relationship between Jackiw-Teitelboim (JT) gravity, a two-dimensional gravitational theory, and certain ensembles of random matrices. JT gravity is one of the gravitational models which has been successfully used in the context $\mathrm{AdS}_2/\mathrm{CFT}_1$ [16]. This in total motivates connecting the study of integrability for CFT's to the BGS conjecture and Random Matrix Theory (RMT). The specific CFT studied in this work is called "$\mathcal{N}=4$ Super Yang-Mills Theory" ($\mathcal{N}=4$ SYM), as it is one of the most popular toy-models used to study the general structure of Quantum Field Theories (QFT's).

Since the 1950's Yang-Mills theories have been the theoretical backbone of particle physics, since they describe the interactions of non-abelian gauge-theories such as the strong and weak nuclear forces [17]. $\mathcal{N}=4$ Super Yang-Mills theory was first developed in [18] in an effort to construct supersymmetric gauge theories in four dimensions. In the 70's supersymmetry was seen as the next extension to particle physics after the success of the Standard Model (SM), however experimental evidence of the particles predicted by supersymmetric extensions of the SM has yet to be found (see [19] for a review of this

search at the LHC). Nevertheless $\mathcal{N} = 4$ SYM is still a useful tool in modern particle physics since its large amount of symmetries simplifies many calculations that are otherwise difficult in general Yang-Mills theories. $\mathcal{N} = 4$ SYM is known to be integrable in the planar limit, where we take the gauge group of the theory to be $SU(N_c), N_c \to \infty$ [20]. Studying this limit is therefor crucial to understanding how integrability manifests itself in QFT's, whether it is a special phenomenon or something that can be deduced from the parameters of the theory. $\mathcal{N} = 4$ SYM is also of interest as it is believed to be the strong side of an $\mathrm{AdS}_5/\mathrm{CFT}_4$ duality with a type-IIB string theory on the AdS side. Integrable QFT's have otherwise only been found for $d = 2$ so perhaps $\mathcal{N} = 4$ SYM can provide insight into whether or not (and how) AdS/CFT correspondence generalises.

It is possible to deform $\mathcal{N} = 4$ SYM in a way that preserves integrability but breaks supersymmetry, called γ_i-twisting. Certain limits of this deformation also break unitarity, meaning that observables in the theory may be complex valued. Of interest in this thesis will be the so-called Fishnet theory[2][21] and a three-scalar theory which we will call "The non-eclectic $SU(3)$ sector" for reasons explained in section 3.2.2[22]. The BGS conjecture has been shown to hold in certain limits of γ_i-twisting [7, 8] but only in the Hermitian case. We expand on this in this thesis by studying non-Hermitian theories.

Now that we know the characters, let's tell the story of this thesis. In chapter 2 we will introduce some basic concepts of Random Matrix Theory, which has played a big role historically in showing the link between quantum chaos and level repulsion [6] – the basis for the BGS conjecture. Specifically we introduce the concepts of level spacings and level spacing ratios as measures for integrability, as well as Gaußian and Ginibre ensembles of random matrices. In chapter 3 we introduce $\mathcal{N} = 4$ SYM as well as the integrability-preserving γ_i-twisting limits hereof. Specifically we look at how the dilatation operator, which describes the scaling of operators in the theory, can be interpreted as a Hamiltonian acting on chains of interacting spins, which in some cases can be solved with a method known as the Bethe Ansatz. We also examine the Heisenberg XXZ spin chain, as it is relevant to the dilatation operator as well as being one of the oldest examples of integrable quantum systems. Finally in chapter 4 we combine our previous work, using results from RMT to analyse the spectral properties of certain limits of the $\mathcal{N} = 4$ SYM dilatation operator. Finally in chapter 5 we tie everything we've learned and analysed together.

[2]The only interaction term present in this theory is a $2 \to 2$ scalar scattering, so all Feynman diagrams in the theory will have a fishnet-like structure

Chapter 2

Random Matrix Theory and Chaotic Quantum Systems

Random Matrix theory is the mathematical study of matrices with elements randomly drawn from probability distributions over fields of numbers. For physicists the eigenvalues and eigenvectors of matrices are often of greatest interest, and so too in this thesis. RMT can be used to determine properties of random matrices such as probability distributions of eigenvalues or eigenvector elements. In this chapter we introduce some of the basics of RMT as well as which properties and results are applied in the study of quantum integrability and chaos. In section 2.1 we introduce the relevant ensembles of random matrices and extract the properties of eigenvalues of large matrices, using an result from a 2×2 ensemble. Then in section 2.2 we relate these properties to chaotic and integrable systems by introducing the concepts of level spacings and level spacing ratios, along with the *Wigner surmise*, which is extended by the BGS conjecture [4] and *Berry-Tabor conjecture* [23].

2.1 Random Matrix Theory and Spectral Integrability

As discussed previously, quantum analogues of integrability and chaos can be difficult to precisely define – in fact there is no such universally accepted definition yet. Great strides have however been made in looking for signatures of integrability in some of the most important features of quantum mechanical systems: eigenvalues of operators. This analysis was pioneered by Wigner [24] and Dyson [25], modeling Hamiltonians as different ensembles of random matrices in order to study universal properties of systems with different symmetries. Originally the goal was to study the spectra of large atoms, but the methods developed, collectively known as Random Matrix Theory (RMT), have proven useful in studying other chaotic quantum systems, such as many body problems in condensed matter physics [26, 27] or indeed quantum field theories [7, 8], as are of interest for this work. When QFT's are said to be "in-

tegrable" we often mean that they are fully solvable, meaning that we can get precise values for observables for all values of the coupling constant – i.e. non-perturbatively. One way to show that a QFT is integrable would be to solve it without the use of perturbation theory in a way that is valid for all values of the coupling, but since this would be exceedingly difficult, and even impossible many important cases like QCD[1], perhaps a slightly simplified starting point would be to look for integrable behavior in the spectra of operators in the theory. Relying on the results of RMT we can then aquire evidence about the integrability of the theory in the first place.

2.1.1 Hermitian Ensembles

A common tactic in RMT is to derive a result for 2×2 matrices and extrapolating these properties to larger systems. To this end we study two types of systems: Those with and without time reversal symmetry. Suppose we have a generic Hermitian 2×2 Hamiltonian

$$H = \begin{pmatrix} e_1 & \frac{\Delta}{\sqrt{2}} \\ \frac{\Delta^*}{\sqrt{2}} & e_2 \end{pmatrix} , \tag{2.1}$$

which can be diagonalized with eigenvalues

$$E_\pm = \frac{e_1 + e_2}{2} \pm \frac{1}{2}\sqrt{(e_1 - e_2)^2 + 2|\Delta|^2} . \tag{2.2}$$

For Hamiltonians of systems with time reversal symmetry we can find a basis in which H is fully real, i.e. $\Delta = \mathrm{Re}(\Delta)$, meaning that we have three independent variables: e_1, e_2 and Δ. H is likewise symmetric, thanks to being Hermitian. If we draw each of the independent variables (e_1, e_2, Δ) from a Gaußian distribution with mean 0 and variance 1 we get a matrix from the *Gaußian Orthogonal Ensemble* (GOE). Likewise if we are looking at a system without time reversal symmetry $\mathrm{Re}(\Delta)$ and $\mathrm{Im}(\Delta)$ can be treated as independent variables and we get a Hermitian matrix from the *Gaußian Unitary Ensemble* (GUE) by drawing $(e_1, e_2, \mathrm{Re}(\Delta), \mathrm{Im}(\Delta))$ from the same standard Gaußian. Since we wish to consider level repulsion as a measure for chaos we could ask about the spacing between the eigenvalues $s = E_+ - E_- = \sqrt{(e_1 - e_2)^2 + 2|\Delta|^2}$. We can find the probability distribution for these spacings $P(s)$ by integrating over the entire parameter space (e_1, e_2, Δ) for the GOE or $(e_1, e_2, \mathrm{Re}(\Delta), \mathrm{Im}(\Delta))$ for the GUE. Since all parameters are real-valued this a three or four dimensional Euclidean integral depending on the ensemble. Taking the GOE our example we let $\mathbf{X} = (e_1, e_2, \Delta)$. For each element X_i we weigh the probability distribution $P(s)$ with a standard Gaußian[2] $(2\pi)^{-1} \exp(-X_i^2/2)$. To ensure that

[1] In fact, we do not expect QCD to behave in an integrable way at all. [8] provides evidence that $\mathcal{N} = 4$ SYM becomes chaotic in the non-planar case, i.e. for gauge group $SU(N)$ with N finite.

[2] We take a "standard Gaußian" to mean 0 and variance 1.

$P(s)$ only returns possible spacings between eigenvalues of H we also weigh by $\delta(\sqrt{(e_1-e_2)^2+2|\Delta|^2}-s)$. Finally we obtain [28]

$$P(s)=\frac{1}{(2\pi)^{3/2}}\int \mathrm{d}^3\mathbf{X}\delta\left(\sqrt{(e_1-e_2)^2+2|\Delta|^2}-s\right)\exp\left(-\frac{|\mathbf{X}|^2}{2}\right), \quad (2.3)$$

and likewise for the GUE with an extra dimension. For both the GOE and the GUE the level spacing distribution exhibits level repulsion, i.e. they are vanishing as $s \to 0$. This is the property we will look for when examining spectral integrability, as it points to a chaotic nature in the system. This distribution of eigenvalue spacings holds true even for general $N \times N$ matrices for $N > 2$ [2, 28].

2.1.2 Non-Hermitian Ensembles

In this work we analyze some operators whose spectra are complex – i.e. the operators are non-Hermitian. The RMT ensembles we've looked at so far all have strictly real eigenvalues, meaning that if we wish to analyse complex spectra using RMT methods, we need ensembles that can replicate the spectral properties of non-Hermitian chaotic operators. We can extend the GOE to complex eigenvalues by not requiring it to be symmetric, i.e. a real valued matrix with random entries drawn from a standard Gaußian distribution, the *Ginibre* Orthogonal Ensemble (GinOE). We can extend the GUE in much the same way, removing the condition for our matrix to be hermitian and simply drawing the real and imaginary parts of every entry from a standard Gaußian. This is what we call the Ginibre Unitary Ensemble (GinUE). These ensembles are named after French mathematician Jean Ginibre who introduced them in [29]. The field of spectral integrability has historically been most focused on Hermitian RMT ensembles, and as such the conjecture of universal chaotic signatures is less studied and less understood for complex spectra. For further discussions of this see [26, 27].

2.2 Measures of Spectral Integrability

Wigner originally used RMT to study the spectra of large atoms [24], leading to the Wigner surmise which states that the energy level spacings of heavy nuclei is described by eq. (2.3). This is extended the BGS conjecture which states that this behavior is true for all chaotic systems invariant under time-reversal [4]. Similarly the Berry-Tabor conjecture claims that the level spacings of an integrable system will follow a Poisson distribution $P(s) = \exp(-s)$. We now introduce the measures of integrability used in this thesis and how they relate to these conjectures.

2.2.1 Level Spacings and Unfolding

As previously discussed, examining the distribution of eigenvalue spacings has lead to most of the key results in spectral integrability. The BGS and Berry-Tabor conjectures state that chaotic and integrable systems carry universal signatures replicable with RMT ensembles. To study these universal signatures we must first eliminate attempt to remove the system dependent fluctuations in the spectra. This removal process is called *unfolding* and there are several ways of doing it. For spectra of Hermitian matrices we define the integrated density of states

$$n(E) = \sum_{i=1}^{N} \Theta(E - E_i) \,, \tag{2.4}$$

with $\Theta(x)$ being the Heaviside step-function. The idea now is to to divide up $n(E)$ into two parts

$$n(E) = n_{\text{avg}}(E) + n_{\text{flux}}(E) \,, \tag{2.5}$$

where $n_{\text{avg}}(E)$ exhibits the universal signatures and $n_{\text{flux}}(E)$ describe the system dependent fluctuations. For large systems the universal RMT signatures are expected to dominate and thus we take $n_{\text{avg}}(E)$ to be some degree p polynomial[3] which we fit to $n(E)$. Constructing $n_{\text{avg}}(E)$ is in general where different methods of unfolding differ. Polynomial unfolding previously been used in the context of $\mathcal{N} = 4$ SYM integrability [7, 8] which is why we use it in this thesis. Another way of removing system dependent fluctuations is by removing a fraction of energies at the high and low end of the spectra, as these are more tightly bounded by system dependent physical effects. The polynomial degree p and the fraction of states removed at each end of the spectrum are non-physical parameters which must be tuned when preforming analysis of level spacings. After unfolding the spectrum we define the *unfolded eigenvalues* as $\varepsilon_i = n_{\text{avg}}(E_i)$. The integrated density of states for a GOE matrix and a random diagonal matrix can be seen in fig. 2.1, illustrating how $n(E)$ can measure the difference between integrable and chaotic spectra. An example of unfolding for a physical system is given in appendix A.3.

2.2.1.1 Real Spectra

Suppose one has a Hamiltonian, H, with a discreet eigenenergy spectrum, $\{E_i\}, E_i \in \mathbb{R} \forall i$. The level spacing, S_i is now defined as the difference between neighboring unfolded energy eigenvalues, ε_i. As such we define

$$S_i = \varepsilon_{i+1} - \varepsilon_i \,. \tag{2.6}$$

For every system we analyse to have spacings in comparable orders of magnitude we use $s_i = {}^{S_i}/_{\bar{s}}$ for any further analysis.

[3] For all computations in this thesis we take $p = 17$ unless otherwise specified.

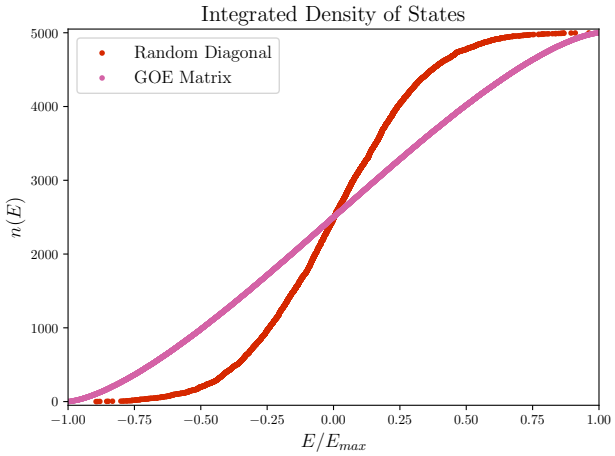

Figure 2.1: Integrated density of states for a random diagonal matrix with elements drawn from a standard Gaußian and a GOE matrix. For both matrices $N = 5000$.

Integrable systems allow for level crossings and in general have uncorrelated eigenvalues. The statement of the Berry-Tabor conjecture is then that these should follow the Poisson distribution,

$$P_{\text{Poi}}(s) = \exp(-s)\,. \tag{2.7}$$

We can generalise the BGS conjecture for chaotic systems by using the *Wigner-Dyson distribution* to describe systems both with and without time reversal symmetry. By preforming the integral in eq. (2.3) we obtain [7, 28]

$$P_{\text{WD}}(s,\alpha) = 2\frac{\Gamma\left(1+\frac{\alpha}{2}\right)^{1+\alpha}}{\Gamma\left(\frac{1+\alpha}{2}\right)^{2+\alpha}} s^{\alpha}\exp\left(-A(\alpha)s^2\right), \quad A(\alpha) = \frac{\Gamma\left(1+\frac{\alpha}{2}\right)^2}{\Gamma\left(\frac{1+\alpha}{2}\right)^2}\,, \tag{2.8}$$

where setting $\alpha = 1$ returns the GOE distribution and $\alpha = 2$ returns the GUE distribution,

$$P_{\text{WD}}(s,1) = P_{\text{GOE}}(s) = \frac{\pi s}{2}\exp\left(-\frac{\pi}{4}s^2\right), \tag{2.9}$$

$$P_{\text{WD}}(s,2) = P_{\text{GUE}}(s) = \frac{32s^2}{\pi^2}\exp\left(-\frac{4}{\pi}s^2\right). \tag{2.10}$$

The Wigner-Dyson distribution is a result extrapolated from 2×2 matrices, but fig. 2.2 shows that these distributions also describe the level spacing distributions of larger matrices.

In some systems there may be a transition between an integrable and chaotic phase, indicated by the level spacings not necessarily being distributed according to $P_{\text{Poi}}(s)$ or $P_{\text{WD}}(s)$. For systems with time reversal this transition can be quantified with the Brody distribution

$$P_B(s,\omega) = \Gamma\left(\frac{\omega+2}{\omega+1}\right)^{1+\omega}(1+\omega)s^{\omega}\exp\left(-\Gamma\left(\frac{\omega+2}{\omega+1}\right)^{1+\omega}s^{1+\omega}\right), \tag{2.11}$$

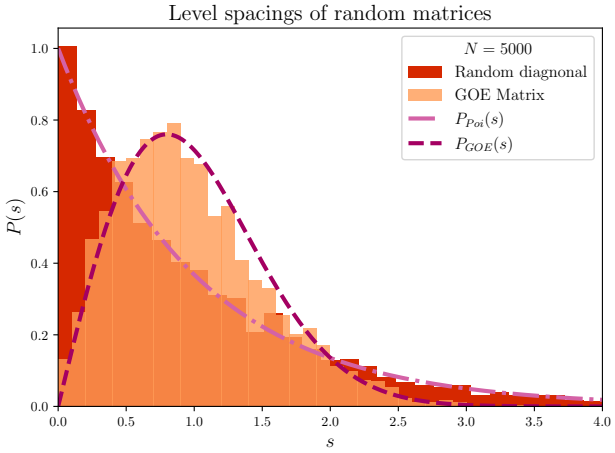

Figure 2.2: Level spacing distributions of a random diagonal matrix and a random symmetric matrix (both real), both $N \times N$. The elements are drawn from a Gaußian distribution with mean 0 and width 1.

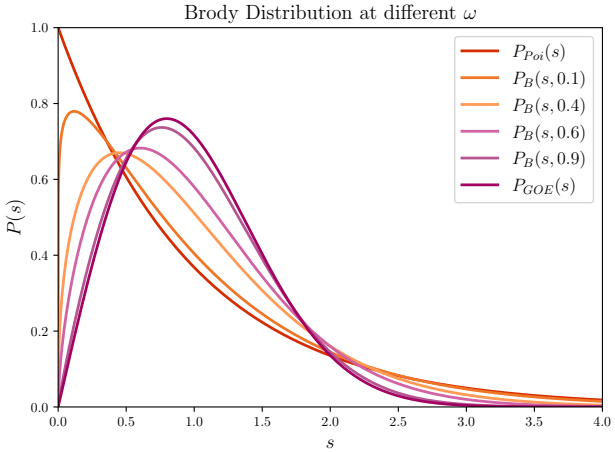

Figure 2.3: Brody distribution $P_B(s)$ at different values of ω along with $P_{\text{Poi}}(s)$ and $P_{\text{GOE}}(s)$.

which is a smooth function on $\omega \in [0, 1]$ with $P_B(s, 0) = P_{\text{Poi}}(s)$ and $P_B(s, 1) = P_{\text{GOE}}$. This transitional behavior is shown in fig. 2.3.

2.2.1.2 Complex Spectra

The concept of level spacing distributions for spectra valued in the complex plane has not been studied as much as real valued spectra and as such there is no universally accepted method to treat analysis of such systems. Furthermore the notion of "spacings" is complicated, as there is no natural ordering to the complex plane. We will in this thesis have to analyse non-Hermitian operators with complex valued spectra, so here we present a method of analysis proposed in [26] where spacing is defined from eigenvalue magnitude. Consider the

spectral density

$$n(E) = \sum_{i=1}^{N} \delta^{(2)}(E_i - E) \,. \tag{2.12}$$

Employing the same procedure as the integrated density of states for real spectra, eq. (2.5), we take this to have a universal part and a system-dependent fluctuating part

$$n(E) = n_{\text{avg}}(E) + n_{\text{flux}}(E) \,, \tag{2.13}$$

$$n_{\text{avg}}(E) = \frac{1}{2\pi\sigma^2 N} \sum_{i=1}^{N} \exp\left(-\frac{1}{2\sigma^2}|E - E_i|^2\right) . \tag{2.14}$$

The Gaußian approximation of $n_{\text{avg}}(E)$ is taken from [26, appendix A]. σ is a free parameter taken to be proportional to, but larger than, the mean spacing of the eigenvalues $\sigma \propto \bar{s} = \overline{|E - E_{\text{NN}}|}$, where E_{NN} is the closest eigenvalue to E using a Euclidean metric in $\mathbb{C}$. We are now ready to define a real-valued level spacing from eigenvalues in the complex plane

$$s_i = \sqrt{n_{\text{avg}}(E_i)}|E_i - E_{\text{NN},i}| \,, \tag{2.15}$$

$$E_{\text{NN},i} \equiv \min\{|E_i - E_j|, E_j \in \text{Spec}(H) \setminus \{E_i\}\} \,. \tag{2.16}$$

$\text{Spec}(H)$ denotes the spectrum of the Hamiltonian H.

Having defined our level spacings, we can expand the BGS and Berry-Tabor conjectures to encompass these complex spacings. We expect integrable systems to exhibit uncorrelated behavior, which in the complex plane corresponds to the two-dimensional Poisson distribution for the spacings,

$$P^{(2D)}_{\text{Poi}}(s) = \frac{\pi s}{2} \exp\left(-\frac{\pi s^2}{4}\right) . \tag{2.17}$$

The level repulsion of chaotic systems are modelled by the Ginibre enesembles (GinOE and GinUE). In [26] it is shown that this projective method of defining level spacings gives the same distribution regardless of ensemble considered, which is found to be

$$P_{\text{GinUE}}(s) \approx 1.14p(1.14s), \quad p(s) = \sum_{j=1}^{\infty} \frac{2s^{2j+1}e^{-s^2}}{\Gamma(j+1,s^2)} \prod_{j=1}^{\infty} \frac{\Gamma(j+1,s^2)}{\Gamma(j+1)} \,. \tag{2.18}$$

We call this distribution "$P_{\text{GinUE}}(s)$" for consistency with [26], but remember that this distribution also applies for GinOE matrices. The factor 1.14 comes from normalisation. Remark that both $P^{(2D)}_{\text{Poi}}(s)$ and $P_{\text{GinUE}}(s)$ show level repulsion, but specifically the GinUE repulsion is cubic, $P_{\text{GinUE}}(s) \sim s^3, s \to 0$ whereas $P^{(2D)}_{\text{Poi}}(s)$ exhibits linear repulsion [30].

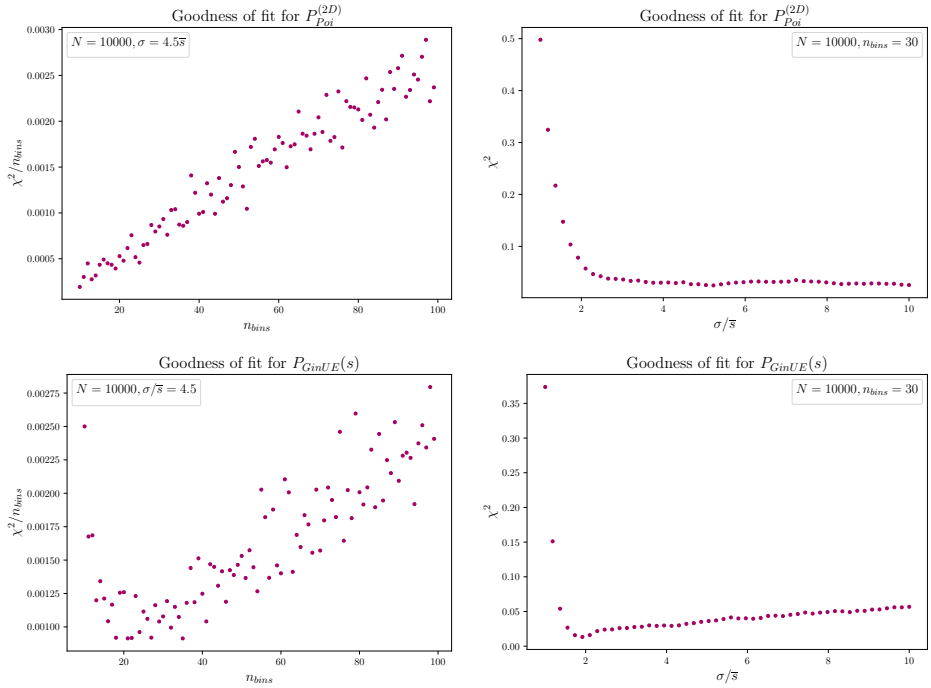

Figure 2.4: χ^2 values for (top) random complex diagonal matrices, varying (top left) the number of bins and (top right) the scaling parameter σ, compared to the analytical expression, eq. (2.17). Same analysis is done for (bottom) a GinUE matrix and compared to eq. (2.18). For both matrices the size is $10^4 \times 10^4$.

In calculating the level spacing distributions of operators numerically, we have two free parameters: The value of σ and the binning of the spacings n_{bins}. To properly fix these parameters, we can look at the χ^2 values[4] of a random diagonal matrix and a GinUE matrix, compared to the analytical level spacing distributions. Figure 2.4 shows these χ^2 values for randomly generated $10^4 \times 10^4$ matrices. The fit is better for low n_{bins}, but this also constitutes a smaller sample size. For Poissonian systems higher values of σ is generally better, but this is not necessarily true for the GinUE sample. Unless otherwise specified values of $n_{\text{bins}} = 50$ and $\sigma/\overline{s} = 4.5$ are used in this thesis when considering complex valued spectra which agrees with results found in [26].

2.2.2 Level Spacing Ratios

Level spacings have proved themselves to be a very robust spectral measure of integrability, but the need for unfolding introduces parameters outside the

[4] $\chi^2 = \sum_{i=1}^{n_{\text{bins}}} \frac{(P_{\text{obs}}(x_{\text{bin},i}) - P_{\text{exp}}(x_{\text{bin},i}))^2}{P_{\text{exp}}(x_{\text{bin},i})}$, the average square difference between the observed and expected distributions. The lower the χ^2 value, the better the observed distribution fits the analytical.

physical system itself (for example the σ in eq. (2.14)) to account for the system dependent local density of states. These parameters need to be fixed in a process that is more statistics than physics and may seem arbitrary given that we a priori know the result we want.

Other spectral integrability measures address this issue by being able to compare eigenvalue statistics without introducing unphysical variables. One such measure is *level spacing ratios*, which for the purposes of this thesis will be used purely to analyze non-Hermitian spectra. As the name implies, level spacing ratios analyzes the ratio between neighboring level spacings. More precisely we define

$$z_k = \frac{E_{k,\mathrm{NN}} - E_k}{E_{k,\mathrm{NNN}} - E_k}\,, \tag{2.19}$$

for some $E_k \in \mathrm{Spec}(H)$. The nearest neighbor (NN) eigenvalue, $E_{k,\mathrm{NN}}$, is defined as the eigenvalue with the smallest Euclidean distance in the complex plane to E_k (and likewise for $E_{k,\mathrm{NNN}}$ with the second-smallest). By definition $|z_k| \leq 1$ and the local density of states is accounted for, removing the need for unfolding. Generally, $z_k \in \mathbb{C}$ so analysis will take place within the complex unit circle. This specific measure is introduced and analyzed in [27], but we shall briefly discuss some of the findings about the spacing ration distribution, $\rho(z)$, here.

For integrable systems the lack of correlation between eigenvalues results in a constant value of $\rho_{\mathrm{Poi}}(z) = {}^1\!/\!_\pi \Theta(1-|z|)$. For chaotic systems, level repulsion plays a role in a few different ways. First we define the partial distributions $\rho(r)$ and $\rho(\theta)$ from polar coordinates $z = re^{i\theta}$,

$$\rho(r) = \int \mathrm{d}\theta r\rho(r,\theta), \quad \rho(\theta) = \int \mathrm{d}r\rho(r,\theta)\,, \tag{2.20}$$

where the extra factor of r in the angular integral comes from the Jacobian $\mathrm{d}x\mathrm{d}y = r\mathrm{d}r\mathrm{d}\theta$. Preforming these integrals we can find the partial distributions explicitly for the Poissonian case

$$\rho_{\mathrm{Poi}}(r) = \frac{r}{\pi}\Theta(1-r)\int_{-\pi}^{\pi}\mathrm{d}\theta = 2r\,, \tag{2.21}$$

$$\rho_{\mathrm{Poi}}(\theta) = \frac{1}{\pi}\int_0^\infty \mathrm{d}r\Theta(1-r) = \frac{1}{\pi}\,. \tag{2.22}$$

The GinUE case is complicated by the fact that $\rho_{\mathrm{GinUE}}(r,\theta)$ is dependent upon the size of the ensemble matrices N. [26, appendix C] derives $\rho_{\mathrm{GinUE}}(r,\theta)$ for both $N = 3$ and asymptotically $N \to \infty$ ensembles,

$$\rho^{(N=3)}_{\mathrm{GinUE}}(r,\theta) = \frac{81r^2(1+r^2-2r\cos\theta)}{8\pi(1+r^2-r\cos\theta)^5}\Theta(1-r)\,, \tag{2.23}$$

$$\rho^{(N\to\infty)}_{\mathrm{GinUE}}(r,\theta) \approx \frac{12r^2(1+r^2-2r\cos\theta)}{\pi(1+r^2)^5}\Theta(1-r)\,. \tag{2.24}$$

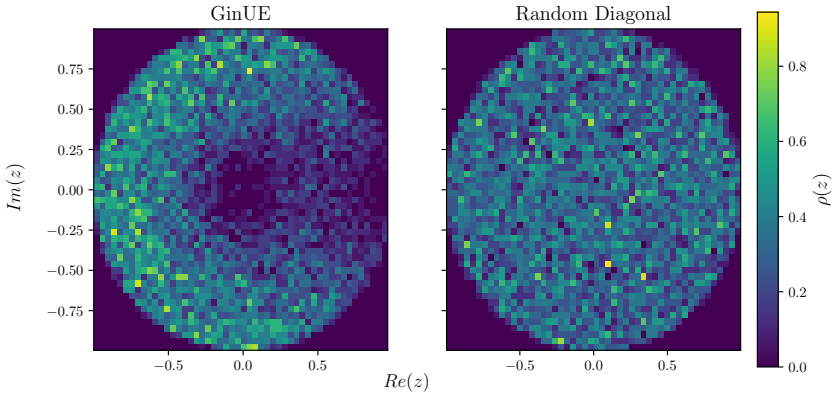

Figure 2.5: Level spacing ratio distributions of (left) a $10^4 \times 10^4$ GinUE matrix, (right) a diagonal matrix with 10^4 random elements taken from a standard complex Gaußian.

Figure 2.5 shows the level spacing ratio density for a $N = 10^4$ GinUE matrix and a random diagonal matrix. Figure 2.6 shows the partial level spacing ratio distributions for these matrices. We observe that even at $N = 10^4$ the large N asymptotics of the ensemble is not captured, meaning that for analysis of operators of smaller sizes $\rho^{(N\to\infty)}_{\text{GinUE}}(r,\theta)$ will not represent an appropriate analytical measure of comparison[5] and we will in general look for level repulsion as the signature of chaotic behavior rater than specifically comparing to this distribution.

[5]The largest operator with chaotic behavior studied in this thesis has $N = 4862$

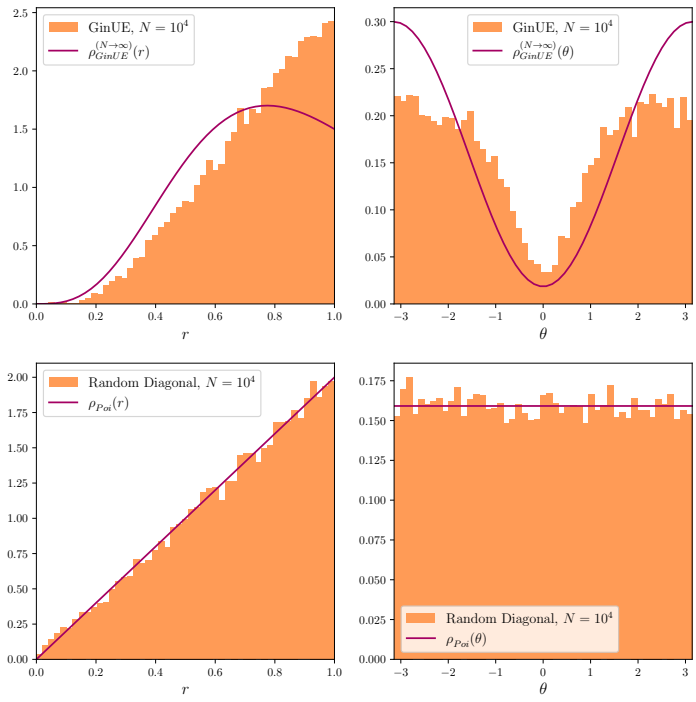

Figure 2.6: Partial level spacing ratio distributions for (top) a GinUE matrix with the partial forms of $\rho^{(N\to\infty)}_{\text{GinUE}}(r,\theta)$ for comparison and (bottom) a random diagonal matrix with entries drawn from a standard Gaußian in the complex plane with the partial forms of $\rho_{\text{Poi}}(r,\theta)$ for comparison. Both matrices are $N = 10^4$.

Chapter 3

Spin Chains and $\mathcal{N} = 4$ Super Yang-Mills Theory

Spin chains appear in many areas of condensed matter physics and have been studied extensively since the late 1920's [31], serving as a model for how magnetism appears in matter. In the early 2000's a link to spin chains was found in a rather surprising area of theoretical physics: supersymmetric Yang-Mills theory [32]. More specifically Minahan and Zarembo found the anomalous dilatation operator of planar $\mathcal{N} = 4$ SYM to have a spin chain interpretation at first loop order and solved it using methods developed for spin chain systems. Spin chains have been a prime example of integrable quantum systems since the 1930's [33] so their discovery in $\mathcal{N} = 4$ SYM motivates further study into its integrability, see [34] for a review. In this chapter we will introduce $\mathcal{N} = 4$ SYM theory and explain how to make the connection to spin chain systems. In section 3.2 we introduce γ_i-twisting of $\mathcal{N} = 4$ SYM along with *Fishnet theory* and the *non-eclectic* $SU(3)$ *sector* which are limits of this twisting. We show that even in these so-called "strong twisting limits" the anomalous dilatation operator retains a spin chain structure. Then in section 3.3 we discuss the Heisenberg XXZ spin chain and use it to demonstrate the spectral integrability methods we developed in chapter 2. This will motivate the study of spectral integrability for strongly twisted $\mathcal{N} = 4$ SYM in chapter 4.

3.1 $\mathcal{N} = 4$ Super Yang-Mills Theory

Yang-Mills theory is the foundation for much of modern particle physics being the mathematical framework underlying the Standard Model. Constructing particle content and dynamics directly from symmetry groups has lead to many of the most groundbreaking discoveries in high-energy physics. It is therefore no wonder that some theoretical physicists in the 1970's would devote much of their attention to extending the symmetries of the Standard Model in order to discover new physics, whether this be through constructing larger gauge groups leading to so-called "Grand Unified Theories" [35] or introducing other

non-gauge symmetries such as *supersymmetry* [36]. It is in the later of these examples where we find $\mathcal{N} = 4$ SYM, originally developed in 1974 [18] as the *maximally supersymmetric* Yang-Mills theory in four space-time dimensions. Due to its many symmetries it has become the go-to toy model for modern particle theorists, because despite supersymmetry being so far unobserved in experiment [19] studying $\mathcal{N} = 4$ SYM can provide insight into the fundamental structure of QFT's. It is conformal, meaning that its β-function is 0 to all orders in perturbation theory. Since QCD is asymptotically free at high energies and is similar in algebraic structure to $\mathcal{N} = 4$ SYM, we may use observables of the later (such as scattering amplitudes) to better understand the former at high energy scales. It is also of interest in the context of AdS/CFT correspondence, linking string theories to conformal field theories.[1] Since one side of this duality is weakly coupled (i.e. able to be studied perturbatively) and the other strongly coupled, it is hoped that a better understanding could further our understanding of some strongly coupled QFT's (for example in condensed matter systems) by studying weakly coupled string theories. In both these cases, the conjectured integrability of $\mathcal{N} = 4$ SYM in the planar limit plays an important role as it allows us to compute observables in a non-perturbative way.

3.1.1 Supersymmetry and Conformality

A field theory is said to be *conformal* (such theories are often called CFT's) if the action of the theory is invariant under a change of the metric such that

$$g_{\mu\nu} \to g'_{\mu\nu} = e^{2\sigma(x)} g_{\mu\nu} \,, \tag{3.1}$$

where $\sigma(x)$ is some real space-time dependent function. Remark that for $g_{\mu\nu} = \eta_{\mu\nu}$ and $\sigma = 0$, these are the Poincaré transformations. We can obtain the generators of this symmetry by applying an infinitesimal transformation $x^\mu \to x^\mu + \epsilon^\mu(x)$, which (to first order in ϵ) gives us the metric equation

$$\partial_\mu \epsilon_\nu + \partial_\nu \epsilon_\mu = 2\sigma(x)\eta_{\mu\nu} \,. \tag{3.2}$$

This thesis restricts itself to flat space-times, so $g_{\mu\nu} = \eta_{\mu\nu}$. Contracting with $\eta^{\mu\nu}$ on both sides we obtain $\partial^\mu \epsilon_\mu = \sigma(x) d$, where d is the space-time dimension ($d = 4$ in this thesis). The solutions $\epsilon^\mu(x)$ to this equation must be no more than second order in x^μ, which is shown more explicitly in chapter 3.2 of [11] and in chapter 4.1 of [37]. We write

$$\epsilon^\mu(x) = \underbrace{a^\mu}_{\text{Translation}} + \overbrace{\omega^\mu_\nu x^\nu}^{\text{Lorentz trans.}} + \underbrace{\lambda x^\mu}_{\text{Scaling (Dilation)}} + \overbrace{2(b\cdot x)x^\mu + x^2 b^\mu}^{\text{Special conformal trans.}} \,. \tag{3.3}$$

[1] It is specifically conjectured to be dual to a type IIB string theory in $\mathrm{AdS}_5 \times \mathrm{S}^5$ target space.

Switching from space-time to fields, we can construct generators of these transformations as

$$\begin{aligned} \text{Translation :} \quad & P_\mu = -\partial_\mu, && (3.4)\\ \text{Lorentz trans. :} \quad & L_{\mu\nu} = -(x_\mu\partial_\nu - x_\nu\partial_\mu), && (3.5)\\ \text{Special conformal trans. :} \quad & K_\mu = 2x_\mu x^\nu\partial_\nu - x^2\partial_\mu, && (3.6)\\ \text{Dilation :} \quad & \mathcal{D} = -x^\mu\partial_\mu\,. && (3.7) \end{aligned}$$

Studying how these generators commute allows us to construct the conformal algebra,

$$\begin{gathered} [L_{\mu\nu}, L_{\rho,\sigma}] = \eta_{\mu\rho}L_{\nu\sigma} + \eta_{\nu\sigma}L_{\mu\rho} - \eta_{\nu\rho}L_{\mu\sigma} - \eta_{\mu\sigma}L_{\nu\rho},\\ [L_{\mu\nu}, P_\rho] = \eta_{\rho\mu}P_\nu - \eta_{\nu\rho}P_\mu, \quad [\mathcal{D}, P_\mu] = P_\mu, \quad [\mathcal{D}, K_\mu] = -K_\mu,\\ [P_\mu, K_\nu] = 2(\eta_{\mu\nu}\mathcal{D} - L_{\mu\nu}), \quad [L_{\mu\nu}, K_\rho] = \eta_{\mu\rho}K_\nu - \eta_{\nu\rho}K_\mu\,, \end{gathered} \tag{3.8}$$

where any commutator not shown is simply 0. If all we wanted was a conformal field theory, we could now start building irreducible representations and discussing what types of particles could exist for this symmetry group, but the "Super" in "Super Yang-Mills theory" means that we have another type of symmetry to discuss.

Where conformality is constructed from an invariance of the metric, supersymmetric theories have actions invariant under certain exchanges of fields. Specifically these symmetry transformations mix fields with their *supersymmetric partner*, where the helicity of the different fields are related as $\lambda_{\text{Field}} = \lambda_{\text{Partner}} \pm 1/2$. Thus super symmetry relates bosonic fields to fermionic fields and vice versa. In principle this is done by introducing *supercharges* Q^a into the conformal algebra eq. (3.8). There is at first glance no limit to the amount of supercharges we can introduce, but the index $a = 1, \ldots, \mathcal{N}$ tells us which one we're dealing with – $\mathcal{N}$ being the total amount. It is in fact this $\mathcal{N}$ which is equal to 4 in "$\mathcal{N} = 4$ SYM". In $d = 4$ only fields with helicity $|\lambda| \leq 1$ are renormalizable, so starting at minimum helicity one needs at most four supersymmetry transformations to reach all other possible helicity states. It is for this reason that $\mathcal{N} = 4$ SYM is often referred to as "maximally supersymmetric".

The supercharges Q^a are spinors[2], and it will prove convenient to write them as Weyl spinors, $Q^a = (Q^a_\alpha, \bar{Q}^{a\dot{\alpha}}), \alpha, \dot{\alpha} \in \{1, 2\}$, with the bar indicating Dirac conjugation. This means that our symmetry algebra now has a fermionic sector and a bosonic sector, upgrading us from a Lie algebra to a *graded* Lie algebra. In addition to our conformal algebra, we now also have the (anti-)commutation relations

$$\begin{gathered} [Q_a, L^{\mu\nu}] = (\sigma^{\mu\nu})^\beta_\alpha Q^a_\beta, \quad [\bar{Q}^{a\dot{\alpha}}, L^{\mu\nu}] = \epsilon_{\dot{\alpha}\dot{\beta}}(\bar{\sigma}^{\mu\nu})^{\dot{\beta}}_{\dot{\gamma}}\bar{Q}^{a\dot{\gamma}},\\ \{Q^a_\alpha, \bar{Q}_{b\dot{\alpha}}\} = 2\sigma^\mu_{\alpha\dot{\alpha}}P_\mu\delta^a_b,\\ \{Q^a_\alpha, Q^b_\beta\} = \epsilon_{\alpha\beta}Z^{ab}, \quad \{\bar{Q}_{a\dot{\alpha}}, \bar{Q}_{b\dot{\beta}}\} = \epsilon_{\dot{\alpha}\dot{\beta}}\bar{Z}_{ab}\,, \end{gathered} \tag{3.9}$$

[2]In contrast to the Poincaré algebra which consists of vectors and scalars

where $\bar{Q}_{a\dot{\alpha}} = (Q^a_\alpha)^*$. As before, all relations not shown vanish. In the convetion of [11, section 3.3] we have $\sigma^\mu = (-\mathbb{I}, \sigma^i)$ and $\bar{\sigma}^\mu = (-\mathbb{I}, -\sigma^i)$ and[3] $(\sigma^{\mu\nu})^\beta_\alpha = {}^i\!/_4(\sigma^\mu_{\alpha\dot{\alpha}}\bar{\sigma}^{\nu\dot{\alpha}\beta} - \sigma^\nu_{\alpha\dot{\alpha}}\bar{\sigma}^{\mu\dot{\alpha}\beta})$. Z^{ab} and $\bar{Z}_{ab}$ are known as the *central charges* of the algebra, which are antisymmetric in a, b and related by $Z^{ab} = (\bar{Z}^\dagger)_{ab}$. This algebra is invariant under a global rotation of the supercharges $Q^a_\alpha \to R^a_b Q^b_\alpha, \bar{Q}_{a\dot{\alpha}} \to \bar{Q}_{b\dot{\alpha}}(R^\dagger)^b_a$, with[4] $R \in SU(4)$, which is called R-symmetry. What we have just constructed is the "super Poincaré algebra", Q^a being the superpartners to P_μ. To fully flesh out the algebraic structure of $\mathcal{N} = 4$ SYM we also include the supercharges S^a_α and $\bar{S}^a_{\dot{\alpha}}$ as superpartners to the special conformal generators K_μ, but at this point the reader should be tired of commutators, so best leave this section of the algebra to textbooks [11, appendix B]. In total we end up with the algebra[5] $\mathfrak{psu}(2,2|4)$, generating the symmetry group $PSU(2,2|4)$. Irreducible representations can be classified with a set of charges: $(\Delta, S_1, S_2, J_1, J_2, J_3)$. Δ is the scaling dimension, more on this in section 3.1.3. (S_1, S_2) are the Lorentz charges for the $SO(3,1) \sim SU(2) \times SU(2)$ subgroup of $PSU(2,2|4)$. Finally the J_i's are charges associated with R-symmetry. Since super symmetry generates transformations between these representations, namely (S_1, S_2), they carry no charge of their own.

3.1.2 Field Contents

$\mathcal{N} = 4$ SYM theory is a gauge theory, in line with all other Yang-Mills theories. For now we will let the gauge group be $SU(N_c)$, meaning that we have a gauge field $A_\mu = \sigma^\mu_{\alpha\dot{\alpha}} A^{\alpha\dot{\alpha}}$ with N_c colors. From the supercharges it's possible to construct raising and lowering operators in helicity to construct the other fields from super symmetry transformations. From this process we get eight fermions, four chiral ψ^a_α and four anti-chiral $\bar{\psi}_{\dot{\alpha}a}$ with $a = 1, 2, 3, 4$, as well as three complex scalar fields ϕ_i and their conjugates $\phi^\dagger_i, i = 1, 2, 3$, all transforming in the adjoint representation of $SU(N_c)$. The action is

$$\begin{aligned} S = \int \mathrm{d}^4x \mathrm{Tr}\Big[&-\frac{1}{4}F^{\mu\nu}F_{\mu\nu} - (D_\mu\phi^\dagger_i)(D_\mu\phi_i) + i\bar{\psi}^{a\dot{\alpha}}D^\alpha_{\dot{\alpha}}\psi_{a\alpha} \\ &+\frac{g_{\mathrm{YM}}}{\sqrt{2}}(i\epsilon^{ijk}\psi^\alpha_i[\phi_j, \psi_{\alpha k}] + 2i\bar{\psi}^i_{\dot{\alpha}}[\phi_i, \bar{\psi}^{4\dot{\alpha}}] + \mathrm{h.c.}) \\ &+\frac{g^2_{\mathrm{YM}}}{\sqrt{2}}(2[\phi^{i\dagger}, \phi^{j\dagger}][\phi_i, \phi_j] - [\phi^{i\dagger}, \phi_i][\phi^{j\dagger}, \phi_j])\Big] . \end{aligned} \tag{3.10}$$

Since all fields are matrix valued the trace is over the gauge group index. We here leave implicit for any field that $\Phi(x) = \Phi(x)^m T_m$ with T_m being the generators of $SU(N)$. Note that this could be defined equivalently with six real scalars ϕ_I, a convention we will use when convenient.

[3] $\bar{\sigma}^{\mu\nu}$ can be found similarly by replacing $\sigma^\mu \leftrightarrow \bar{\sigma}^\mu$ and permuting the indices appropriately, summing over the un-dotted rather than the dotted.

[4] For general $\mathcal{N}$ we have $R \in U(\mathcal{N})$, but for $\mathcal{N} = 4$ SYM this is the structure.

[5] Read as "p s u two two grade four" or "p s u two comma two slash four".

3.1.3 Spin Chains and the Dilatation Operator

In the study of CFT's "the spectral problem" refers to solving the spectrum of the dilatation operator $\mathcal{D}$, which generates the scalings of conformal transformations. In general we say that an operator $\mathcal{O}(x)$ has scaling dimension Δ when the transformation $x \to \lambda x$ transforms the operator as $\lambda^{-\Delta}\mathcal{O}(\lambda x)$ where Δ is an eigenvalue of $\mathcal{D}$. In the case of gauge invariant operators which can represent observables in the theory, it is useful to first study gauge covariant operators, i.e. operators transforming like

$$\chi(x) \to \chi(x) + [\epsilon(x), \chi(x)] \,, \tag{3.11}$$

with $\epsilon(x)$ generating the gauge transformation. The gauge covariant fields are the scalars, fermions and field strength $F_{\mu\nu}$ as well as covariant derivatives hereof.[6] From this definition we can construct local gauge invariant operators as traces

$$\mathcal{O}(x) = \mathrm{Tr}[\chi_1(x)\chi_2(x)\dots\chi_L(x)] \,. \tag{3.12}$$

Trace operators and products of trace operators form a basis for all local gauge invariant operators which are the observables of the theory, meaning we can solve the spectral problem by only considering traces of gauge covariant operators. For large N_c the scaling dimension of the product of trace operators becomes the sum of the dimensions of the single trace operators, so in this limit we need only solve the spectrum of single trace operators. We can find the scaling dimension of a single such operator by investigating the two-point correlation function between itself and its conjugate

$$\left\langle \mathcal{O}(x)\bar{\mathcal{O}}(y) \right\rangle \propto \frac{1}{|x-y|^{\Delta}} \,. \tag{3.13}$$

The dilatation operator commutes with the generators of $SU(4)$ R-symmetry, meaning its action is closed under operators with equal R-charges. To this end we define the scalar fields $\varphi_n = {}^1\!/\!_{\sqrt{2}}(\phi^{2n+1} + i\phi^{2n+2})$, with $\varphi_0 = Z, \varphi_1 = W, \varphi_2 = X$. These have charges $(1,0,0,1,0,0)$,$(1,0,0,0,1,0)$ and $(1,0,0,0,0,1)$ respectively. Charges of single trace operators can be found as a sum of their component fields, so an operator $\mathcal{O}(x) \propto \mathrm{Tr}[ZWWZ\dots]$ with $L-M$ Z's and M W's will have charge $(L,0,0,L-M,M,0)$ and transform in a closed sector of equal charges under scaling, which from now on will be referred to as an (L,M) sector. This specific sector of operators built form traces of Z's and W's is often referred to as the $SU(2)$ sector, as (Z,W) transform as an $SU(2)$ duplet under R-symmetry.

Investigating only operators within such (L,M) sectors, we can restrict the action of $\mathcal{D}$ heavily to a sum of possible exchanges of Z,W. We can draw these

[6] There are some combinations of derivatives that may be replaced by non-derivative terms, for example any contraction $D^\mu D_\mu \phi_i$ can be replaced from the equations of motion for the scalar fields. More details in [34, section 4]

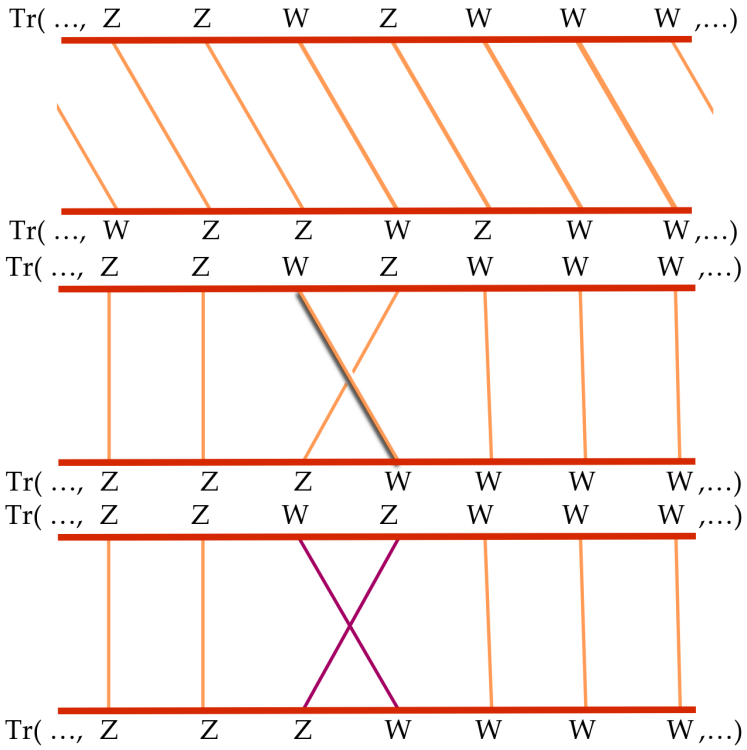

Figure 3.1: Examples of diagrams that appear in the computation of eq. (3.13). **Top**: A tree level planar diagram. **Middle**: A tree level diagram with crossing. **Bottom**: A planar one loop diagram.

exchanges as diagrams, as in fig. 3.1. When taking the limit $N_c \to \infty$ for the rank of the gauge group $SU(N_c)$, diagrams with crossing lines are suppressed as $1/N_c^2$, meaning that planar diagrams will dominate. This limit is therefore called the planar limit, as we need only consider diagrams that can be drawn on a plane (crossing lines need at least a torus). More specifically we also take $g_{\text{YM}} \to 0$ in such a way that $g_{\text{YM}}^2 N_c$ stays fixed. This limit was originally introduced by Gerard 't Hooft [38], which is why it is also referred to as the *'t Hooft limit*. This means that at tree level we can only have interactions that leave the operator invariant or move all fields a single space in the same direction, but since traces are cyclic, all operators in the (L, M) sector are invariant under such interactions. At one-loop order we can add a vertex factor, allowing for exchanges of neighboring fields without crossings - a so called Nearest Neighbor (NN) interaction. For every loop order we go up, we can introduce longer range interactions, so Next-Nearest Neighbor (NNN) at two-loop, NNNN at three-loop and so on.

Evaluating these types of interactions allows us to calculate the anomalous correction γ to the scaling dimension $\Delta = \Delta_0 + \gamma$, where the bare dimension Δ_0 can be found from counting the component fields. Explicitly the anomalous

part of $\mathcal{D}$ can be found as

$$\delta\mathcal{D}^{(\text{one loop})}_{SU(2)} = \frac{\lambda}{16\pi^2}\sum_{l=1}^{L}(1 - 2P_{l,l+1}) \ , \tag{3.14}$$

at first loop order in the $SU(2)$ sector. $P_{l,l+1}$ is the exchange operator, exchanging the fields on sites l and $l+1$. $\lambda = g^2_{\text{YM}}N_c$ is called the 't Hooft coupling. Identifying Z with spin-up ($\uparrow$) and W with spin-down ($\downarrow$) we can imagine these single trace operators as closed chains of spin-½ particles on L sites with M magnons (letting $|\uparrow\uparrow\uparrow\ldots\uparrow\rangle$ be the ground state). We can the rewrite the anomalous dimension operator in terms of spin operators $\vec{S}_i$ acting on cites i and one finds [34]

$$\delta\mathcal{D}^{(\text{one loop})}_{SU(2)} = \frac{\lambda}{16\pi^2}\sum_{l=1}^{L}\left(1 - 2\vec{S}_l \cdot \vec{S}_{l+1}\right) \ , \tag{3.15}$$

which is the Hamiltonian for the Heisenberg XXX spin chain. Remarkably, this is one of the oldest examples of integrable quantum systems studied, originally solved by Hans Bethe [33]. The action of the dilatation operator then becomes propagating the magnons around the chain. More information on this system can be found in section 3.3.

We can solve for the eigenvalues of $\delta\mathcal{D}^{(\text{one loop})}_{SU(2)}$ using the method presented in [34, section 8]. In sectors where $M = 1$, we can find the eigenstates as states of definite momentum,

$$|p\rangle = \frac{1}{\sqrt{L}}\sum_{l=1}^{L} e^{ipl}\,|l\rangle \ , \tag{3.16}$$

where $|l\rangle$ denotes a state with a magnon on site l. The associated eigenenergies are

$$E(p) = \frac{\lambda}{2\pi^2}\sin^2\frac{p}{2} \, . \tag{3.17}$$

Jumping to arbitrary M it becomes useful to introduce rapidities u_i for each magnon, where

$$e^{ip_i} = \frac{u_i + i/2}{u_i - i/2} \, . \tag{3.18}$$

The energy associated with each rapidity becomes

$$E(u) = \frac{\lambda}{8\pi^2}\frac{1}{u^2 + \frac{1}{4}} \, . \tag{3.19}$$

Exchanging two magnons on the chain can be likened to a scattering, meaning we can construct an S-matrix to describe them. Exchanging two magnons will result in a phase factor

$$S_{ij} = \frac{u_i - u_j - i}{u_i - u_j + i} \, . \tag{3.20}$$

Since the chain is closed, shifting a single magnon from site l to $l + L$ should leave the chain invariant, meaning that

$$e^{ipl} = e^{ip(l+L)} \Rightarrow (e^{ip})^L = 1\,, \tag{3.21}$$

if $M = 1$. When $M > 1$ then $(e^{ip})^L$ should equal the phase factors picked up from scattering the other magnons along the chain. Using this we can impose a condition on the rapidities,

$$\left(\frac{u_j + i/2}{u_j - i/2}\right)^L = \prod_{k\neq j}^{M} \frac{u_j - u_k - i}{u_j - u_k - i}\,. \tag{3.22}$$

We may also impose that we are dealing with single trace operators, meaning that we actually have invariance under a global $l_i \to l_i + 1$ for all magnons. We now make the ansatz that a general M-magnon eigenstate can be written as

$$\begin{aligned} |p_1, p_2, \ldots, p_M\rangle = &\sum_{l_1<l_{k\neq 1}} e^{i\sum_{j=1}^{M} p_j l_j}\, |l_1 l_2 \ldots l_M\rangle \\ &+\text{permutations assuming other orderings of } l_k\text{'s}\,, \end{aligned} \tag{3.23}$$

this requires that the common phase factor $\exp\left(i\sum_{j=1}^{M} p_j l_j\right)$ have the property that

$$\begin{aligned} &\exp\left(i\sum_{j=1}^{M} p_j l_j\right) = \exp\left(i\sum_{j=1}^{M} p_j (l_j + 1)\right) \\ \Rightarrow &\exp\left(i\sum_{j=1}^{M} p_j l_j\right) = \exp\left(i\sum_{j=1}^{M} p_j\right)\exp\left(i\sum_{j=1}^{M} p_j l_j\right) \\ \Rightarrow &\exp\left(i\sum_{j=1}^{M} p_j\right) = 1 \Rightarrow \sum_{j=1}^{M} p_j = 0 \mod 2\pi\,. \end{aligned} \tag{3.24}$$

We can impose this on the rapidities as

$$\exp\left(i\sum_{j=1}^{M} p_j\right) = \prod_{j=1}^{M} \frac{u_j + i/2}{u_j - i/2} = 1\,. \tag{3.25}$$

Solving eqs. (3.22) and (3.25) for the rapidities u_j, we can get the total anomalous dimension as

$$\gamma^{(\text{one loop})} = \sum_{j=1}^{M} E(u_j)\,. \tag{3.26}$$

Having explicitely computed the anomalous dimension, we know the spectral problem of $\mathcal{N} = 4$ SYM to be integrable at first loop order in the planar

limit of the $SU(2)$ sector, which was some of the first evidence collected to support the conjectured integrability of $\mathcal{N} = 4$ SYM at large. This method of diagonalizing the XXX (and other spin chain Hamiltonians) is known as the Coordinate Bethe Ansatz (CBA), with eqs. (3.22) and (3.25) being referred to as the "Bethe equations" for $\delta\mathcal{D}^{(\text{one loop})}_{SU(2)}$. There are different Bethe ansatz methods, but these will not be explored in this work. In this thesis we will only work with the anomalous part of the dilatation operator, hence every time the dilatation operator is mentioned we refer to the anomalous part – as such we will use "anomalous dilatation operator" and "dilatation operator" interchangeably.

3.2 γ_i-Twisted $\mathcal{N} = 4$ SYM

Having studied the historical origins of spin chains in $\mathcal{N} = 4$ SYM, we now turn to investigate how integrability is affected when deforming the action in different ways. In order to study the properties of theories with smaller degrees of supersymmetry, deformations of $\mathcal{N} = 4$ SYM [39, 40] were developed. Originally to study gravity duals in AdS/CFT, these deformations have also proved themselves to be of use in the context of integrability, especially in the spectral problem [7, 8, 41].

Specifically we will look at γ_i-twisted $\mathcal{N} = 4$ SYM where twisting parameters $q_i = e^{-\frac{i}{2}\gamma_i}$ are introduced. The Lagrangian for this theory (in the formalism presented in [42, appendix A]) is given as

$$\mathcal{L} = N \operatorname{Tr}\left[-\frac{1}{4}F_{\mu\nu}F^{\mu\nu} - \frac{1}{2}D^\mu\phi_i^\dagger D_\mu\phi^i + i\bar{\psi}_a^{\dot{\alpha}} D_{\dot{\alpha}}^\alpha \psi_\alpha^a\right] + \mathcal{L}_{\text{int}}\,. \tag{3.27}$$

The interaction part of the Lagrangian, in which the twisting is implemented reads

$$\begin{aligned}\mathcal{L}_{\text{int}} =& N g_{\text{YM}} \operatorname{Tr}\left[\frac{g_{\text{YM}}}{4}\{\phi_i^\dagger,\phi^i\}\{\phi_j^\dagger,\phi^j\} - g_{\text{YM}} e^{-i\epsilon^{ijk}\gamma_k}\phi_i^\dagger\phi_j^\dagger\phi^i\phi^j\right.\\ &- e^{-\frac{i}{2}\gamma_j^-}\bar{\psi}_j\phi^j\bar{\psi}_4 + e^{\frac{i}{2}\gamma_j^-}\bar{\psi}_4\phi^j\bar{\psi}_j + i\epsilon_{ijk}e^{\frac{i}{2}\epsilon_{jkm}\gamma_m^+}\psi^k\phi^i\psi^j\\ &\left.- e^{\frac{i}{2}\gamma_j^-}\psi^4\phi_j^\dagger\psi^j + e^{-\frac{i}{2}\gamma_j^-}\psi^j\phi_j^\dagger\psi^4 + i\epsilon^{ijk}e^{\frac{i}{2}\epsilon_{jkm}\gamma_m^+}\bar{\psi}_k\phi_i^\dagger\bar{\psi}_j\right].\end{aligned} \tag{3.28}$$

Here we use the shorthand $\gamma_1^\pm = {}^{\gamma_2\pm\gamma_3}/_2$ with $\gamma_2^\pm, \gamma_3^\pm$ from cyclic permutations of the indices. Limits of this theory are especially interesting. In the 't Hooft limit the gauge fields decouple, massively simplifying the dynamics of the theory. Combining this with letting the twisting parameters $\gamma_i \to \pm i\infty$ ($q_i \to \infty, 0$) leads to eight different strong twisting limits. We classify these limits by the sign of the limit for each γ_i, so $(+,+,+)$ would mean $\gamma_i \to +i\infty, \forall i$ and $(+,+,-)$ would mean $\gamma_{1,2} \to +i\infty$ and $\gamma_3 \to -i\infty$. In practice we introduce a parameter $\epsilon \to 0$ and let $g_{\text{YM}} \to \epsilon g_{\text{YM}}$ and $q_i = \epsilon^{\mp 1}\xi_i^\pm$. In the $(+)$ twisting

limits, we take $g_{\text{YM}} q_i = \xi_i^+ = \text{constant}$ and $q_i / g_{\text{YM}} = \xi_i^- = \text{constant}$ in the $(-)$ limits.

An important thing to notice is that in the case of large imaginary γ_i, the theory is no longer unitary. Non-unitary quantum mechanics might seem like and unphysical consideration, but it is actually a common study in the context of open quantum systems and statistical mechanics, see [26, 30] for discussions. However since our goal is a better understanding of integrability – which is not a physical observable, but rather a mathematical property – we may think of it as a toy model.[7]

The $(+,+,+)$ case has been studied most historically. The case wherein[8] $\xi_1 = \xi_2 = \xi_3$ has historically been called *strongly β-twisted* (sβt), defining $\xi_i = \beta$. The case where $\xi_1 = \xi_2 = 0$ and $\xi_3 = \xi$ is called *Fishnet theory* (FN) after the look of the resulting Feynman diagrams.

3.2.1 Fishnet Theory

Taking the $(+,+,+)$ limit and letting $\xi_1 = \xi_2 = 0, \xi_3 = \xi$ we get Fishnet theory, in which most fields decouple and we are left with a ϕ^4 Lagrangian [43, section 2.2.3]

$$\mathcal{L} = \frac{N}{2} \operatorname{Tr}\Big[-\partial^\mu \phi_1^\dagger \partial_\mu \phi_1 + \partial^\mu \phi_2^\dagger \partial_\mu \phi_2 + 2\xi^2 \phi_1^\dagger \phi_2^\dagger \phi_1 \phi_2 \Big] . \tag{3.29}$$

Since the only interaction term we have in this theory is a four-point vertex, all possible planar Feynman diagrams have a fishnet-like structure, hence the name, see fig. 3.2 for an example.

Since so many fields decouple or vanish in this theory, parts of the internal R-symmetry are broken. Specifically we go from $SU(4)$ to $U(1)^2$, corresponding to replacing $\phi_i \to e^{i\theta} \phi_i$, i.e. a single global $U(1)$ symmetry for each of the fields. Furthermore the theory is invariant under the discrete internal symmetries that are products of the replacements $\phi_{1,2} \to \phi_{2,1}^T, \phi_1 \to \phi_2^\dagger, \phi_2 \to \phi_1$, which is the group of discrete symmetries of a square, D_4. Thus we have a total internal symmetry of $D_4 \ltimes U(1)^2$ for Fishnet theory.[9]

Like the case of un-twisted $\mathcal{N} = 4$ theory, the Fishnet dilatation operator has closed sectors of the scalar fields ϕ_1, ϕ_2 or their conjugates, meaning that we can once again translate local gauge invariant operators to $SU(2)$ spin chains in closed (L, M) sectors. This is sometimes referred to as the "broken $SU(2)$" sector, referring to the fact that we are studying a sector of the broken $SU(4)$ R-symmetry. We do however run into issues with Fishnet theory as it is not fully conformal. In [44] it is shown that Fishnet theory contains

[7] $\mathcal{N} = 4$ SYM is already an extremely simple toy model.

[8] Since we are dealing with the $(+,+,+)$ case, the signs on the ξ's are suppressed.

[9] The symbol $\cdot \ltimes \cdot$ signifies a *semidirect product*. The action is that of a direct product, but it also denotes that the group on the left side is a normal subgroup of the total product group, and that all unique compositions of elements from D_4 and $U(1)^2$ correspond to a unique element in the total internal symmetry group.

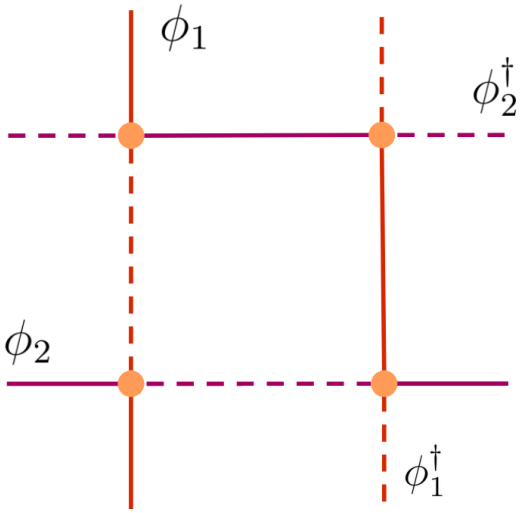

Figure 3.2: A Feynman diagram in Fishnet theory. All possible diagrams are built from the same four-point vertex shown here four times, hence why all diagrams look like fishing nets.

double trace operators with non-vanishing β-functions,[10] breaking conformal symmetry. Conformality can be reinstated by introducing counter terms to the Lagrangian, which would affect computation of the dilatation operator. These counter terms only impact gauge invariant operators of length 2, however the focus of this work is spectral statistics and due to the cyclicity of trace operators $(2, M)$ sectors are at most one-dimensional and thus cannot be analysed in this framework. We therefore only consider sectors of $L \geq 3$ (and in practice $L \geq 10$).

All possible operators on closed spin chains of fixed length and magnon number can be expressed as sums of operators of the form

$$\chi(\dots, a, b, c, \dots) = \sum_{i=1}^{L} \dots \sigma_{i+1}^{+} \sigma_{i+1+a}^{-} \sigma_{i+1}^{+} \sigma_{i+1+b}^{-} \sigma_{i+1}^{+} \sigma_{i+1+c}^{-} \dots \,, \tag{3.30}$$

which swap spins that are *chirally ordered* with different interaction lengths, meaning operations of the type $|\dots\downarrow\dots\uparrow\dots\rangle \to |\dots\uparrow\dots\downarrow\dots\rangle$. This can be seen from the fact that $\sigma_i^{\pm}$ are the usual Pauli raising and lowering operators for spin-$1/2$ particles. Note that operators which swap spins in the other direction (anti-chirally) can also be constructed using operators of the type $\chi(L+a-1)$ since the chains are closed. The anomalous part of the dilatation operator for Fishnet theory in the planar limit is found to be [42, section 5.1]

$$\delta\mathcal{D}_{\text{Fishnet}} = -2(\xi^2\chi(1) + \xi^4(\chi(1,2) + \chi(2,1))) + \mathcal{O}(\xi^6) \,, \tag{3.31}$$

up to second loop order. The factor -2 comes from the subtraction scheme, where we here follow the convention of [42]. Writing this out and truncating

[10] "Double trace" referring to the amount of traces, not their length, e.g. operators of the type $\mathrm{Tr}[\chi_i \dots \chi_j]\,\mathrm{Tr}[\chi_l \dots \chi_m]$

at first and second order we get the operators

$$\delta\mathcal{D}^{(\text{one loop})}_{\text{Fishnet}} = -2\xi^2 \sum_{i=1}^{L} \sigma_i^+ \sigma_{i+1}^- \,, \tag{3.32}$$

$$\delta\mathcal{D}^{(\text{two loop})}_{\text{Fishnet}} = -2\xi^2 \sum_{i=1}^{L} \left(\sigma_i^+ \sigma_{i+1}^- + \xi^2 \left[\sigma_i^+ \sigma_{i+2}^- + \sigma_{i+2}^+ \sigma_i^-\right]\right) \,, \tag{3.33}$$

the spectra of which are studied extensively in section 4.1. The one loop operator can be diagonalized using CBA, which is done in detail in [43, section 3.2]. Here we present the resulting Bethe equations:

$$\prod_{i=1}^{M} \alpha_i = 1 \,, \tag{3.34}$$

$$(\alpha_i)^L = (-1)^{M-1} \,, \tag{3.35}$$

$$E = -2 \sum_{i=1}^{M} \frac{1}{\alpha_i} \,. \tag{3.36}$$

The $\alpha_k = e^{ip_k}$'s play a role similar to the rapidities u_j introduced in eq. (3.18) used to simplify the Bethe equations for the XXZ spin chain. From here on the α_k's will be referred to as *Bethe roots*. Having diagonalized $\delta\mathcal{D}^{(\text{one loop})}_{\text{Fishnet}}$ using Bethe ansatz methods, we know it to be integrable. It is actually possible to show that Fishnet theory in general is integrable at all loop orders [20] in the 't Hooft limit, however when considering truncated orders this is not always true. In section 4.1 we provide evidence that while $\delta\mathcal{D}^{(\text{one loop})}_{\text{Fishnet}}$ is integrable, $\delta\mathcal{D}^{(\text{two loop})}_{\text{Fishnet}}$ has chaotic behavior in its spectrum. It is important to note here that since $\delta\mathcal{D}^{(\text{one loop})}_{\text{Fishnet}}$ is not unitary, we were not guaranteed diagonlisability. In this work we will only deal with diagonalisable operators, but an insight into some non-diagonalisable sectors of general strong γ_i-twisted theories can be found in [22].

3.2.2 The Non-Eclectic $SU(3)$ Sector

Going beyond just two scalars the anomalous dilatation operator for strongly twisted planar $\mathcal{N}=4$ SYM retains its spin chain interpretation, albeit with chains that have more than two possible spin states on each site. In the full theory we consider all operators acting on $SU(4) \cong SO(6)$ spin chains with some NN interaction terms. Here we consider a subsector with three scalars, so instead of labelling our sites with $\uparrow$ or $\downarrow$, we simply use $1, 2, 3$ – 1 denoting vacuum and $2, 3$ being the possible excitations – we'll call this the $SU(3)$ sector. We can model the twisted dilation operator at one loop order as [22, section 1]

$$\delta\mathcal{D}_{SU(3)} = \sum_{i=1}^{L} \tilde{P}^{(q_1,q_2,q_3)}_{i,i+1} \,, \tag{3.37}$$

where the "one loop" superscript is suppressed, as higher loop orders will not be considered for this sector. Here $\tilde{P}_{i,i+1}^{(q_1,q_2,q_3)}$ swaps the state on site i with the state on site $i+1$ and multiplies with a factor $q_j^{\pm 1}$ depending on which states are swapped and in what order. For example $\tilde{P}^{(q_1,q_2,q_3)}\,|23\rangle = {}^1\!/_{q_1}\,|32\rangle$ and $\tilde{P}^{(q_1,q_2,q_3)}\,|23\rangle = q_1\,|32\rangle$. Full detail on the action of this operator is given in [22], but the actions relevant to this thesis are shown in eq. (3.39).

Since we only permute spin states, we can analyse this operator in closed sectors (L, M, K) with L being the length of the chains, M being the total amount of excitations and K being the number of excitations of a specific type. Here we choose $|11\ldots11\rangle$ to be the ground state and K to be the number of 3's, i.e. the state $|1123\rangle$ is in the $(4, 2, 1)$ sector. By definition we have $L \geq M \geq K$. Using $q_i = e^{-i\gamma_i/2}$ we can apply the strong twisting limits to the dilatation operator. In the $(-)$ limits $\tilde{P}^{q_1,q_2,q_3}$ is dominated by the terms with a factor q_i, in effect annihilating all other permutations – and vice versa for the $(+)$ limits and terms with a factor q_i^{-1}. In the $(+,+,+)$ limit the $\delta\mathcal{D}_{SU(3)}$ can be shown to be nilpotent, which means that there exists some n for which $(\delta\mathcal{D}_{SU(3)}^{(+,+,+)})^n = 0$, and non-diagonalisable [41, section 2.3] with vanishing generalized eigenvalues. These sectors are called *eclectic* and are studied extensively in [22], however since our analysis focuses on spectral statistics, vanishing eigenvalues are not ideal. Note that the $(+,+,+)$ limit is equal to the $(-,-,-)$ limit up to parity and relabeling, so this limit is also not ideal. For this reason the work done in this thesis focuses on the $(+,+,-)$ limit, which is diagonalisable in the $SU(3)$ sector – we'll refer to this as the *non-eclectic $SU(3)$ sector*. Note that by appropriate relabeling this limit is equivalent to $(+,-,+), (-,+,+), (-,-,+), (-,+,-)$ and $(+,-,-)$. Using the notation introduced in section 3.2 we get

$$\delta\mathcal{D}_{SU(3)}^{(+,+,-)} = \sum_{i=1}^{L} \tilde{P}_{i,i+1}^{(+,+,-)}\,, \tag{3.38}$$

where the action of $\tilde{P}_{i,i+1}^{(+,+,-)}$ is

$$\begin{gathered}\tilde{P}_{i,i+1}^{(+,+,-)}\,|21\rangle = \xi_3\,|12\rangle\,, \quad \tilde{P}_{i,i+1}^{(+,+,-)}\,|32\rangle = \xi_1\,|23\rangle\,, \\ \tilde{P}_{i,i+1}^{(+,+,-)}\,|31\rangle = \xi_2^{-1}\,|13\rangle\ ,\end{gathered} \tag{3.39}$$

annihilating all other spin state orderings. The twisting deformation is known to be integrability preserving. How this is reflected in the spectral statistics of this operator is studied in section 4.2.

3.3 The XXZ Spin Chain

Having seen multiple ways in which spin chains arise in the study of planar $\mathcal{N} = 4$ SYM, it is worthwhile to spend some time studying the XXZ spin chain

on its own, especially in the context of spectral integrability. The Hamiltonian for this system is

$$H_{\mathrm{XXZ}} = \sum_{i=1}^{L} \left(S_i^- S_{i+1}^+ + S_i^+ S_{i+1}^- + \Delta S_i^z S_{i+1}^z \right) + E_0 \mathbb{I} \,. \tag{3.40}$$

$S_i^{\pm,z}$ are the usual spin operators acting on site i in units of $\hbar = 1$. When working with this and other spin chain Hamiltonians, we introduce the site-basis, written as $|\uparrow\downarrow \ldots \uparrow\rangle$, indicating the direction of spin at each site in the chain, where the site $L+1$ is identified with the site 1. This basis is in principle infinite dimensional, but can be restricted to sectors (L, M) of finite size.

$$|(L, M)| = \binom{L}{M} \,, \tag{3.41}$$

where L indicates the length of the chain, i.e. the number of sites, and M is the magnon number. E_0 is an energy off-set, but since we're mainly interested in energy spacings and not the energies themselves, we take $E_0 = 0$ unless otherwise specified. The name "XXZ" comes from the parameter Δ which indicates that the coupling to the z-axis is different from the coupling to the x and y-axies.

A more general Hamiltonian with different couplings in all directions, $H = \sum_i^L J_a S_i^a S_{i+1}^a, a = x, y, z$, is called an XYZ chain. If we set $\Delta = 1$ we get the XXX chain model. We now briefly review the symmetries of the XXZ spin chain.

- **Spin rotation**: The Hamiltonian commutes with $S_i^z, \forall i$, meaning that we can label eigenstates with a quantum number M for the operator $S^z_{\mathrm{Total}} = \sum_{i=1}^L S_i^z$, which measures the total spin along the z-axis. M corresponds to either the number of up-spins or down-spins in the site basis, depending on convention, but we will see later that this is equivalent. In the XXX case ($\Delta = 1$) we have full $SU(2)$ symmetry, as H_{XXX} commutes with $S_i^{x,y,z} \forall i$ which generate an $\mathfrak{su}(2)$ algebra. In the more general XXZ case this breaks down to a $U(1)$ symmetry. Notice that since M is a quantum number for the site basis, H_{XXZ} does not mix sites with different numbers of magnons. It also does not mix states of different length L, meaning that the Hamiltonian is closed under sectors of equal L and M. Physically this symmetry corresponds to rotating all spins in the chain by the same angle around the z-axis.

- **Translation**: In this thesis we exclusively investigate closed spin chains, meaning that we identify the site $L+1$ with 1, applying periodic boundary conditions. With this identification H_{XXZ} is left invariant by any global translation of sites $i \to i + L$, which can be achieved by applying $i \to i + 1$ L times. This means that we can label each magnon with a definite momentum p_j but, as discussed previously with eq. (3.25), the

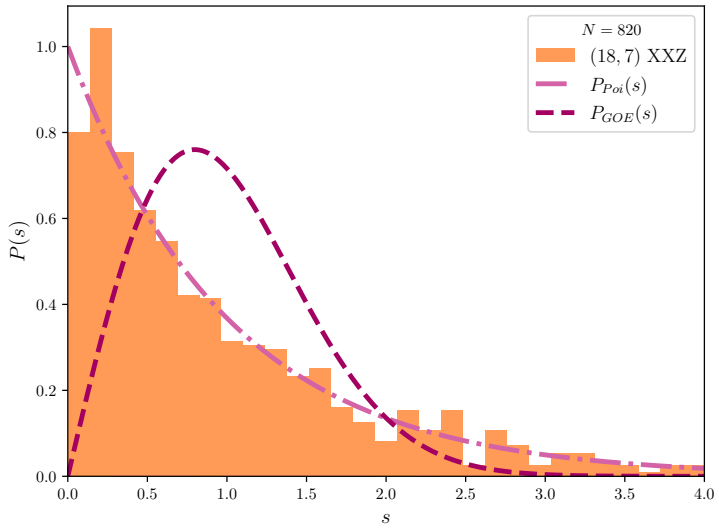

Figure 3.3: Level spacing distribution in the $(18, 7)$ sector of H_{XXZ} with $\Delta = 1$.

total momentum must be $P = \sum_{i=1}^{M} p_i = 0$. In the Hamiltonian itself, this corresponds to reordering the terms of the sum.

- **Parity**: Also called reflection symmetry, H_{XXZ} is left invariant under reversing the order of spins in the site basis, e.g. $|\downarrow\downarrow\uparrow\downarrow\uparrow\uparrow\uparrow\rangle \to |\uparrow\uparrow\uparrow\downarrow\uparrow\downarrow\downarrow\rangle$. Note that this can not generally be achieved by global translations. This corresponds to replacing the terms $S_i^{\pm} S_{i+1}^{\mp} \to S_i^{\mp} S_{i+1}^{\pm}$, which again reorders the terms of the Hamiltonian.

- **Spin flip**: By flipping all spins in a chain, we switch between sectors (L, M) and $(L, L - M)$. These have the same size, as can be seen from eq. (3.41). In H_{XXZ} we achieve this by replacing $S_i^{\pm} \to S_i^{\mp}$ and $S_i^z \to -S_i^z$, leaving the Hamiltonian invariant. For a given L only the $(L, L/2)$ sector is closed under such transformations, but more generally this means that the energies in the (L, M) and $(L, L - M)$ sectors are equal, meaning that we only have to investigate one of them.

We now briefly review and reproduce some of the results for the level statistics of the XXZ spin chain found in [45, chapter 4], which contains a more in-depth analysis.

3.3.1 Deformations and Integrability Breaking

The XXZ spin chain can be solved using the Bethe Ansatz, making it integrable. This integrability is reflected in the level statistics which follow a Poissonian distribution, as seen in fig. 3.3. We can break this integrability by adding new terms to the Hamiltonian that introduce a chaotic signature in the level spacings.

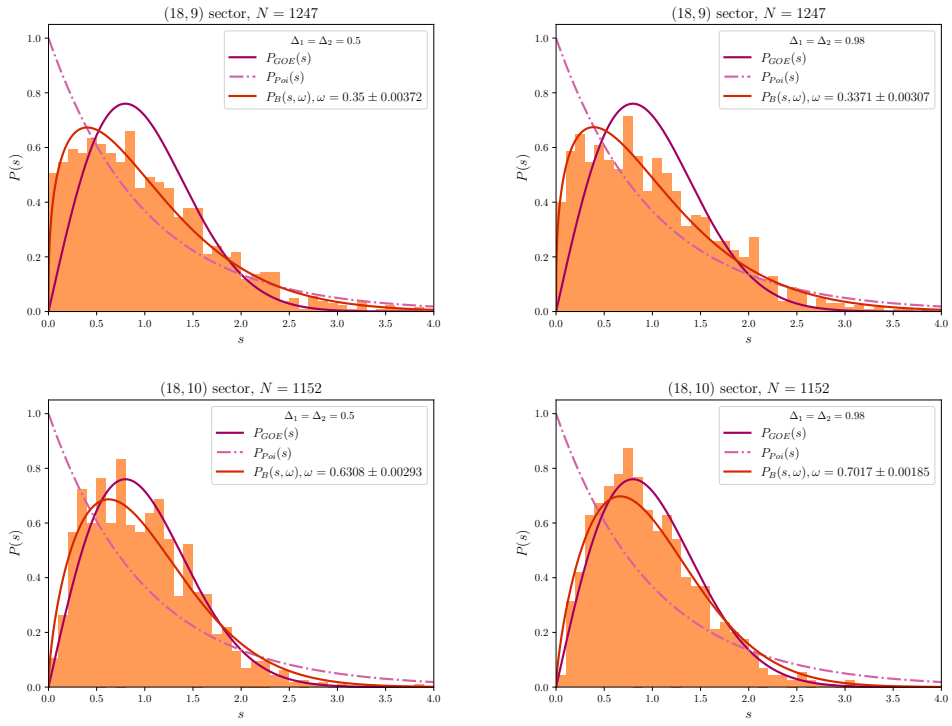

Figure 3.4: Level spacing distributions for the $(18, 9)$ and $(18, 10)$ sectors of H_{NNN} with different values of Δ_1 and Δ_2. The distributions are fitted with $P_B(s, \omega)$ to quantify the transition between integrable and chaotic phases. For all calculations we set $J_2 = 1$.

3.3.1.1 NNN Coupling

Non-integrable behavior can appear if the spin chain has not only a NN coupling, but also a Next Nearest Neighbor (NNN) coupling,

$$\begin{aligned} H_{\text{NNN}} = J_1 \sum_{i=1}^{L} \left(S_i^- S_{i+1}^+ + S_i^+ S_{i+1}^- + \Delta_1 S_i^z S_{i+1}^z \right) \\ + J_2 \sum_{i=1}^{L} \left(S_i^- S_{i+2}^+ + S_i^+ S_{i+2}^- + \Delta_2 S_i^z S_{i+2}^z \right) + E_0 \mathbb{I} \,. \end{aligned} \tag{3.42}$$

Here we have four parameters, $(J_1, \Delta_1, J_2, \Delta_2)$, that we can tune in order to amplify or suppress different interactions in the chains. At different values of these parameters the system may be integrable or chaotic, but this is not an instant transition. We can parameterize this as a phase transition between an integrable and a chaotic phase using the Brody distribution, eq. (2.11). Figures 3.4 and 3.5 show level spacing distributions for different values of these parameters.

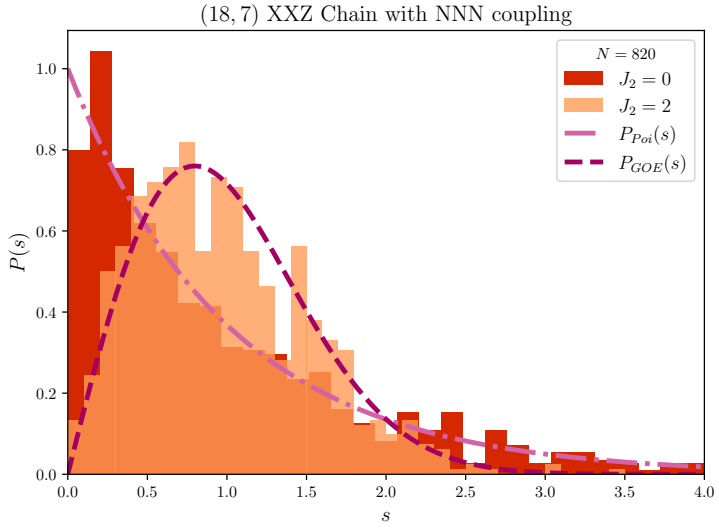

Figure 3.5: Level spacing distribution of the $(18, 7)$ sector of H_{NNN}. The two distributions correspond to different strengths of the NNN coupling strength J_2. For both distributions we set $\Delta_1 = \Delta_2 = 1$.

3.3.1.2 Random Magnetic Field

Another way to break the integrable structure of the XXZ Hamiltonian is to introduce a random magnetic field in the z direction on each site,

$$H_{\text{RND}} = \sum_{i=1}^{L} \left(S_i^- S_{i+1}^+ + S_i^+ S_{i+1}^- + \Delta_1 S_i^z S_{i+1}^z + h_i S_i^z \right) + E_0 \mathbb{I} \,. \tag{3.43}$$

We get the field strengths h_i from a Gaußian with zero mean and width h. Since in general $h_{i-1} \neq h_i \neq h_{i+1}$ symmetry under parity transformations is broken. The same argument can show that translational symmetry is also broken, since the magnetic field is in general different on all sites. Lastly spin flip transformation only preserve the energies in the case where $M = {}^{L}/_{2}$, meaning that only spin rotation symmetry is left. The chaotic level spacing distribution of an XXZ chain in such a field can be seen in fig. 3.6.

3.4 Desymmetrisation

Desymmetrisation is the process of splitting up the eigenstates of an operator into different closed sectors with respect to all symmetries of the operator. This is important, especially when studying level spacings as different closed sectors can by definition not be correlated and will therefore exhibit integrable behavior (or even degeneracies) when compared, regardless of the actual structure of the Hamiltonian. For an illustration of this see fig. 3.7.

For the XXZ Hamiltonian we first desymmetrise with respect spin rotation by only considering states within the same (L, M) sector. We then desym-

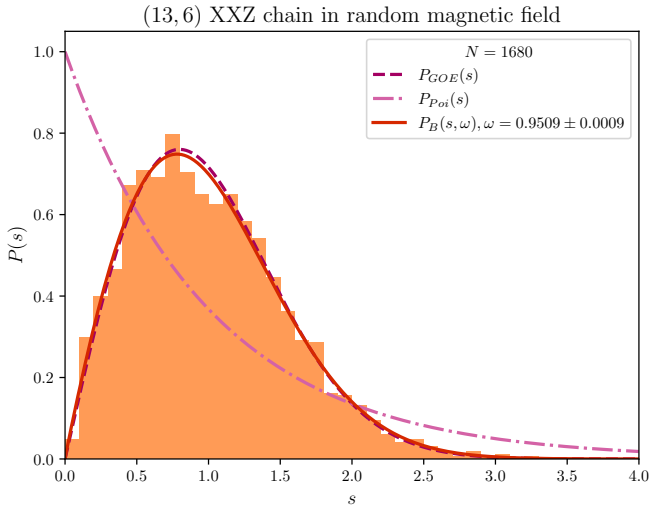

Figure 3.6: Level spacing distribution in the $(13, 6)$ sector of H_{RND} with $h = 1$. The level spacing distribution is fitted with the Brody distribution. Since we find ω close to 1, the spectrum is best described by GOE statistics which signifies chaos.

metrise with respect to translations by only considering states that can not be found as a translation of other states. In practice we choose our basis to be in *canonical order*, which is best explained by example. Take the state $|{\downarrow}{\uparrow}{\uparrow}{\downarrow}{\downarrow}\rangle$ and identify $\uparrow \to 1$ and $\downarrow \to 0$, so $|01100\rangle$. Reading this as a binary number we find the smallest possible number achievable by global translation of the spins, in this case $|00011\rangle$. All other states that are equal to this ordering up to translation are discarded. In the $(5, 2)$ sector there are two such orderings

$$|{\downarrow}{\downarrow}{\downarrow}{\uparrow}{\uparrow}\rangle \quad \text{and} \quad |{\downarrow}{\downarrow}{\uparrow}{\downarrow}{\uparrow}\rangle \ , \tag{3.44}$$

meaning this sector is two-dimensional after translation-desymmetrisation, compared to $\binom{5}{2} = 10$ dimensional before.

From these canonically ordered states we desymmetrise with respect to parity by constructing states of definite parity. This can be done for any state by simply considering

$$|\psi\rangle \to |\psi_\pm\rangle \propto |\psi\rangle \pm P\,|\psi\rangle \tag{3.45}$$

$$P\,|\psi_\pm\rangle = \pm\,|\psi_\pm\rangle \tag{3.46}$$

with P being the parity operator and $|\psi_\pm\rangle$ being appropriately normalized. We can now consider two sectors of either positive or negative parity, but in general the positive sector will be used as it is always larger than the negative sector (if $|\psi\rangle = P\,|\psi\rangle$ this state will only add to the positive sector).

We need only desymmetrise with respect to spin flipping in sectors where $M = L/2$, since otherwise this transformation is not closed under the desymmetrisation we've already performed. The desymmetrisation is performed in

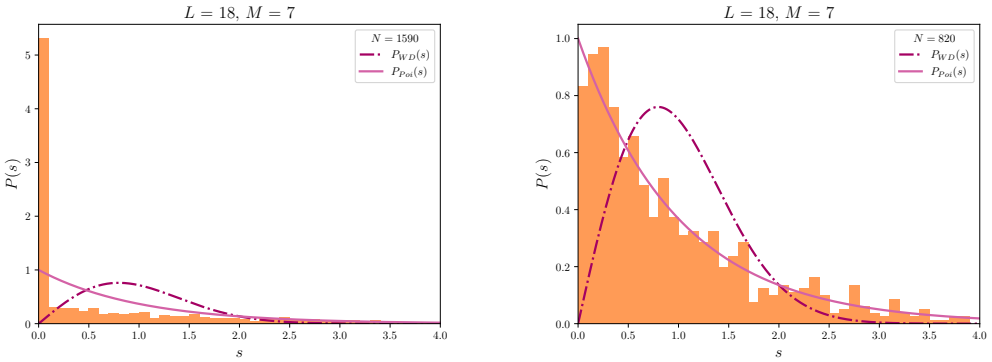

Figure 3.7: Level spacing distribution for the $(18, 7)$ sector of the XXZ spin chain (left) before and (right) after desymmetrising with respect to parity.

the same way as for the parity operator, but in general we will not consider this sector.

Chapter 4

Spectral Integrability Methods for Strongly Twisted $\mathcal{N} = 4$ Super Yang-Mills

Integrability can be difficult to prove. Even when $\mathcal{N} = 4$ SYM lends itself to a spin chain interpretation, the process of solving this spin chain with Bethe ansatz methods can be highly non-trivial, especially at all orders of the coupling constant. This is where the application of numerical measures of integrability comes into play, as they can provide evidence for integrability without the need for rigorous proofs. This needs however not be the case, as some integrable systems have extra structure in their spectra, causing their level spacings to deviate from the otherwise expected Poissonian distribution[1]. Analysing the spectrum of $\mathcal{N} = 4$ SYM in order to understand the integrable structure of the theory has in the past few years been a successful endeavor. In [7, 8] real level spacings are used to study how integrability is affected outside the planar limit of $\mathcal{N} = 4$ SYM, finding that for finite N the spectrum is chaotic, but that integrability is recovered as $N \to \infty$. The same is observed for the β-twisted theory, albeit only for $\beta \in \mathbb{R}$.

In this chapter Fishnet theory and the non-eclectic $SU(3)$ sector, which we found in the strong imaginary twisting limits of planar $\mathcal{N} = 4$ SYM, are studied using level spacings and level spacing ratios. This differs from previous work integrability in the spectral problem of strongly twisted $\mathcal{N} = 4$ SYM [7, 8] as the limits considered here are non-unitary, introducing the possibility of complex eigenvalues. This means our analysis must expand to that of open quantum systems, which we described in sections 2.2.1.2 and 2.2.2. In section 4.1 we analyse the spectrum of different (L, M) sectors of $\delta\mathcal{D}_{\text{Fishnet}}$ at first and second loop order. We consider the spectra themselves as well as their level spacing distributions and level spacing ratio distribution. The same analysis is preformed for $\delta\mathcal{D}_{SU(3)}$ at first loop order in section 4.2. Finally in

[1] A great example of this is the hydrogen atom. Not accounting for any pertubative effects like Zeeman splitting or spin-orbit coupling the spectrum is exactly solveable but does not exhibit Poissonian level spacings.

section 4.3 we discuss the findings of the previous sections as propose some reasons for the observed deviations and degeneracies.

4.1 Fishnet Theory

In this section we analyze the spectrum of the dilitation operator for Fishnet theory, given by eqs. (3.31) and (3.32). First we comment on the spectra themselves as they appear in the complex plane, where the spectrum of a given (L, M) sector appears in the shape of an M-pointed star at first loop order and how this structure is broken at second loop order. We comment on how the Bethe equations lead to this structure, and what effect this might have on the measures of integrability deployed.

We then analyze the level spacing rations of the operator, commenting on how the aforementioned structure appears both in the one loop and two-loop ratios. We then look at the level spacings for this theory and discover degeneracies for all considered chains of even L at one loop order, which disappear at two loop order. Degeneracies are also in some odd L sectors, but not by methods used in this section, see section 4.3 for more detail. However even in chains of odd L, we discover deviations from Poissonian structure in the one loop spacings. It is discussed whether the degeneracies are accidental or point to a hidden symmetry of the operators, and evidence pointing towards degeneracies arising from combinatorics of the Bethe equations is presented. All numerical evaluations are done with $\xi = 1$. It should be noted that whenever we refer to "two loop" or "second loop" order, we refer to the perturbative expansion of $\delta\mathcal{D}_{\text{Fishnet}}$ truncated at ξ^4.

4.1.1 Spectra

The spectrum is obtained by explicitly constructing a matrix representation of the one loop and two loop operators for a given sector (L, M) and diagonalizing it numerically (technical details in appendix A). The matrix for both the one loop and two loop operator is always real valued in the chain basis and as such all eigenvalues are either real or come in complex conjugate pairs. However the spectra exhibit more structure than just reflection about the real axis. At one loop order, the spectrum in a given (L, M) sector is shaped like an M-pointed star. It is worth noting that the "points" of the spectral star align with the M roots of unity, as is seen in fig. 4.1. At two loop order this structure is broken, but since $\delta\mathcal{D}^{(\text{two loop})}_{\text{Fishnet}}$ is still real valued in the chain basis, the spectrum is still symmetric about the real axis. There is also a tendency for the spectra to "spread out" towards larger positive real values, but this is only observed numerically.

It is worthwhile noting that the lines at the M roots of unity do not constitute symmetry axes for the one loop spectrum, but rather a tendency for the eigenvalues to have greater magnitudes at these angles. The star shaped

spectra of the Fishnet theory dilatation operator is derived analytically in [43, section 4.1] for $M = 3$ and $M = 4$, but only as a sum of all $(L, 3)$ and $(L, 4)$ sectors explicitly, however since any sector with $M = 3$ and a specified L would be a subset of all $(L, 3)$ combined, that sector will also have the same bounds – same for $M = 4$. It is likewise commented in in [43] that the spectrum of any (L, M) sector is bounded by a convex M-gon, matching the star shapes found in this thesis.[2]

Furthermore, as the Bethe roots, eq. (3.36), are L'th roots of unity, there are only certain possible values for the magnitude of their reciprocal sum at a given angle (the eigenvalues). This is less pronounced in the bulk of the spectrum. towards the middle, but it causes some straight line structures to appear for the more extremal energies. How (if at all) this structure affects level spacings and level spacing ratios is discussed in sections 4.1.2 and 4.1.3. We can get an idea as to how the level spacings are impacted by comparing the spectra to the RMT counterparts for integrable and chaotic behavior. Looking at fig. 4.2, we observe that the $(19, 9)$ sector exhibits structure, both in extremal states as well as in the central bulk, that is not present for randomly distributed values. Generally the $(19, 9)$ bulk values tend to "clump" together forming clusters or lines in the complex plane. At two loop order, fig. 4.3, this clumping is gone pointing towards the chaotic nature of the model. In general the two loop shares more similarities with its chaotic RMT counterparts, albeit with an apparent preference for values on the real axis. $\delta\mathcal{D}^{(\text{two loop})}_{\text{Fishnet}}$ has 132 real eigenvalues in the $(19, 9)$ sector, as opposed to 54 and 0 for GinOE and GinUE matrices of the same size respectively.

In the spectra analyzed we find degeneracies in most chains of even L for $L \geq 10$. This may point towards a further symmetry of the Hamiltonian, meaning we would have to further desymmetrise our basis, but no such symmetry was found during the process of this thesis. In [46] it is shown that one can always explicitly construct an anti-unitary operator to act as a symmetry protector for a two-fold degeneracy, however the proof fails for non-unitary systems (due to the difference between left and right eigenvectors) meaning that accidental degeneracies could still be a possibility for the DS theories studied in this thesis. It is however worth mentioning that whatever degeneracies are observed at one loop order is gone at truncated two loop order. This discussion is expanded in section 4.3.1.

[2]The spectrum of the (L, M) sector is equal to that of the $(L, L-M)$ sector (see section 4.1 of [43] for this) and map to one another through spin-flipping, so the trend will only persist until then – for example the $(20, 11)$ spectrum has 9 points.

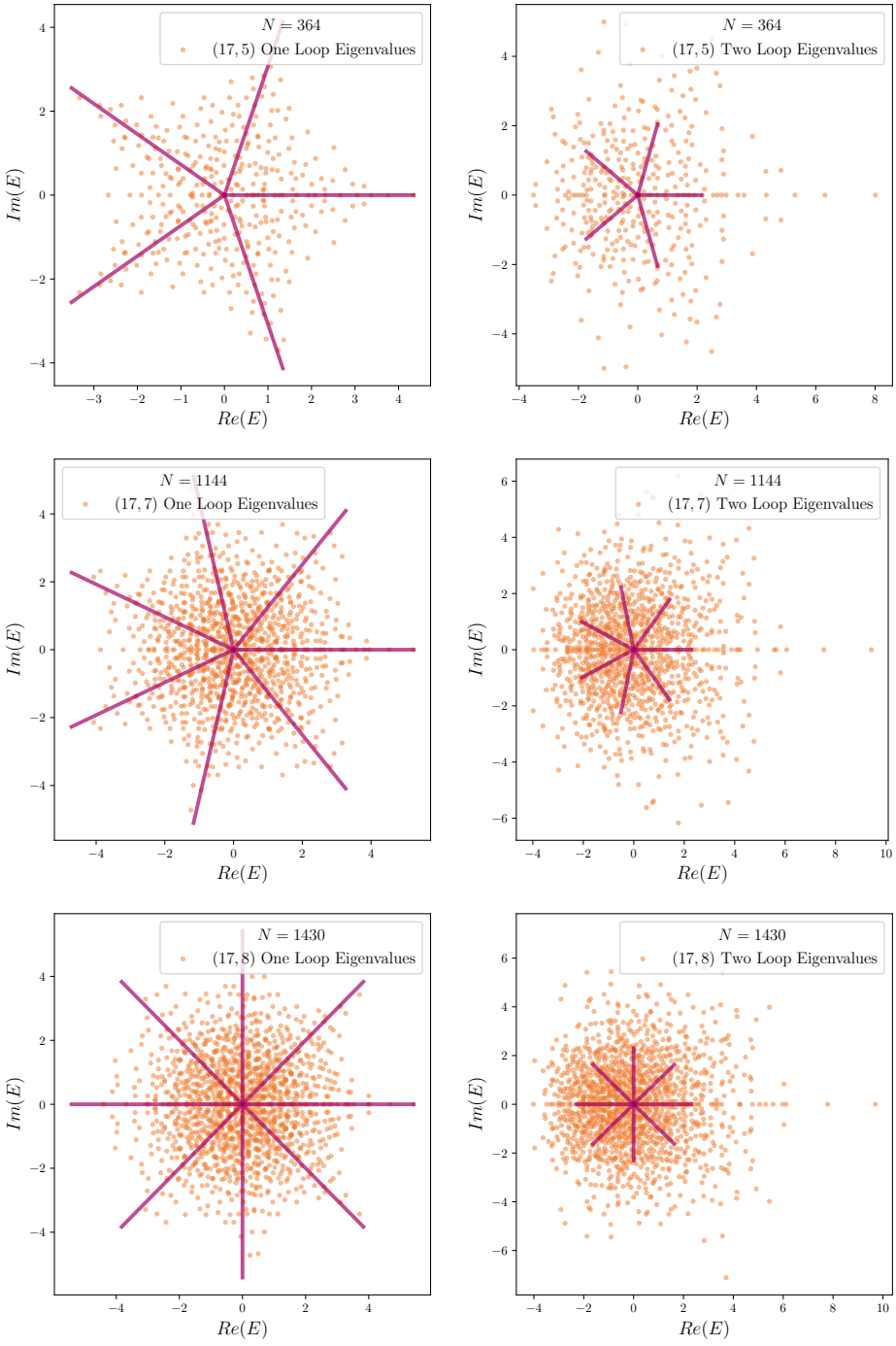

Figure 4.1: Spectra for $\delta\mathcal{D}_{\text{Fishnet}}$ at (left) one loop and (right) two loop order for $L = 17, M = 5, 7$ and 8. To illustrate the shape of the spectra, lines have been drawn at $\theta = 2\pi k/M, k = 0, \ldots, M - 1$.

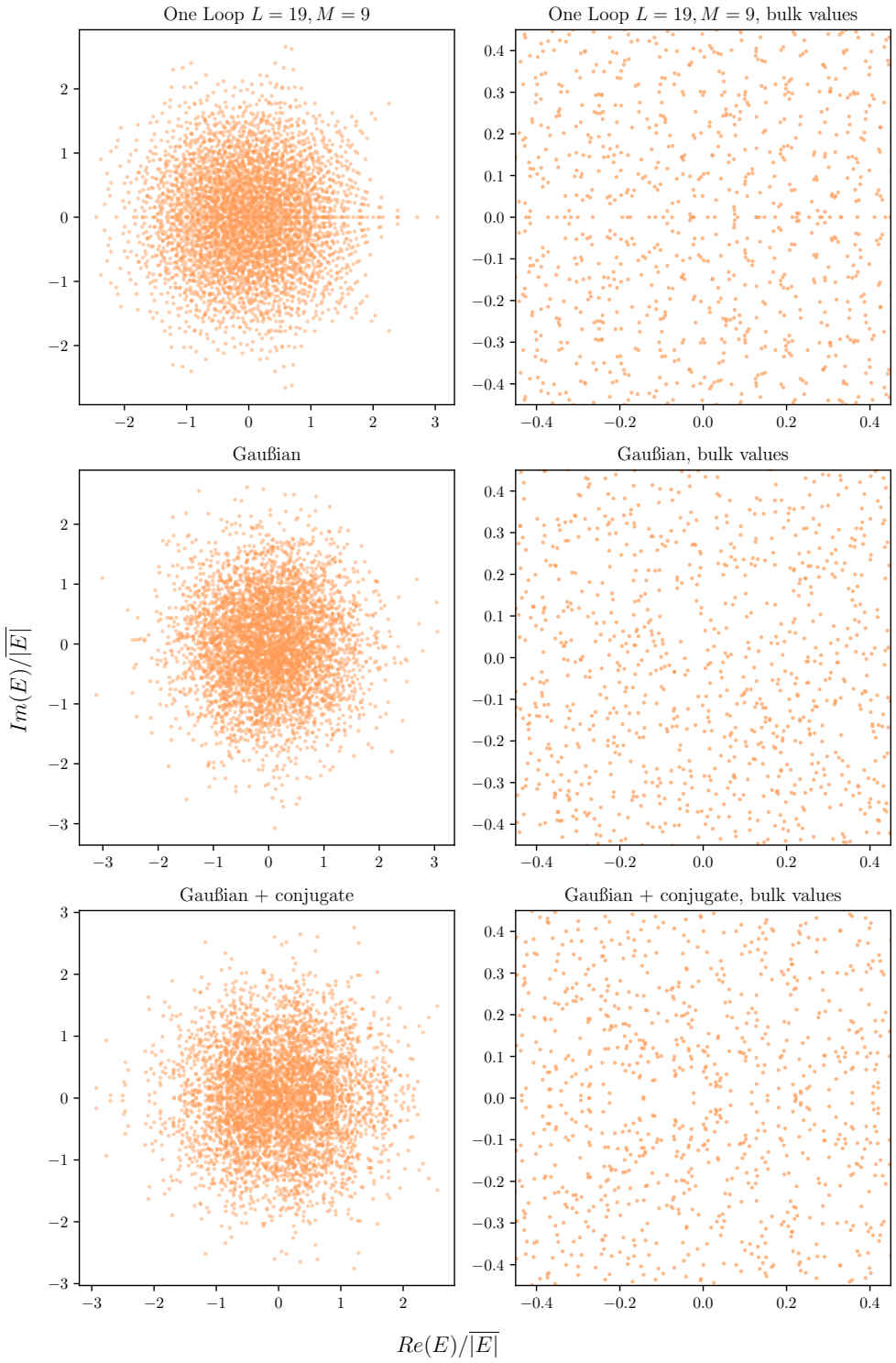

Figure 4.2: **Top**: Eigenvalues for $\delta\mathcal{D}^{(\text{one loop})}_{\text{Fishnet}}$ in the $(19, 9)$ sector ($N = 4862$). The plot to the left displays all eigenvalues in $\mathbb{C}$ whereas the plot to the right is zoomed in on the bulk. **Middle**: Random values with their real and imaginary parts drawn from a standard Gaußian. The number of values is equal to the number eigenvalues for the (19,9) sector, the plot to the right is again zoomed in on the bulk. **Bottom**: The same as the middle row, but with the complex conjugates of the random values added to have the same symmetry about the real axis as the Fishnet dilatation operator. The plot on the left contains the same number of values as the plots above, while the plot on the right is again zoomed in on the bulk.

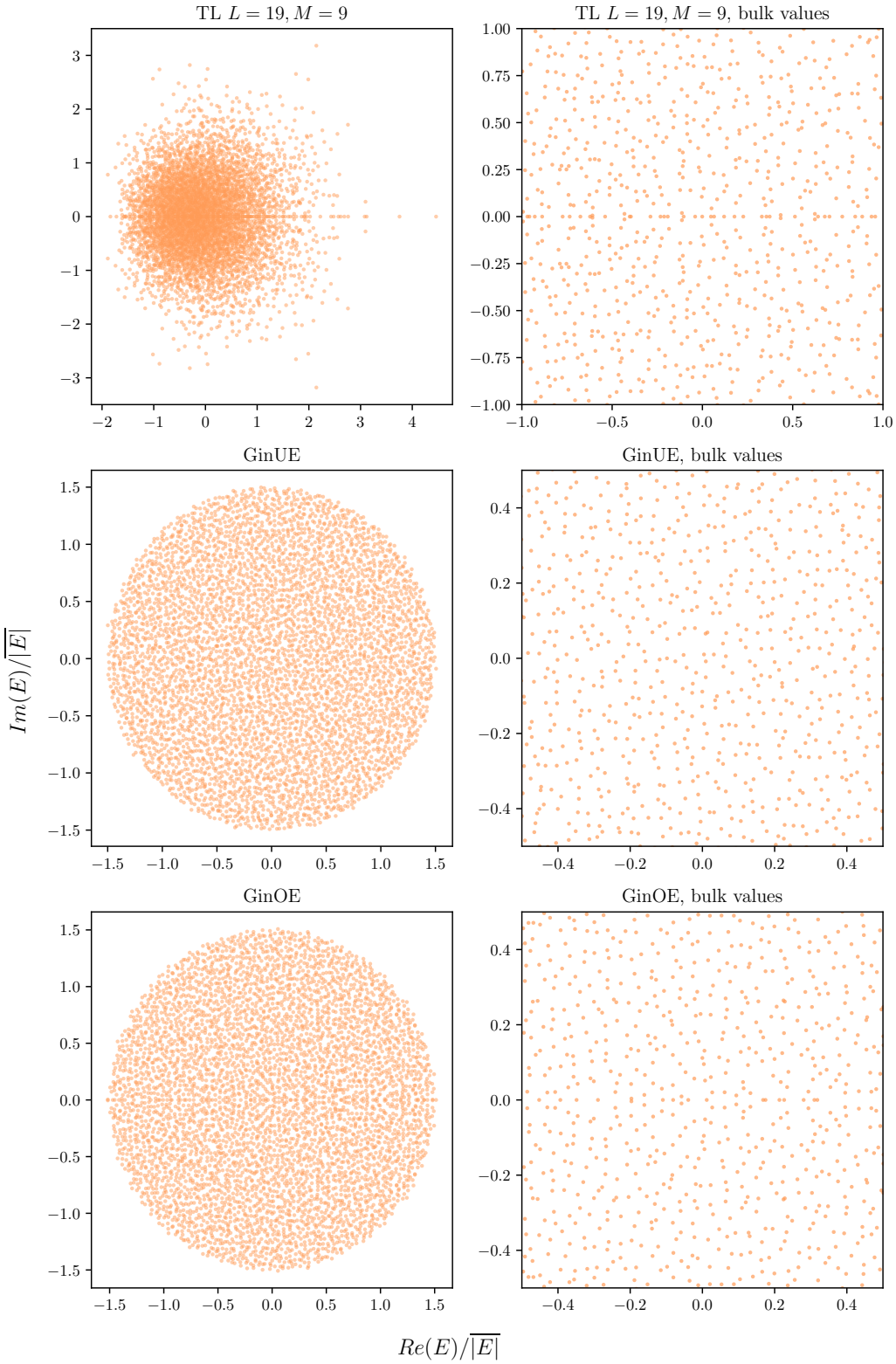

Figure 4.3: **Top**: Eigenvalues for $\delta\mathcal{D}_{\text{Fishnet}}$ in the $(19, 9)$ sector ($N = 4862$) at two loop order. The plot to the left displays all the values in the complex plane whereas the plot to the right is zoomed in on the bulk. **Middle and bottom**: Eigenvalues for a $N \times N$ GinUE (middle) and GinOE (bottom) matrix. As GinOE and GinUE are are both normalized such that $|E| \leq 1$. The bulk of these spectra (the plots on the right) are chosen such that roughly the same amount of points appear as for the bulk of the two loop Fishnet.

4.1.2 Level Spacings

Since the spectra belong in the complex plane, we'll analyze them using the level spacing definition given in section 2.2.1.2. For even L the degeneracies discussed previously become apparent in the level spacings since $s_i \propto |E_i - E_{i,\mathrm{NN}}|$. Figure 4.4 shows the level spacings for the $(18, 7)$ and $(17, 7)$ sectors. In the $(18, 7)$ sector the degeneracies cause a large deviation from $P^{(2D)}_{\mathrm{Poi}}(s)$. These degeneracies are no longer present at two loop order, which does have better agreement with $P_{\mathrm{GinUE}}(s)$, albeit with overcounting $s \lesssim 0.6$ and $s \gtrsim 1.5$ and undercounting elsewhere. As stated previously the level spacing statistics employed in this project are not equipped to deal with degeneracies, therefore the rest of this analysis will focus on odd L sectors.

In real level spacings a common practice is to remove states at the extremes of the spectrum, as these are bounded by the physical properties of the system and integrability is found in the bulk spacings. One might then think that the same procedure could fix the deviations observed above in the complex case. However, this is not observed when extremal states are removed and the level spacings computed numerically, as can be seen in fig. 4.5. The clipping of large magnitude states has a neutral, if not detrimental effect on the deviations of the level spacing distributions from their RMT counterparts in both the one loop and two loop case, albeit less so at two loop order. Figures 4.2 and 4.3 show that even in the bulk of the spectrum, there are noticeable differences between $\delta\mathcal{D}_{\mathrm{Fishnet}}$ and the RMT ensembles, suggesting that whatever deviations are observed in the level spacing distributions they may persist when only considering the bulk. Furthermore, the agreement with $P^{(2D)}_{\mathrm{Poi}}(s)$ actually becomes better as more states are included in the one loop case, but this may also be a consequence of worse statistics in the bulk, as less values are included.

One could also consider the unfolding parameter σ in eq. (2.14) as the cause of these deviations, given that especially the one loop spectrum has this "clumping" property (top of fig. 4.2), it may be sensitive to the width of the Gaußian functions used to calculate $n_{\mathrm{avg}}(E)$. Numerically it is observed that while the value of σ does effect the level spacing distributions, the change become minimal for σ's larger than 4.5, especially in the one loop case where the χ^2 value stabilizes.

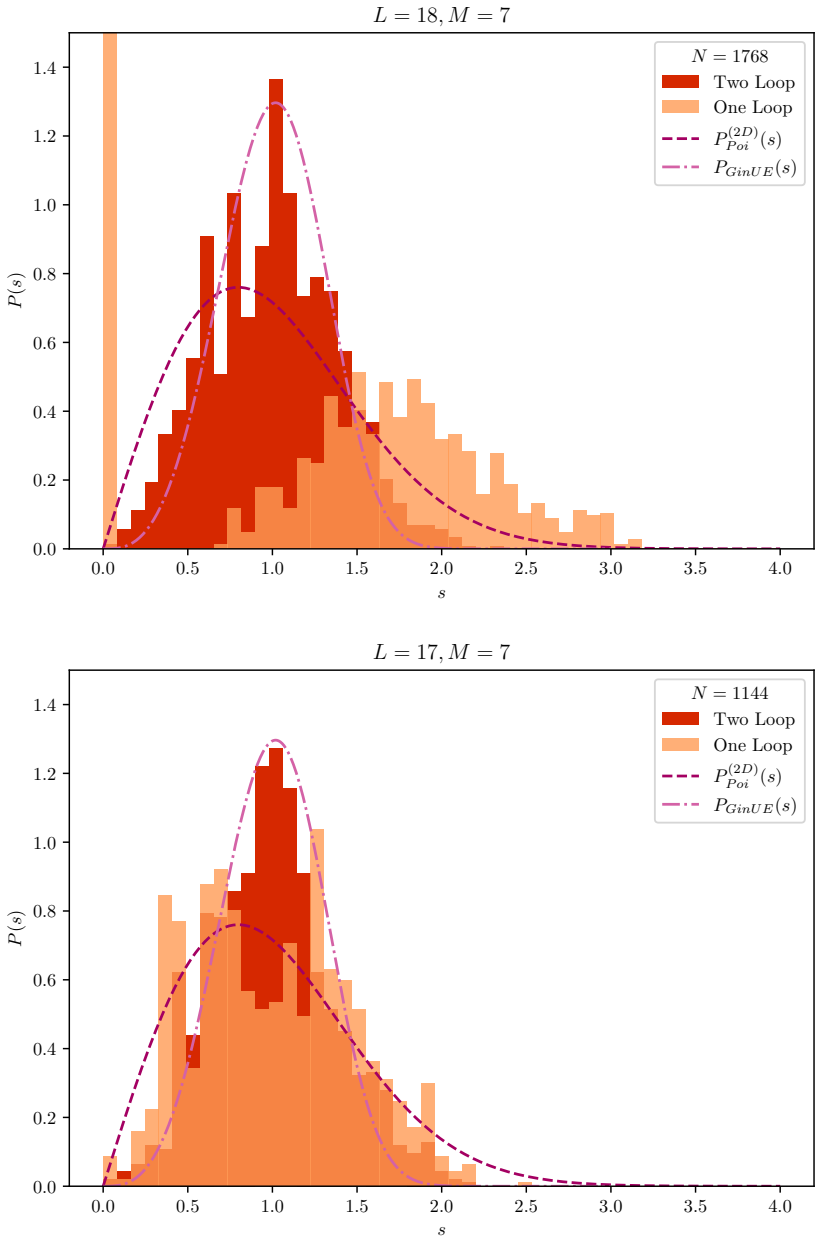

Figure 4.4: Level spacings for the (top) $(18, 7)$ and (bottom) $(17, 7)$ sectors $\delta\mathcal{D}^{(oneloop)}_{\text{Fishnet}}$. The dashed line in both plots is the two-dimensional Poisson distribution which integrable spectra are expected to follow. The dashed and dotted line is the level spacing distribution for the GinUE, which chaotic spectra are expected to follow. The degeneracies in the $(18, 7)$ sector can be seen as the large count of spacings at $s = 0$.

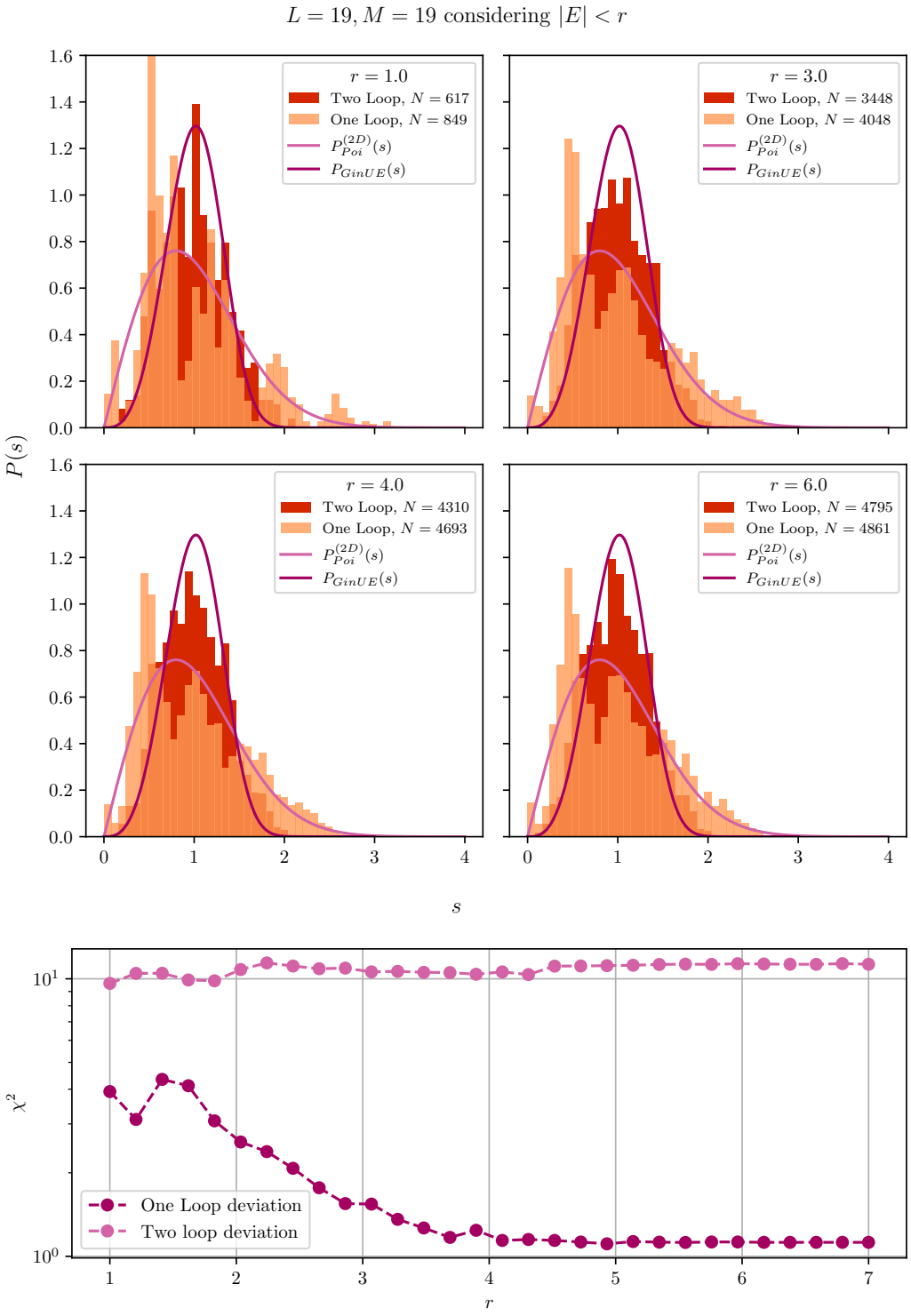

Figure 4.5: **Top**: Level spacing distributions of the $(19, 9)$ sector of $\delta\mathcal{D}_{\text{Fishnet}}$ only considering eigenvalues with $E \leq r$. In the unfolding process we set $\sigma = 4.5$ for all cases. **Bottom**: χ^2 values for the observed distributions (compared to $P^{(2D)}_{\text{Poi}}(s)$ for the one loop distribution and $P_{\text{GinUE}}(s)$ for the two loop distribution) at different cut-off radii.

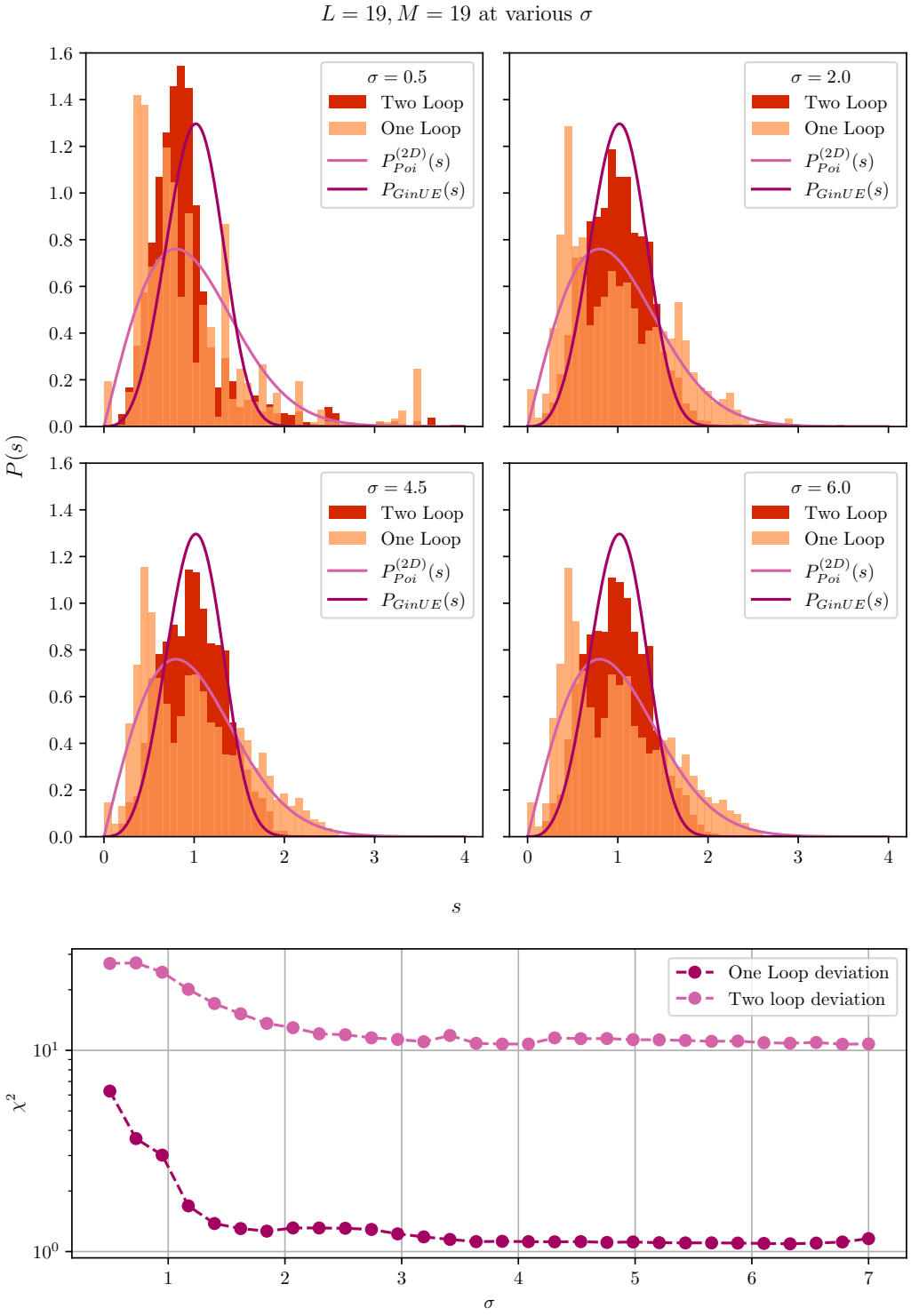

Figure 4.6: **Top**: Level spacing distributions in the $(19, 9)$ sector of $\delta\mathcal{D}_{\text{Fishnet}}$ at various values of the unfolding parameter σ. **Bottom**: χ^2 values for the observed distributions (compared to $P^{(2D)}_{\text{Poi}}(s)$ for the one loop distribution and $P_{\text{GinUE}}(s)$ for the two loop distribution) at different values of σ.

4.1.3 Level Spacing Ratios

Having explored the level spacing distributions of Fishnet theory, we turn our attention to level spacing ratios, defined in section 2.2.2. It is worthwhile to once again note that level spacing ratios, by definition, do not require unfolding and thus we have no free parameters to tune. Whereas the RMT prediction for an integrable system would be a perfectly flat distribution, $\delta\mathcal{D}_{\text{Fishnet}}^{(\text{one loop})}$ once again deviates from this result, this time in a very pronounced way as seen in fig. 4.7. In the $(18, 7)$ sector we again observe degeneracies, as most of the spacing ratios are at the origin. This pattern is present in other even L sectors. In the $(19, 9)$ sector we do not see degeneracies, but the distribution of level spacing ratios are still far from Poissonian, as there are certain ratios that are much more probable than others. In both cases the two loop correction breaks this structure and we find a result more reminiscent of the GinOE distribution expected from RMT, albeit with much more pronounced level repulsion in the $(19, 9)$ sector. In this sector we also see an overcounting of ratios at $\arg(z) \approx \pi$ which can be attributed to the straight line structures seen in the spectra at larger values of $|E|$. Figure 4.8 shows this structure in the one loop $(19, 9)$ sector. This overcounting disappears when limiting the analysis to the bulk of the spectra.

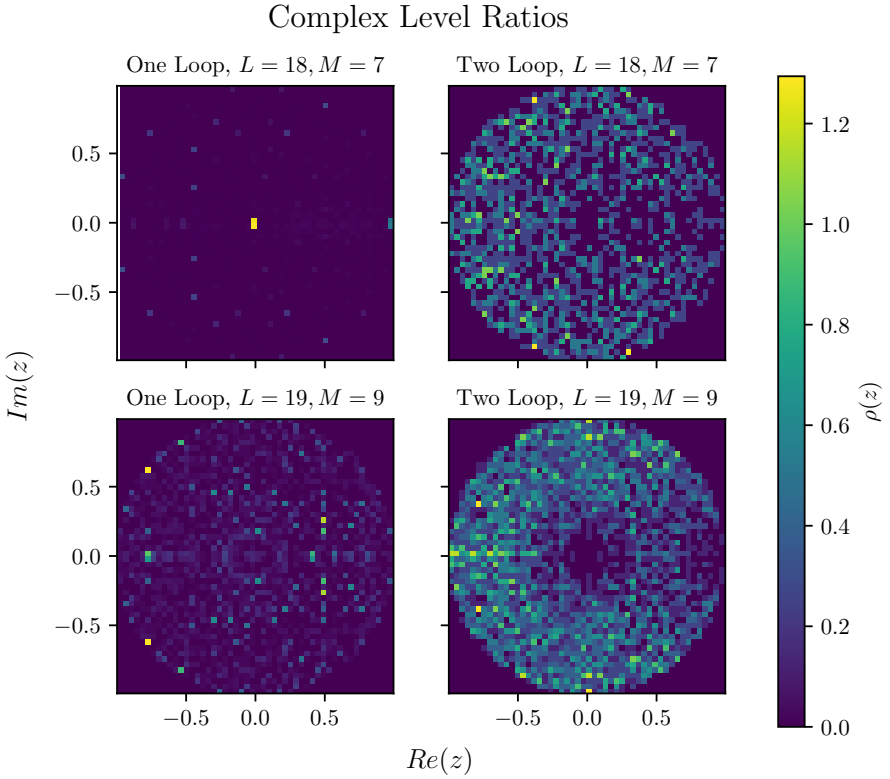

Figure 4.7: Level spacing ratios for the $(18, 7)$ and $(19, 9)$ sectors of $\delta\mathcal{D}_{\text{Fishnet}}$ at one loop and two loop order. In the $(18, 7)$ sector $N = 1768$ and in the $(19, 9)$ sector $N = 4862$

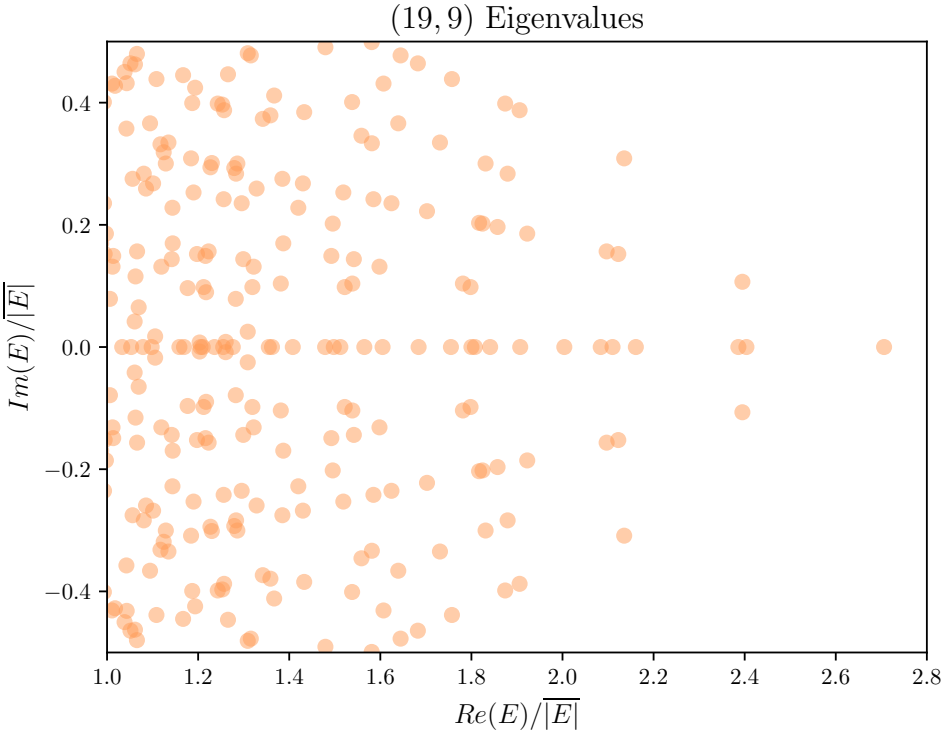

Figure 4.8: Spectrum of $\delta\mathcal{D}^{(\text{one loop})}_{\text{Fishnet}}$ in the $(19, 9)$ sector zoomed in on one of the "points". Five straight lines of eigenvalues can be seen in the spectrum, one on the real axis, two above it and two below it.

Considering the partial level spacing ratio distributions, eq. (2.20), we run into an issue in comparing the distributions to RMT expectations, namely for $\delta\mathcal{D}^{(\text{two loop})}_{\text{Fishnet}}$ in which we have already observed chaotic behavior. Since $\rho^{(N)}_{\text{GinUE}}(r, \theta)$ is dependent on the size of the ensemble matrices N and the asymptotic behavior of $\rho^{(N\to\infty)}_{\text{GinUE}}(r, \theta)$ is not captured even for $N = 10^4$ matrices, see fig. 2.6, we have no analytical distribution to compare to. What we can do instead is to compare the level spacing ratios of the $\delta\mathcal{D}^{(\text{two loop})}_{\text{Fishnet}}$ to those of an ensemble of GinOE matrices with $N = |(19, 9)| = 4862$. For the integrable case we can still use $\rho_{\text{Poi}}(r, \theta)$. Figure 4.9 shows the $(19, 9)$ level spacing ratio distributions along with the RMT distributions just described. Here we actually observe better agreement with RMT expectations in the two loop case than the one loop case. $\delta\mathcal{D}^{(\text{two loop})}_{\text{Fishnet}}$ actually provides a better fit to the RMT level spacing ratio distributions than any of the level spacing distributions considered.

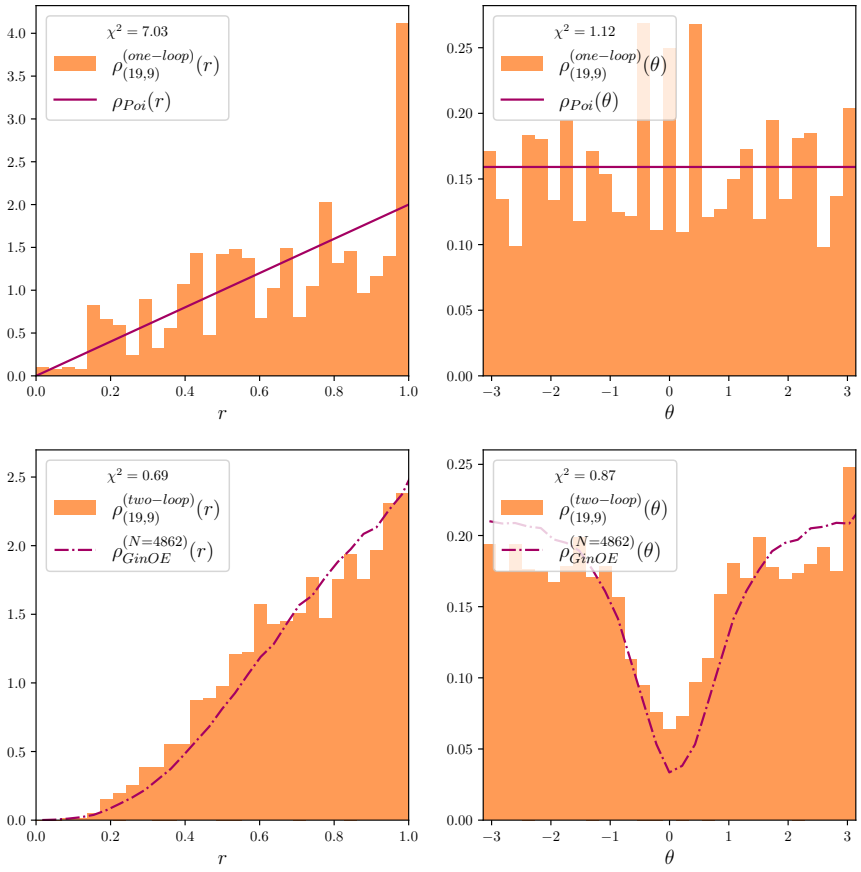

Figure 4.9: Partial level spacing ratio distributions in the $(19, 9)$ sector of $\delta\mathcal{D}_{\text{Fishnet}}$. **Top**: $\rho^{(\text{one loop})}_{(19,9)}(r)$ (left) and $\rho^{(\text{one loop})}_{(19,9)}(\theta)$ (right) shown alongside the partial distributions of $\rho_{\text{Poi}}(r, \theta)$. **Bottom**: $\rho^{(\text{two loop})}_{(19,9)}(r)$ (left) and $\rho^{(\text{two loop})}_{(19,9)}(\theta)$ (right) shown alongside the partial distributions of $\rho_{\text{GinOE}}(r, \theta)$. The RMT distribution is calculated from 100 GinOE matrices with $N = |(19, 9)| = 4862$ to account for the N-dependence of the distribution. All plots show the χ^2 between the Fishnet distribution shown and the matching RMT distribution.

4.2 Non-Eclectic SU(3) Sector

We now turn our attention to the non-eclectic $SU(3)$ sector, which we will analyse in the same way as we did Fishnet theory in section 4.1, albeit only at first loop order. Once again we find the spectra to be M-pointed stars, despite there now being two different types of excitations. In general when considering level spacings and level spacing ratios, we find better agreement with RMT expectations for integrable systems for $\delta\mathcal{D}_{SU(3)}$ than for $\delta\mathcal{D}^{(\text{one loop})}_{\text{Fishnet}}$. For all calculations presented we take $\xi_{1,2,3} = 1$.

4.2.1 Spectra

Many of the properties of the spectrum of $\delta\mathcal{D}^{(\text{one loop})}_{\text{Fishnet}}$ also hold true for the spectrum of $\delta\mathcal{D}_{SU(3)}$. Recall that for $\delta\mathcal{D}_{SU(3)}$, we consider closed sectors labeled by (L, M, K), L being the length, M being the magnon number and K being the number of those magnons that are in the $|3\rangle$ spin state. The spectra are shapes with M points, regardless of L and K as illustrated in fig. 4.10, similarly to Fishnet theory. Unlike for Fishnet theory, there is yet to be found an analytical bound to the spectra of $\delta\mathcal{D}_{SU(3)}$. The Bethe equations are presented, but not solved, in [41, section 5.1] and analytic solutions to some small sectors are given in [43, section 4.2]. The spectrum is less dense at larger magnitudes, but the straight lines of eigenvalues that appeared in Fishnet theory is absent – or at least suppressed to a point where we can no longer see it. There is however a much more prominent "clumping" of the eigenvalues in the bulk, especially when compared to a random spectrum as seen in fig. 4.11. All of these observations are empirical, and only verified for the sectors studied as part of this work which are $(12, 4, 2)$, $(13, 4, 3)$, $(13, 5, 3)$, $(13, 6, 2)$, $(14, 5, 3)$, $(13, 6, 2)$ and $(14, 7, 4)$.

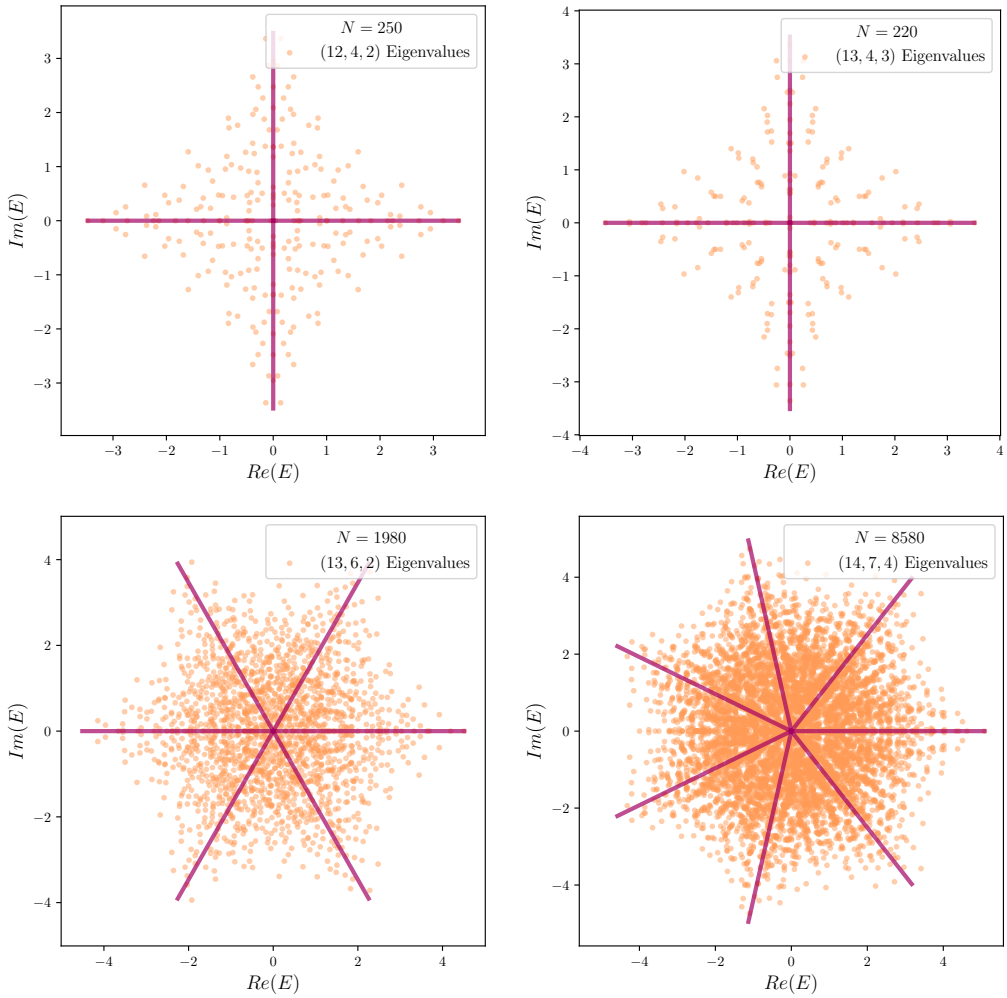

Figure 4.10: Spectrum of $\delta\mathcal{D}_{SU(3)}$ in different (L, M, K) sectors. Lines have been drawn in the direction of the M roots of unity to illustrate the shape of each spectrum.

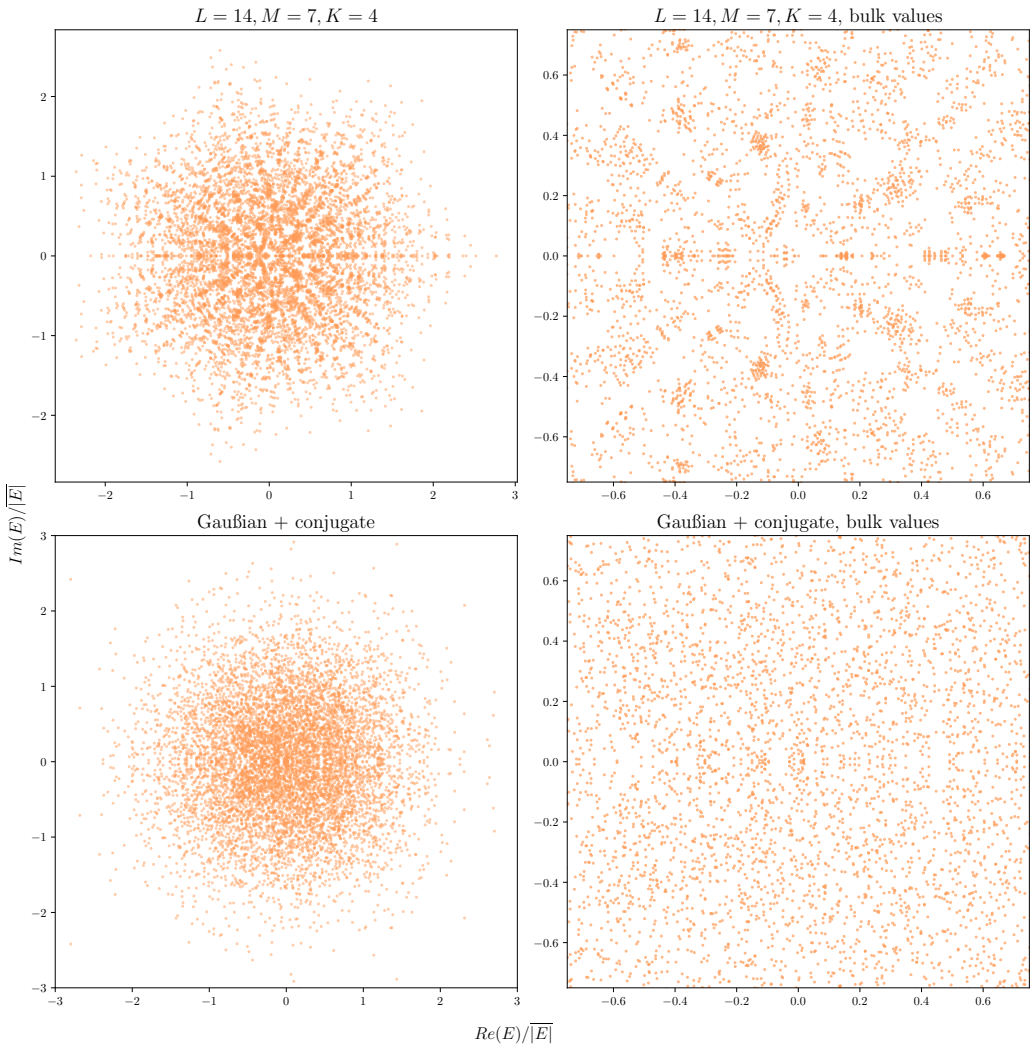

Figure 4.11: **Top**: Spectrum of the $(14, 7, 4)$ sector. To the left all values are shown and to the right the plot is zoomed in on the bulk, showing the clumping of eigenvalues. **Bottom**: Random values with their real and imaginary parts taken from a standard Gaußian distribution. To the left we see the full set of values and to the right the plot is zoomed in on the bulk.

4.2.2 Level Spacings

Considering the level spacings of $\delta\mathcal{D}_{SU(3)}$, we in general find better agreement between our observed distributions and $P^{(2D)}_{\text{Poi}}(s)$ than for Fishnet theory. This is readily apparent when looking at fig. 4.12, albeit still with some deviations. In some cases the deviations can be explained by the small size of the sector, such as for $(13, 4, 3)$, but even for larger sectors we see deviations. However crucially we do not see cubic level repulsion in any sector, which would indicate chaotic behavior.

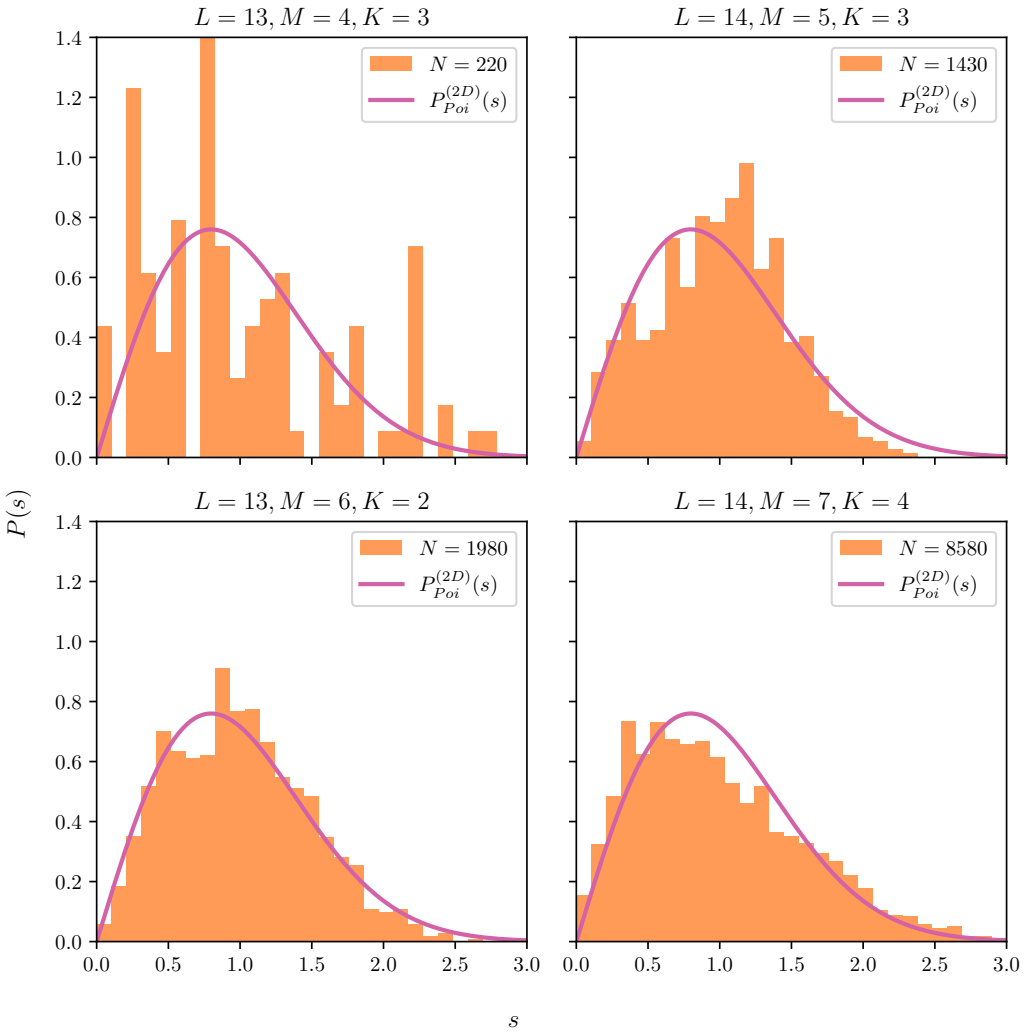

Figure 4.12: Level spacing distributions for different closed sectors of $\delta\mathcal{D}_{SU(3)}$.

We can quantify this claim by again looking at the χ^2 value as a "goodness of fit" parameter[3] when comparing the level spacing distributions of $\delta\mathcal{D}_{SU(3)}$ to $P_{\text{Poi}}^{(2D)}(s)$. Where as $\chi^2 > 1$ for all values of σ in Fishnet theory, in the non-eclectic $SU(3)$ theory, we see a universally better fit with the expected integrable distribution, as can be seen in fig. 4.13. The χ^2 values stabilize when $\sigma \gtrsim 5.2$, but curiously has a minima at $\sigma \approx 2.2$ in the $(14, 7, 4)$ sector. Since σ defines the width of the Gaußians used to calculate the average density of points, see eq. (2.14), it may be that this value is correlated with the average size of the "clumps" in the spectrum. In general we find very good agreement with RMT expectations across larger sectors.

[3]Using reduced χ^2 is usually standard for comparing different fits with different parameters, but since all our distributions have the same binnings we can used standard χ^2 values for analysis.

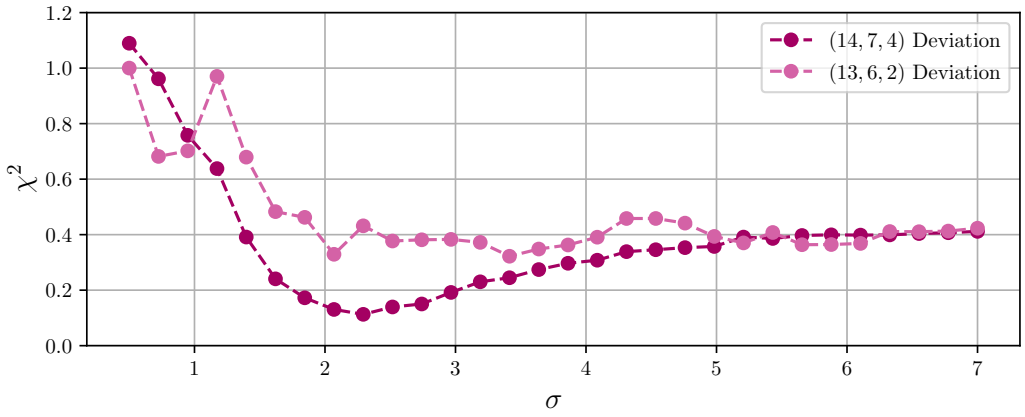

Figure 4.13: χ^2 values for different values of σ comparing the level spacing distributions in the $(13, 6, 2)$ and $(14, 7, 2)$ sectors to $P^{(2D)}_{\text{Poi}}$.

4.2.3 Level Spacing Ratios

Considering the level spacing ratios, we find considerable agreement between different (L, M, K) sectors and RMT expectations for integrable systems. Looking at the full distributions in fig. 4.14 we observe in general that is the size of the sector grows, we approach the flat distribution expected for integrable systems. Looking at fig. 4.15 we find that the partial distributions $\rho(r)$ and $\rho(\theta)$ cooperate this picture – especially for the $(14, 7, 4)$ sector.

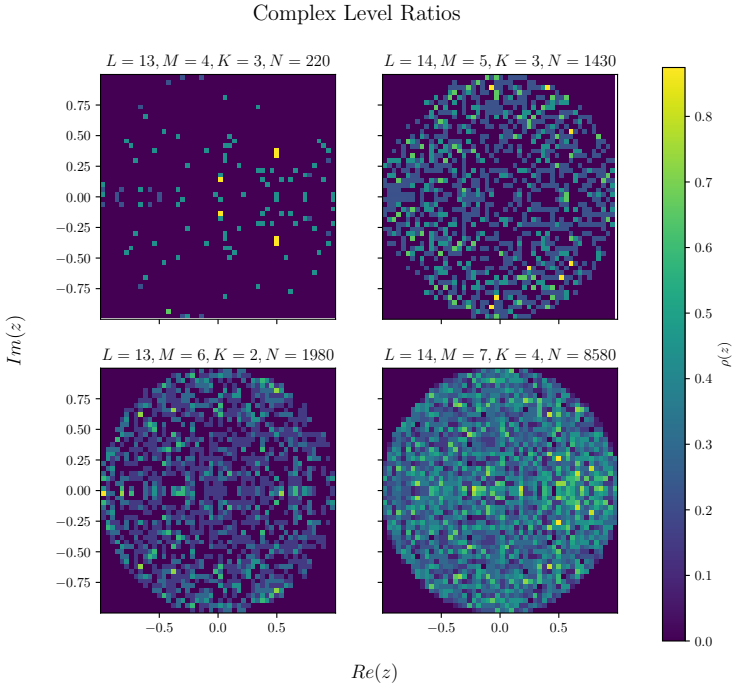

Figure 4.14: Level spacing ratios in four closed sectors of $\delta\mathcal{D}_{SU(3)}$. Here N indicates the size of the sector.

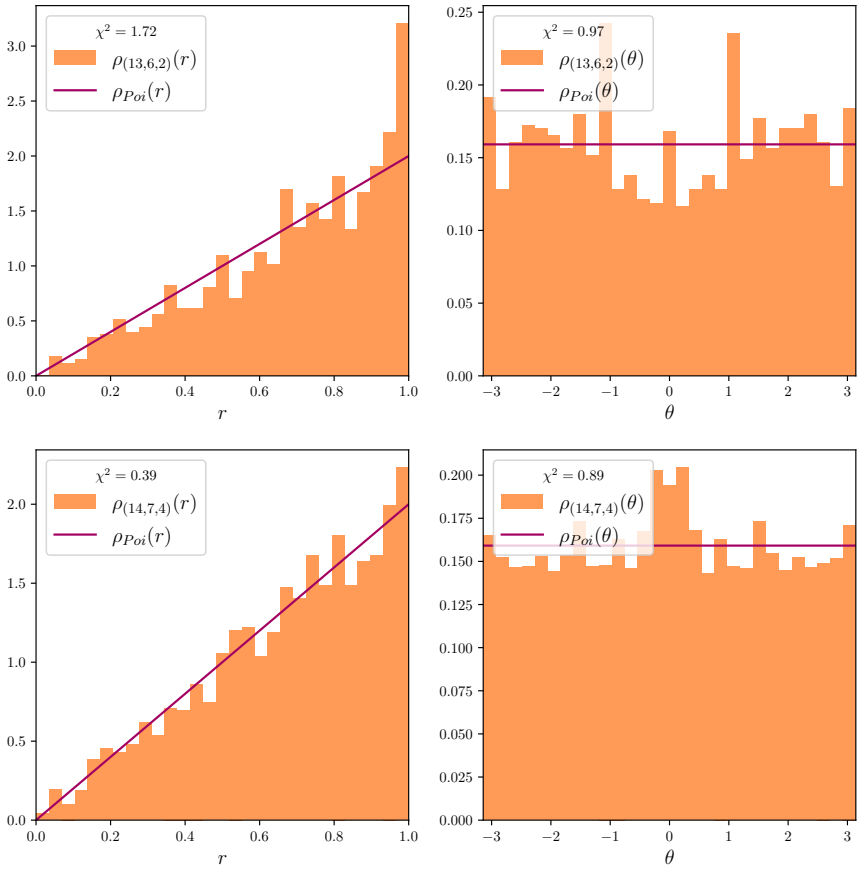

Figure 4.15: Partial level spacing ratio distributions $\rho(r)$ and $\rho(\theta)$ for the $(13, 6, 2)$ sector (top) and the $(14, 7, 4)$ sector (bottom). The purple lines are the partial distributions for a perfectly flat total distribution – the expectation for integrable systems. For each plot the χ^2 value for our observed distribution and the expected distribution is given and found to be lower for the larger sector.

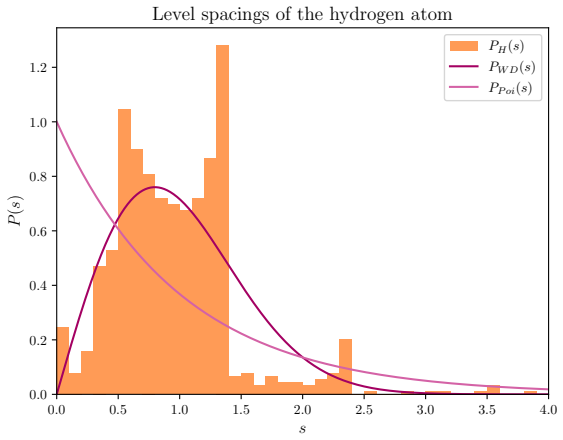

Figure 4.16: Level spacing distribution for the first 10^4 energy levels of the hydrogen atom.

4.3 Discussion

The deviations of the spectral statistics of Fishnet theory from the predictions of RMT raises som questions about the validity of extending the BGS conjecture for analysis of integrability in strongly twisted planar $\mathcal{N} = 4$ SYM. The study of level spacing distributions have proved useful in the spectral problem strongly β-twisted theory [7, 8] at first loop order. In the $SU(2)$ sector of untwisted planar $\mathcal{N} = 4$ SYM we found the anomalous dilatation operator to be an XXX spin chain, which has been shown to have integrable spectral characteristics, both in this thesis and in other works, see fig. 3.3[4] and [2, section 3.1]. We point out in section 4.1.1 that perhaps the prominent internal structure of the spectra is the cause of the deviations observed in our analysis. Removing states at the low and high energy ends of spectra is a common part of the unfolding process for real valued spectra, as extrema of the energies are more tightly bounded by system dependent properties, however we did not observe an improvement when only considering bulk states, see fig. 4.5 . If the system dependent structure persists at all energy scales, it can cause deviations from RMT expectations. A good example of this is the hydrogen atom, which is integrable in the sense that we can solve it by analytical means, but the system itself exhibits far from Poissonian level spacings, as seen in fig. 4.16. In systems with very simple dynamics, the internal structure can dominate, making RMT an unideal tool for analysing integrability. This may explain the deviations we see in Fishnet theory, as well as why they are suppressed when considering the non-eclectic $SU(3)$ sector as it has more complicated dynamics. However further work is necessary to understand the ways in which the spectral structure affect both the level spacings and level spacing ratios.

[4]Recall that an XXX chain is simply an XXZ chain with $\Delta = 1$.

4.3.1 Fishnet Degeneracies From Bethe Root Combinatorics

In section 4.1.2 we found degeneracies in some (L, M) sectors of Fishnet theory with even L. Typically in quantum mechanics we associate degenerate eigenvalues with a symmetry, implying that the spectrum is not fully desymmetrised. In [46] it is shown that any degeneracy of a Hermitian Hamiltonian is protected by an anti-unitary symmetry operator, but the argument requires the orthogonality of eigenvectors and does therefore not generalise to systems with non-Hermitian Hamiltonians, see [47, chapter 8]. It is therefore not clear whether or not the degeneracies we observe are protected by a larger symmetry of $\delta\mathcal{D}^{(\text{one loop})}_{\text{Fishnet}}$ or are "accidental", i.e. not originating from a symmetry. Looking at a sector where $M = L/2$ we can actually identify a larger symmetry as a combination of parity and spin reversal, as these both rearrange the ordering of $\uparrow\downarrow$ pairs, but since spin reversal in general is not a closed operation on (L, M) sectors this does not generalise. Whether or not this symmetry accounts for all degeneracies in $(L, L/2)$ sectors remains to be analysed.

[48, 49] present methods for classifying the degeneracies of a model similar to $\delta\mathcal{D}^{(\text{one loop})}_{\text{Fishnet}}$ called the "Totally Antisymmetric Exclusion Process" (TASEP). TASEP is a Hamiltonian similar to the XXZ spin chain, but with different boundary conditions that make it, in general, non-unitary. The degeneracies of TASEP are not found to be due to a symmetry of the system, but rather a property of its Bethe equations. [48] shows that by swapping "packages" of Bethe roots that contribute the same to the total energy and momentum degeneracies can occur. Since we know the Bethe equations for $\delta\mathcal{D}^{(\text{one loop})}_{\text{Fishnet}}$, we might try a similar approach in an attempt to classify the degeneracies we found in section 4.1.2. Looking at the Bethe equations we have

$$E = -2\sum_{i=1}^{M}\frac{1}{\alpha_i}\,, \tag{4.1}$$

$$(\alpha_i)^L = (-1)^{M-1}\,, \tag{4.2}$$

$$\prod_{i=1}^{M}\alpha_i = 1\,. \tag{4.3}$$

$\alpha_i^L = (-1)^{M-1}$ implies that the Bethe roots α_i are L'th roots of unity or negative unity, depending on the parity of M. If L is even then both α_i and $-\alpha_i$ are L'th roots of (negative) unity, since $\alpha_i^{2l} = (-\alpha_i)^{2l}, l \in \mathbb{N}, l = L/2$. So if a set of M Bethe roots adding up to an eigenvalue in eq. (4.1) contains both α_i and $(-\alpha_i)$ these cancel out. If one can replace $(\alpha_i, -\alpha_i)$ with another pair $(\alpha_k, -\alpha_k)$ in a way such that eqs. (4.2) and (4.3) are still satisfied, this would constitute a degeneracy. If this constitutes all degeneracies they would only occur for sectors of even L. By finding the Bethe roots corresponding to degenerate eigenvalues numerically we can examine whether this is the process by which degeneracies occur. Figures 4.17 and 4.18 show that this pattern can account

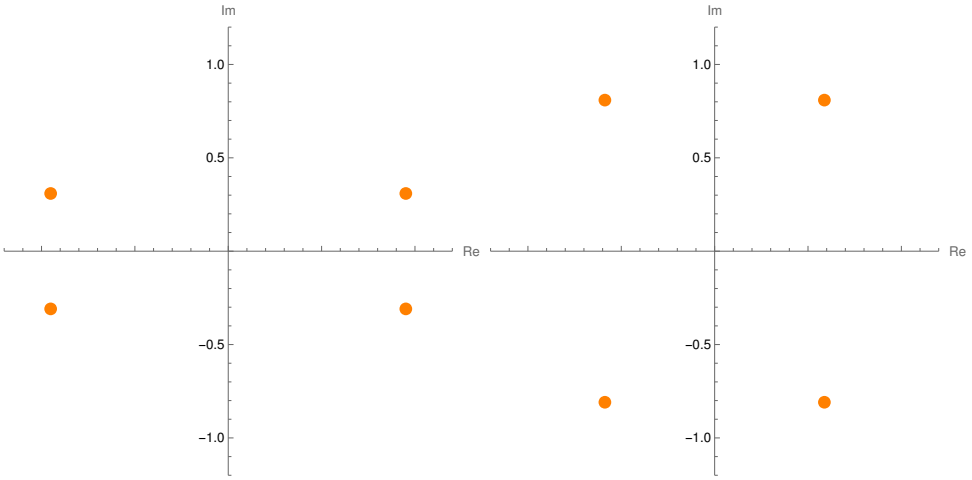

Figure 4.17: All possible Bethe root combinations in the $(10, 4)$ sector that produce the eigenvalue $E = 0$. Both the left and right plot consist of two canceling pairs of roots, hence why E vanishes. This is the only degeneracy found in the $(10, 4)$ sector.

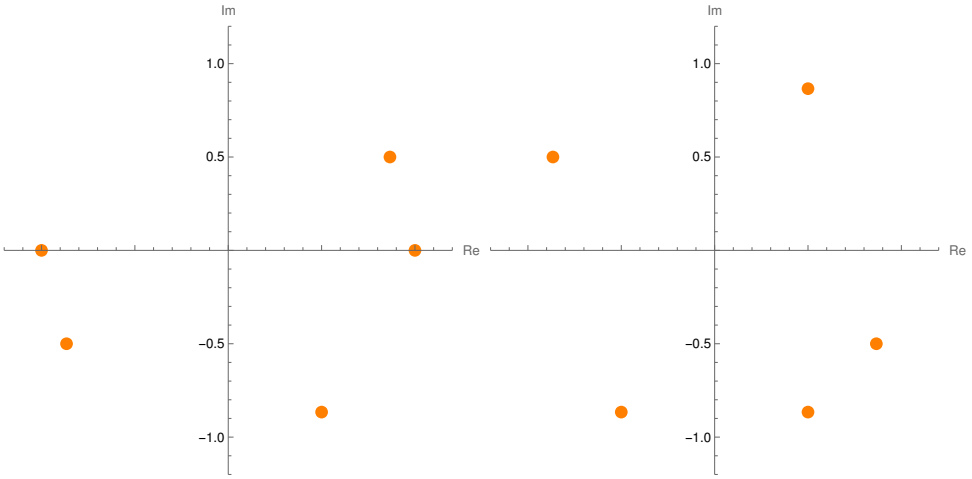

Figure 4.18: All possible Bethe root combinations in the $(12, 5)$ sector that produce the eigenvalue $E = -2e^{i\pi/3}$.

for some degeneracies, and numerical analysis shows that all degeneracies in the $(10, 4), (12, 4), (12, 5)$ and $(14, 5)$ sectors come from swapping out cancelling pairs of Bethe roots.

Of sectors where $M \neq L/2$ the $(10, 4)$ sector is the smallest to have any degeneracies, which has been verified numerically. This pattern persists throughout all sectors up to $(15, 5)$, where we only find degeneracies in even L sectors. In the $(15, 6)$ sector we find that $E = 0$ is a two-fold degeneracy, which disproves the conjecture of degeneracies only occurring for even L. However looking at fig. 4.19 we find that the degeneracy is caused by three pairs of roots that add to a canceling triplet. So in general the idea of exchangeable packages of Bethe roots constitute all the degeneracies up to the $(15, 6)$ sector. $(15, 6)$

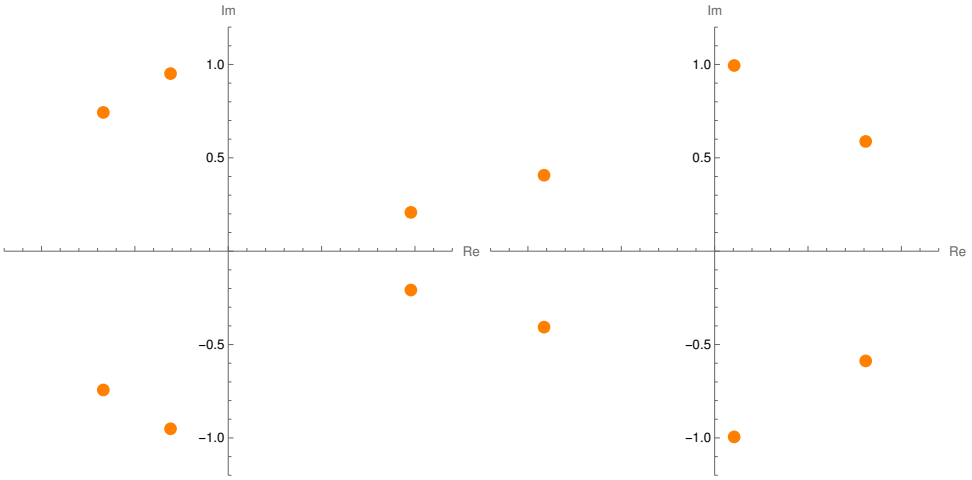

Figure 4.19: All possible Bethe root combinations in the $(15, 6)$ sector that produce the eigenvalue $E = 0$. This is the only degeneracy in the $(15, 6)$ sector, which is the only odd L sector found to have degeneracies in this analysis.

is the largest sector analysed in this work, as larger sectors introduce computational and runtime difficulties, more on this in appendix A. Whether this result is general and whether it reveals an underlying symmetry of $\delta\mathcal{D}^{(\text{one loop})}_{\text{Fishnet}}$ is not understood. Going back to the non-degenerate cases it is also not fully understood how the underlying structure of the spectra emerge from the Bethe equations and what effect this has on the level spacing distributions and level spacing ratio distributions.

Chapter 5

Conclusions

The study of spectral statistics has proved a useful tool in the field of quantum chaos and integrability. The Berry-Tabor and BGS conjectures along with Wigner-Dyson statistics are universally accepted measures of integrability and for Hermitian quantum systems with real valued spectra, such as the XXZ spin chain, which is seen both in this thesis and the literature in general [1, 2, 6, 45]. The field of non-Hermitian physics is not by any means new and appears in the study of open or dissipative quantum systems where the usual requirement of probability conservation which leads to Hermicity is dropped, see [50] for a review. Even the concept of level statistics in the complex plane has been studied since the late 1980's with [30] discovering the universality of cubic level repulsion for dissipative quantum systems. However a universally accepted methodology for the spectral statistics of integrable and chaotic quantum systems in $\mathbb{C}$ is yet to be found. [26] proposes the projective level spacing distributions described in section 2.2.1.2 but points out that it is not understood how RMT signatures appear in the spectra of non-Hermitian chaotic systems. [27] proposes using level spacing ratios, section 2.2.2, as a measure in non-Hermitian systems but also discusses how this warrants further analysis as it is unclear which RMT ensembles should be considered due to the slow appearance of large N asymptotics in GinOE and GinUE matrices, see fig. 2.6.

We can take strongly twisted planar $\mathcal{N} = 4$ SYM as a microcosm of the larger story of non-Hermitian spectral statistics. Spectral integrability methods have previously been used to analyse Hermitian strong twisting limits [7, 8] and our goal was to extend this analysis to certain non-unitary limits: Fishnet theory and the non-eclectic $SU(3)$ sector. For Fishnet theory we found degeneracies in most (L, M) sectors for even L, which we discussed the origins of by looking at different combinations of Bethe roots. We believe these symmetries to be accidental, but further work is needed in order to know if all these degeneracies can be classified in the way discussed in section 4.3.1. In all cases studied these degeneracies are only present at first loop order and are broken at second loop order. Looking at larger odd L sectors we found level spacing distributions resembling the RMT expectations, $P^{(2D)}_{\text{Poi}}(s)$ for the integrable first loop order and $P_{\text{GinUE}}(s)$ for the chaotic second loop order. However both

loop orders analysed deviated in significant ways, which we conjectured was due to further internal structure in the spectrum. Looking at the level spacing ratios for Fishnet theory we found a similar story. At first loop order we saw a pattern very different from the RMT expectation – even for larger (L, M) sectors – which we again conjectured might be caused by the internal structure of the spectra. This was somewhat remedied at second loop order, were we found good agreement with the RMT results. In general we found that for Fishnet theory level spacings distribution provided a better description of the one loop dilatation, whereas the truncated two loop dilatation operator showed better agreement with RMT expectations when using level spacing ratio distributions.

Moving on to the non-eclectic $SU(3)$ sector we found that $\delta\mathcal{D}_{SU(3)}$ in general provided better agreement with RMT predictions for both methods used. For the level spacings specifically the fit was up to an order of magnitude better than Fishnet theory when comparing the χ^2 values. The level spacing ratios also provided better agreement with RMT predictions, as larger sectors such as $(13, 6, 2)$ and $(14, 7, 4)$ actually resembled the perfectly flat $\rho_{\text{Poi}}(z)$. However both in the level spacings and the level spacing ratios we still found deviations that may once again point to the internal structure in the spectra. In general, further investigation into how the spectral structure of Fishnet theory affects the one loop level spacings and level spacing ratios and why this is suppressed in the non-eclectic $SU(3)$ sector is needed.

One way to deepen our understanding of spectral statistics as a probe for integrability in the strong twisting limits studied in this thesis is to vary the value of the couplings ξ_i. For Fishnet theory this would introduce a difference in the strength of the one loop and two loop correction terms, which may suppress or enhance the chaotic signatures observed in the truncated two loop dilatation operator, possibly leading to chaotic phase transitions like the ones described in [26]. The non-eclectic $SU(3)$ sector has three couplings $\xi_{1,2,3}$, the relative size of which could play a role in the structure of the spectra, as taking $\xi_{1,2} \to 0$ while keeping $\xi_3 = 1$ one would regain Fishnet theory and with it the prominent spectral structure. Studying how this structure emerges could help our understanding of how it affects the level spacing and level spacing ratio distributions, for which in general the non-eclectic $SU(3)$ sector shows better agreement than Fishnet theory.

Integrability in the one loop spectral problem of planar $\mathcal{N} = 4$ SYM is a well established result, both in the twisted and untwisted theories [7, 32, 34, 43]. The results presented in this thesis indicate that for non-Hermitian sectors of strongly twisted theories RMT signatures appear, but are in the case of Fishnet theory suppressed by other effects which we believe to be internal spectral structure. The fact that this structure is less present in the non-eclectic $SU(3)$ sector, which has more complicated dynamics, points to the fact that in larger sectors, and in the full strongly twisted theory, spectral statistics and RMT could serve as a good indicator for integrability and chaos in the non-Hermitian limits as it has in the Hermitian ones.

Acknowledgments

I would like to thank my primary supervisor Anne Spiering for her invaluable insight into my work and for always helping me find the right direction to move forward. I would also like to thank my co-supervisor Matthias Wilhelm for providing a level of experience and coordination, without which this project certainly would not have run as smoothly as it did. Furthermore I want to thank my master thesis journal club: Rune, Oliver, Rasmus, Jakob and Unik, for providing lively discussions and in general being great friends. Lastly I extend my thanks to all my friends and family who've been with me through this project and helped keep me from entering "The Swamp" – special thanks to my girlfriend Sofie finishing their PhD at exactly the same time so we could be in this together.

Appendix A

Numerical Details

All numerical results in this thesis are achieved using Wolfram Mathematica and Python. All code used and written for this project is available in a public GitHub repository [51].[1] All computations have been preformed locally on an ASUS VivoBook 15 X512 running Ubuntu 22.04.01.

Most numerical computations in this thesis consist of the following steps:

1. Construct a matrix, either a representation of a spin chain Hamiltonian or a matrix from an RMT ensemble.
2. Diagonalise the matrix to find its eigenvalues.
3. Analyse spectral statistics of the eigenvalues (level spacings or level spacing ratios).

If the desired matrix is a representation of a spin chain Hamiltonian, it is constructed in Mathematica, since the language allows for some abstractions (like using undeclared functions) that simplify the process of constructing these matrices. The RMT matrices are generated with Python. Python is in general a faster language and thus is used for as many computations as possible, such as diagonalisation, computing level spacings and level spacing distributions. Documentation for the languages and packages used can be found in [52, 53, 54].

All one dimensional histograms shown in this thesis are normalised such that

$$\sum_{i=1}^{n_{\text{bins}}} h_i \Delta_{\text{bin}} = 1 \,, \tag{A.1}$$

with h_i being the value of the histogram on the i'th bin and Δ_{bin} being the width of each bin. n_{bins} is the total amount of bins. The normalisation is preformed in Python using the `matplotlib.pyplot` package's `hist(density=True)` function.

[1] Reader beware: most of it is un-commented and rather messy.

Likewise for the two dimensional histograms they are normalised such that

$$\sum_{i=1}^{n_{\text{bins,h}}} \sum_{j=1}^{n_{\text{bins,v}}} h_{ij} \Delta_{\text{bin,h}} \Delta_{\text{bin,v}} = 1 \,, \tag{A.2}$$

with $n_{\text{bins,h}}, n_{\text{bins,v}}$ being the amount horisontal and vertical bins respectively. Since the histogram is now a matrix h_{ij} indicates the value of the histogram in the i'th horisontal and j'th vertical bin. $\Delta_{\text{bin,h}}$ and $\Delta_{\text{bin,v}}$ are the horisontal and vertical binwidths. In practice we always take $n_{\text{bins,h}} = n_{\text{bins,v}}$. The normalisation is again preformed in Python using the `matplotlib.pyplot` package and the `hist2d(density=True)` function.

A.1 Constructing Spin Chain Hamiltonians

To construct a matrix representation of a Hamiltonian we first pick a basis. For all operators analysed, except $\delta\mathcal{D}_{SU(3)}$, the basis used is known as the "site basis", which labels each site with either $\uparrow$ or $\downarrow$ depending on the spin state at the site, e.g. states of the form $|\uparrow\uparrow\downarrow \ldots \uparrow\downarrow\rangle$. $\delta\mathcal{D}_{SU(3)}$ represented in a variant of the site basis with spin states $1, 2$ and 3. Here we present the method used for the standard site basis.

We start by using Mathematica to construct the basis. We identify $\uparrow \to 1$ and $\downarrow \to 0$.

```
chains[L_]:=Tuples[{1,0},L];

States[L_,M_]:=Select[chains[L], Plus @@ # == M &];
```

This gives us the site basis in the (L, M) sector. We now implement desymmetrisation by removing states from the site basis that are identical up to a given symmetry transformation. Desymmetrising with respect to cyclicity and parity is done in the following way:

```
canonical[lst_] := Sort[RotateLeft[lst, #] & /@ Range[Length@lst]] // First;

Traces[L_, M_] := canonical /@ States[L, M] // DeleteDuplicates;

PosPar[state_] := Ch[canonical[state]] + Ch[canonical[Reverse[state]]];

PosParStates[L_, M_] := PosPar /@ Traces[L, M] // DeleteDuplicates;
```

Having constructed our basis, we move on to constructing the matrix by finding the matrix elements. For a Hamiltonian H in a basis $\{|e_i\rangle\}$ these are found by

$$\mathbf{H}_{ij} = \langle e_i | \, H \, | e_j \rangle \,. \tag{A.3}$$

So in code we construct a function $\mathbf{H} : |\psi\rangle \to H\,|\psi\rangle$ for some $|\psi\rangle$ in the site basis. For the XXZ Hamiltonian this is done like so

```
HXXZ[State_] :=
Sum[If[Part[State,i] == 1 && Part[State,i+1] == 0,
Ch[ReplacePart[ReplacePart[State,i->0],i+1->1]],0] +
If[Part[State,i] == 0 && Part[State,i+1] == 1,
Ch[ReplacePart[ReplacePart[State,i->1],i+1->0]],0] +
```

```
\[CapitalDelta](Part[State,i]-1/2) (Part[State,i+1]-1/2) Ch[State],
{i,1,Length[State]-1}] +
If[Part[State,Length[State]] == 1 && Part[State,1] == 0,
Ch[ReplacePart[ReplacePart[State,Length[State]->0],1->1]],0] +
If[Part[State, Length[State]]==0 && Part[State,1] == 1,
Ch[ReplacePart[ReplacePart[State,Length[State]->1],1->0]],0] +
\[CapitalDelta] (Part[State,Length[State]]- 1/2)
(Part[State,1]-1/2) Ch[State] + E0 Ch[State]
```

As an example, we can use the state $|\downarrow\downarrow\uparrow\uparrow\rangle$. We get H_{XXZ} from eq. (3.40) and in units of $\hbar = 1$ we find

$$\sum_{i=1}^{4} S_i^- S_{i+1}^+ |\downarrow\downarrow\uparrow\uparrow\rangle = |\downarrow\uparrow\downarrow\uparrow\rangle \ , \tag{A.4}$$

$$\sum_{i=1}^{4} S_i^+ S_{i+1}^- |\downarrow\downarrow\uparrow\uparrow\rangle = |\uparrow\downarrow\uparrow\downarrow\rangle \ , \tag{A.5}$$

$$\sum_{i=1}^{4} S_i^z S_{i+1}^z |\downarrow\downarrow\uparrow\uparrow\rangle = \left[\left(-\frac{1}{2}\right)^2 - \frac{1}{4} + \left(\frac{1}{2}\right)^2 - \frac{1}{4}\right] |\downarrow\downarrow\uparrow\uparrow\rangle = 0 \, , \tag{A.6}$$

$$\begin{aligned} H_{\mathrm{XXZ}} |\downarrow\downarrow\uparrow\uparrow\rangle &= E_0 |\downarrow\downarrow\uparrow\uparrow\rangle + |\downarrow\uparrow\downarrow\uparrow\rangle + |\uparrow\downarrow\uparrow\downarrow\rangle \\ &= E_0 |\downarrow\downarrow\uparrow\uparrow\rangle + 2 |\downarrow\uparrow\downarrow\uparrow\rangle \ . \end{aligned} \tag{A.7}$$

Where the last equality comes from putting all states in canonical order, i.e. desymmetrising w.r.t. cyclicity. In code this looks like

```
In[] := HXXZ[{0, 0, 1, 1}] /. Ch[a_] :> Ch[canonical[a]]
Out[] = E0 Ch[{0, 0, 1, 1}] + 2 Ch[{0, 1, 0, 1}]
```

where the `Ch[]` function is an undeclared function that makes sure the spin chain states are not added as vectors. We construct the matrix by finding the coefficients between the original desymmetrised site basis states and the states obtained from acting with H_{XXZ}

```
HXXZMatrixPos[L_, M_] := Module[{St = PosParStates[L, M]},
Transpose@Map[Coefficient[#, Last /@ St] &, (St /. Ch[a_] :> HXXZ@a)
/.Ch[a_] :> Ch[canonical[a]] /Coefficient[St, Last /@ St]]]
```

For instance in the $(5, 2)$ sector we get

$$\mathbf{H}_{\mathrm{XXZ}}^{(5,2)} = 2 \begin{pmatrix} \frac{E_0}{2} + \frac{\Delta}{8} & 1 \\ 1 & 1 + \frac{E_0}{2} + \frac{\Delta}{8} \end{pmatrix} . \tag{A.8}$$

The matrices found in Mathematica are exported and diagonalised in Python. This was done because I believed Python to be a faster language, epsecially when considering linear algebra computations. Tables A.1 and A.2 show the runtimes of constructing and diagonalising some matrices in Mathematica and Python. Python is generally faster, but never by more than a few seconds, and in one case Python is even slower. However the small time gains do add up over the course of the time spent on this thesis (9 months) and Python has more tools for data visualisation so something is still gained from using multiple programming languages.

Time [s]/Sector	$(16,7), N = 375$	$(17,7), N = 600$	$(18,7), N = 912$
Matrix construction	39.6	101.5	256.1
Diagonalisation (Mathematica)	0.08 ± 0.01	0.2 ± 0.03	0.6 ± 0.17
Diagonalisation (Python)	0.057 ± 0.012	0.22 ± 0.04	0.65 ± 0.07

Table A.1: Times for constructing and diagonalising different (L, M) sectors of H_{NNN} in Mathematica and Python. The matrices are constructed symbolically in Mathematica only, but all eigenvalues are evaluated numerically with $\Delta = 1$. The matrix construction is only preformed once, but other times are averages of 10 runs.

Time [s]/Sector	$(13,6,2), N = 1980$	$(14,5,3), N = 1430$
Matrix construction	33.9	37.0
Diagonalisation (Mathematica)	6.0 ± 2.3	1.7 ± 0.1
Diagonalisation (Python)	4.5 ± 0.4	2.2 ± 0.2

Table A.2: Times for constructing and diagonalising different (L, M, K) sectors of $\delta\mathcal{D}_{SU(3)}$ in Mathematica and Python. Matrices are only constructed in Mathematica. Matrices and eigenvalues are evaluated numerically with $\xi_{1,2,3} = 1$. The matrix construction is only preformed once, but other times are averages of 10 runs.

A.2 Generating RMT Matrices

All RMT ensembles are generated in Python using the `numpy.random` library and the function `standard_normal()` which takes a tuple of integers as input and returns an array of numbers randomly drawn from a standard Gaußian distribution with the same shape as the input tuple. For example `standard_normal((2,5))` returns a 2×5 matrix with random entries. All RMT ensembles are found using the following functions:

```
import numpy as np

def RealUncorrelated(size):
        return np.random.standard_normal(size)

def GOE(size):
        A = np.random.standard_normal((size,size))
        return 0.5*(A + A.T)

def ComplexUncorrelated(size):
        return np.random.standard_normal(size) + 1.j * np.random.standard_normal(size)

def GinOE(size):
        return np.random.standard_normal((size,size))

def GinUE(size):
        return (np.random.standard_normal((size,size))
                + 1.j*np.random.standard_normal((size,size)))/np.sqrt(2*size)
```

The Gaußian and Ginibre ensembles are diagonalised with the `numpy.linalg` library using the `eigvals()` function. For the uncorrelated ensembles we simply generate the eigenvalues directly.

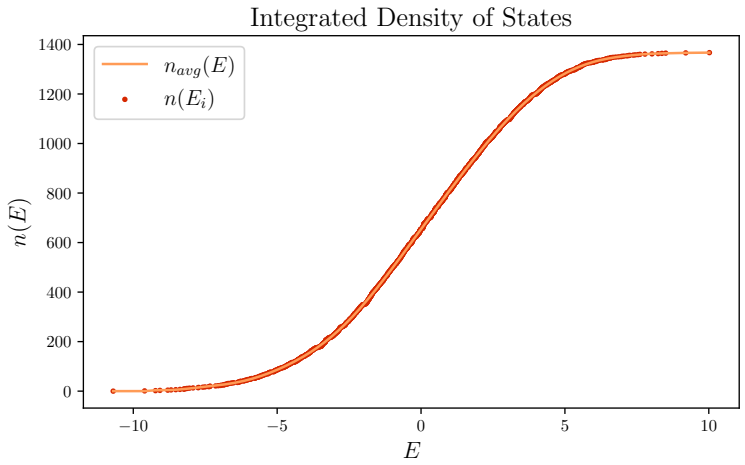

Figure A.1: Integrated density of states for the $(19, 7)$ sector of H_{XXZ} fitted with a degree 17 polynomial $n_{\mathrm{avg}}(E)$.

A.3 Unfolding the XXZ Spin Chain

Here we explain in more detail the process of unfolding (section 2.2.1) for the spectrum of the $(19, 7)$ sector of the XXZ spin chain, see section 3.3 for the physical details.

We start by removing the extreme ends of the spectrum as these are more sensitive to system dependent parameters. The percentage of states removed is a free parameter of the unfolding process and we choose to remove 5% at each end in line with [6]. We proceed by finding the integrated density of states $n(E)$ and fitting a degree 17 polynomial to it. The polynomial degree p is another free parameter in the unfolding process and we find $p = 17$ to work just fine for our purposes. [7] finds their results to be insensitives to variations in p for $p \geq 11$, albeit for a different physical system. We let this polynomial be $n_{\mathrm{avg}}(E)$. Both $n(E)$ and $n_{\mathrm{avg}}(E)$ are shown in fig. A.1. Having defined $n_{\mathrm{avg}}(E)$ we can define the unfolded energy levels $\varepsilon_i = n_{\mathrm{avg}}(E_i)$ and the level spacings $S_i = \varepsilon_{i+1} - \varepsilon_i$, $s_i = {}^{S_i}/_{\bar{s}}$. Unfolding is used to remove the system dependent fluctuations in the analysed spectra. The effect of unfolding on level spacing distributions can be seen in fig. A.2 which shows the distribution of level spacings for the unfolded eigenvalues ε_i and the raw eigenvalues E_i for the $(19, 7)$ sector of H_{XXZ}.

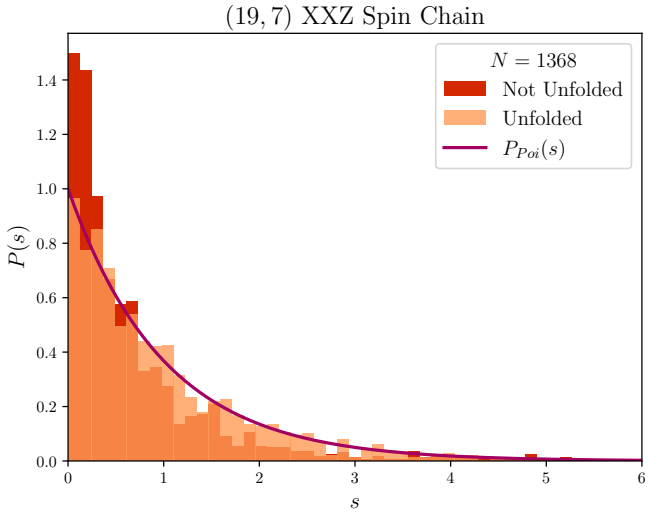

Figure A.2: Level spacing distribution for the $(19, 7)$ sector of the XXZ spin chain, with and without unfolding.

A.4 Solving Fishnet Bethe Equations

Mathematica is used to compute the Bethe roots and energies of the Fishnet Bethe equations

$$E = -2\sum_{i=1}^{M} \frac{1}{\alpha_i}\,, \tag{A.9}$$

$$(\alpha_i)^L = (-1)^{M-1}\,, \tag{A.10}$$

$$\prod_{i=1}^{M} \alpha_i = 1\,. \tag{A.11}$$

Mathematica is chosen due to supporting symbolic computations without the use of external packages. The process for solving these equations is

1. Find all complex numbers that solve eq. (A.10).
2. Find all sets of M unique solutions to eq. (A.10) that solve eq. (A.11).
3. Use eq. (A.9) on the sets that solve eq. (A.11) to find the energies.

These steps are fulfilled with the following functions:

```
FishnetBetheRoots[L_, M_] := Last /@ Last /@ Solve[x^L == (-1)^(M - 1), x, Complexes];

EigenValueRootSets[L_, M_] :=
Select[DeleteDuplicates /@ Select[Tuples[FishnetBetheRoots[L, M], {M}],
Times @@ # == 1 &]//DeleteDuplicatesBy[Sort], Length[#] == M &];

EigenValue[RootSet_] := Sum[-2/RootSet[[i]], {i, Length[RootSet]}] // FullSimplify;

EigenValues[L_, M_] := FullSimplify /@ EigenValue /@ EigenValueRootSets[L, M]
```

We also define a function that gives us the Bethe roots of a given eigenvalue:

```
RootOfEigval[eigval_,rootsets_] := Select[rootsets,EigenValue[#] == eigval &]
```

We then use these functions to find the degenerate eigenvalues and their corresponding Bethe roots. The use of `FullSimplify` in the `EigenValues[L_,M_]` function is crucial since the eigenvalues are not evaluated numerically, so the expression needs to be simplified as much as possible for Mathematica to recognise the degenerate eigenvalues as equal. The precision with which Mathematica evaluates values means that eigenvalues that are equal will sometimes be different to the 5th or 6th decimal place if determined numerically and not symbolically. The $(15, 6)$ sector of $\delta\mathcal{D}^{(\text{one loop})}_{\text{Fishnet}}$ is the largest analysed in this thesis and finding all its degenerate eigenvalues and their corresponding Bethe roots takes ~ 300s. Attempting to solve larger sectors caused Mathematica to crash, but this should not happen on a better computer.

Bibliography

[1] G. Tanner G. Vattay and P. Cvitanovi. *Chaos: Classical and Quantum*. 2020. URL chaosbook.org/version16.

[2] Luca D'Alessio, Yariv Kafri, Anatoli Polkovnikov, and Marcos Rigol. From quantum chaos and eigenstate thermalization to statistical mechanics and thermodynamics. *Advances in Physics*, 65(3):239–362, may 2016. doi: 10.1080/00018732.2016.1198134. URL https://doi.org/10.1080%2F00018732.2016.1198134.

[3] Fritz Haake. *Quantum Signatures of Chaos, 3rd Edition*.

[4] O. Bohigas, M. J. Giannoni, and C. Schmit. Characterization of chaotic quantum spectra and universality of level fluctuation laws. *Phys. Rev. Lett.*, 52:1–4, Jan 1984. doi: 10.1103/PhysRevLett.52.1. URL https://link.aps.org/doi/10.1103/PhysRevLett.52.1.

[5] O Bohigas, MJ Giannoni, and C Schmit. Spectral properties of the laplacian and random matrix theories. *Journal de Physique Lettres*, 45(21):1015–1022, 1984. URL https://doi.org/10.1051/jphyslet:0198400450210101500.

[6] Aviva Gubin and Lea F. Santos. Quantum chaos: An introduction via chains of interacting spins 1/2. *American Journal of Physics*, 80(3):246–251, mar 2012. doi: 10.1119/1.3671068. URL https://doi.org/10.1119%2F1.3671068.

[7] Tristan McLoughlin, Raul Pereira, and Anne Spiering. One-loop nonplanar anomalous dimensions in super yang-mills theory. *Journal of High Energy Physics*, 2020(10), oct 2020. doi: 10.1007/jhep10(2020)124. URL https://doi.org/10.1007%2Fjhep10%282020%29124.

[8] Tristan McLoughlin, Raul Pereira, and Anne Spiering. Quantum chaos in perturbative super-yang-mills theory, 2020. URL https://doi.org/10.48550/arXiv.2011.04633.

[9] Darrell F. Schroeter David J. Griffiths. *Introduction to Quantum Mechanics, 3rd Edition*. Cambridge University Press, 2018.

[10] Veronika E Hubeny. The AdS/CFT correspondence. *Classical and Quantum Gravity*, 32(12):124010, jun 2015. doi: 10.1088/0264-9381/32/12/124010. URL https://doi.org/10.1088%2F0264-9381%2F32%2F12%2F124010.

[11] J. Erdmenger M. Ammon. *Gauge/Gravity Duality: Foundations and Applications*. 2015.

[12] Don Page. Hawking radiation and black hole thermodynamics. *New Journal of Physics*, 7, 09 2005. doi: 10.1088/1367-2630/7/1/203. URL https://doi.org/10.48550/arXiv.hep-th/0409024.

[13] Stephen H. Shenker and Douglas Stanford. Black holes and the butterfly effect. *Journal of High Energy Physics*, 2014(3), mar 2014. doi: 10.1007/jhep03(2014)067. URL https://doi.org/10.1007%2Fjhep03%282014%29067.

[14] P.Di Francesco, P. Ginsparg, and J. Zinn-Justin. 2d gravity and random matrices. *Physics Reports*, 254(1-2):1–133, mar 1995. doi: 10.1016/0370-1573(94)00084-g. URL https://doi.org/10.1016%2F0370-1573%2894%2900084-g.

[15] Douglas Stanford and Edward Witten. Jt gravity and the ensembles of random matrix theory, 2020. URL https://doi.org/10.48550/arXiv.1907.03363.

[16] Ahmed Almheiri and Joseph Polchinski. Models of ads$_2$ backreaction and holography, 2015. URL https://doi.org/10.48550/arXiv.1402.6334.

[17] C. N. Yang and R. L. Mills. Conservation of isotopic spin and isotopic gauge invariance. *Phys. Rev.*, 96:191–195, Oct 1954. doi: 10.1103/PhysRev.96.191. URL https://link.aps.org/doi/10.1103/PhysRev.96.191.

[18] Lars Brink, John H. Schwarz, and Joel Scherk. Supersymmetric Yang-Mills Theories. *Nucl. Phys. B*, 121:77–92, 1977. doi: 10.1016/0550-3213(77)90328-5. URL https://doi.org/10.1016/0550-3213(77)90328-5.

[19] Anadi Canepa. Searches for supersymmetry at the large hadron collider. *Reviews in Physics*, 4:100033, 2019. ISSN 2405-4283. doi: https://doi.org/10.1016/j.revip.2019.100033. URL https://www.sciencedirect.com/science/article/pii/S2405428318300091.

[20] Niklas Beisert. On yangian symmetry in planar $\mathcal{N} = 4$ sym. In *Gribov-80 Memorial Volume*. WORLD SCIENTIFIC, apr 2011. doi: 10.1142/9789814350198_0039. URL https://doi.org/10.1142%2F9789814350198_0039.

[21] Ömer Gürdoğan and Vladimir Kazakov. New Integrable 4D Quantum Field Theories from Strongly Deformed Planar N = 4 Supersymmetric Yang-Mills Theory. *Phys. Rev. Lett.*, 117(20):201602, 2016. doi: 10.1103/PhysRevLett.117.201602. URL https://inspirehep.net/literature/1410933. [Addendum: Phys.Rev.Lett. 117, 259903 (2016)].

[22] Changrim Ahn and Matthias Staudacher. The Integrable (Hyper)eclectic Spin Chain. *JHEP*, 02:019, 2021. doi: 10.1007/JHEP02(2021)019. URL https://doi.org/10.48550/arXiv.2010.14515.

[23] M. V. Berry and M. Tabor. Level clustering in the regular spectrum. *Proceedings of the Royal Society of London. Series A, Mathematical and Physical Sciences*, 356(1686):375–394, 1977. ISSN 00804630. URL http://www.jstor.org/stable/79349.

[24] Eugene P. Wigner. On the distribution of the roots of certain symmetric matrices. *Annals of Mathematics*, 67(2):325–327, 1958. ISSN 0003486X. URL http://www.jstor.org/stable/1970008.

[25] Freeman J. Dyson. Statistical Theory of the Energy Levels of Complex Systems. III. *Journal of Mathematical Physics*, 3(1):166–175, 12 2004. ISSN 0022-2488. doi: 10.1063/1.1703775. URL https://doi.org/10.1063/1.1703775.

[26] Gernot Akemann, Mario Kieburg, Adam Mielke, and Toma ž Prosen. Universal signature from integrability to chaos in dissipative open quantum systems. *Phys. Rev. Lett.*, 123:254101, Dec 2019. doi: 10.1103/PhysRevLett.123.254101. URL https://link.aps.org/doi/10.1103/PhysRevLett.123.254101.

[27] Lucas Sá , Pedro Ribeiro, and Tomaž Prosen. Complex spacing ratios: A signature of dissipative quantum chaos. *Physical Review X*, 10(2), apr 2020. doi: 10.1103/physrevx.10.021019. URL https://doi.org/10.1103%2Fphysrevx.10.021019.

[28] V. E. Kravtsov. Random matrix theory: Wigner-dyson statistics and beyond. (lecture notes of a course given at sissa (trieste, italy)), 2012. URL https://doi.org/10.48550/arXiv.0911.0639.

[29] Jean Ginibre. Statistical ensembles of complex, quaternion, and real matrices. *J. Math. Phys.*, 6:440–449, 1965. URL https://doi.org/10.1063/1.1704292.

[30] Rainer Grobe and Fritz Haake. Universality of cubic-level repulsion for dissipative quantum chaos. *Phys. Rev. Lett.*, 62:2893–2896, Jun 1989. doi: 10.1103/PhysRevLett.62.2893. URL https://link.aps.org/doi/10.1103/PhysRevLett.62.2893.

[31] Werner Heisenberg. Zur theorie des ferromagnetismus (english: "on the theory of ferromagnetism"). 1928. URL https://doi.org/10.1007/BF01328601.

[32] Joseph A Minahan and Konstantin Zarembo. The bethe-ansatz for script n = 4 super yang-mills. *Journal of High Energy Physics*, 2003(03):013–013, mar 2003. doi: 10.1088/1126-6708/2003/03/013. URL https://doi.org/10.1088%2F1126-6708%2F2003%2F03%2F013.

[33] H. Bethe. On the theory of metals. 1. Eigenvalues and eigenfunctions for the linear atomic chain. *Z. Phys.*, 71:205–226, 1931. doi: 10.1007/BF01341708. URL https://doi.org/10.1007/BF01341708.

[34] Joseph A. Minahan. Review of AdS/CFT Integrability, Chapter I.1: Spin Chains in N=4 Super Yang-Mills. *Lett. Math. Phys.*, 99:33–58, 2012. doi: 10.1007/s11005-011-0522-9. URL https://doi.org/10.48550/arXiv.1012.3983.

[35] Howard Georgi and S. L. Glashow. Unity of all elementary-particle forces. *Phys. Rev. Lett.*, 32:438–441, Feb 1974. doi: 10.1103/PhysRevLett.32.438. URL https://link.aps.org/doi/10.1103/PhysRevLett.32.438.

[36] J.-L. Gervais and B. Sakita. Field theory interpretation of supergauges in dual models. *Nuclear Physics B*, 34(2):632–639, 1971. ISSN 0550-3213. doi: https://doi.org/10.1016/0550-3213(71)90351-8. URL https://www.sciencedirect.com/science/article/pii/0550321371903518.

[37] D. Sénéchal P. D. Francsesco, P. Mathieu. *Conformal Field Theory*. Springer.

[38] G.'t Hooft. A planar diagram theory for strong interactions. *Nuclear Physics B*, 72(3):461–473, 1974. ISSN 0550-3213. doi: https://doi.org/10.1016/0550-3213(74)90154-0. URL https://www.sciencedirect.com/science/article/pii/0550321374901540.

[39] Oleg Lunin and Juan Maldacena. Deforming field theories with u(1) × u(1) global symmetry and their gravity duals. *Journal of High Energy Physics*, 2005(05):033–033, may 2005. doi: 10.1088/1126-6708/2005/05/033. URL https://doi.org/10.1088%2F1126-6708%2F2005%2F05%2F033.

[40] S.A. Frolov, R. Roiban, and A.A. Tseytlin. Gauge-string duality for (non)supersymmetric deformations of super-yang–mills theory. *Nuclear Physics B*, 731(1-2):1–44, dec 2005. doi: 10.1016/j.nuclphysb.2005.10.004. URL https://doi.org/10.1016%2Fj.nuclphysb.2005.10.004.

[41] Asger C. Ipsen, Matthias Staudacher, and Leonard Zippelius. The one-loop spectral problem of strongly twisted $\mathcal{N} = 4$ Super Yang-Mills theory.

JHEP, 04:044, 2019. doi: 10.1007/JHEP04(2019)044. URL https://doi.org/10.48550/arXiv.1812.08794.

[42] João Caetano, Ömer Gürdoğan, and Vladimir Kazakov. Chiral limit of $\mathcal{N} = 4$ SYM and ABJM and integrable Feynman graphs. *JHEP*, 03: 077, 2018. doi: 10.1007/JHEP03(2018)077. URL https://doi.org/10.48550/arXiv.1612.05895.

[43] Friedrich Leonard Zippelius. *On the One-Loop Dilatation Operator of Strongly-Twisted N=4 Super Yang-Mills Theory*. PhD thesis, Humboldt U., Berlin, Humboldt U., Berlin, 2020. URL https://inspirehep.net/literature/1794560.

[44] Jan Fokken, Christoph Sieg, and Matthias Wilhelm. Non-conformality of γ_i-deformed $\mathcal{N} = 4$ SYM theory. *Journal of Physics A: Mathematical and Theoretical*, 47(45):455401, oct 2014. doi: 10.1088/1751-8113/47/45/455401. URL https://doi.org/10.1088%2F1751-8113%2F47%2F45%2F455401.

[45] Kazue Kudo. Statistical and dynamical properties in the energy spectra of xxz spin chains, 2005. URL https://www.researchgate.net/publication/268441867_Statistical_and_Dynamical_Properties_in_the_Energy_Spectra_of_XXZ_Spin_Chains.

[46] Jing-Min Hou and Wei Chen. Hidden antiunitary symmetry behind "accidental" degeneracy and its protection of degeneracy. *Frontiers of Physics*, 13(1), sep 2017. doi: 10.1007/s11467-017-0712-8. URL https://doi.org/10.1007%2Fs11467-017-0712-8.

[47] Henrik Schlichtkrull. *Advanced Vector Spaces*. Department of Mathematical Sciences, University of Copenhagen, 2021.

[48] O. Golinelli and K. Mallick. Spectral degeneracies in the totally asymmetric exclusion process. *Journal of Statistical Physics*, 120(5-6):779–798, sep 2005. doi: 10.1007/s10955-005-6972-7. URL https://doi.org/10.1007%2Fs10955-005-6972-7.

[49] Olivier Golinelli and Kirone Mallick. The asymmetric simple exclusion process: an integrable model for non-equilibrium statistical mechanics. *Journal of Physics A: Mathematical and General*, 39(41):12679–12705, sep 2006. doi: 10.1088/0305-4470/39/41/s03. URL https://doi.org/10.1088%2F0305-4470%2F39%2F41%2Fs03.

[50] Yuto Ashida, Zongping Gong, and Masahito Ueda. Non-hermitian physics. *Advances in Physics*, 69(3):249–435, jul 2020. doi: 10.1080/00018732.2021.1876991. URL https://doi.org/10.1080%2F00018732.2021.1876991.

[51] Anna Liv Paludan Bjerregaard. Code for this thesis, 2023. URL `https://git.ku.dk/vpd462/anna-bjerregaard-master-thesis-code`.

[52] Wolfram. Wolfram language documentation. URL `https://reference.wolfram.com/language/`.

[53] The Matplotlib development team. Matplotlib 3.7.1 documentation. URL `https://matplotlib.org/stable/index.html`.

[54] NumPy. Numpy documentation. URL `https://numpy.org/doc/`.